Development of Near-Infrared Spectroscopic Chronometers for Galaxy Evolution: Critical Testing With Nearby Galaxies

Jesse Miner

A dissertation submitted to the faculty of the University of North Carolina at Chapel Hill in partial fulfillment of the requirements for the degree of Doctor of Philosophy in the Department of Physics & Astronomy.

Chapel Hill
2011

Approved by:

James A. Rose, Advisor
Gerald Cecil, Reader
Sheila Kannappan, Reader
Bruce Carney, Reader
Christian Iliadis, Reader

ABSTRACT

JESSE MINER: Development of Near-Infrared Spectroscopic Chronometers for Galaxy Evolution: Critical Testing With Nearby Galaxies
(Under the Direction of James A. Rose)

I present preliminary results in the development of a near-infrared (NIR) spectroscopic chronometer for studying stellar populations in galaxies. By examining NIR IRTF/SpeX spectroscopy of the young post-starburst galaxy NGC 5102, and the compact elliptical M32, I have defined six indices that measure the strength of features due to thermally-pulsing asymptotic giant branch (TP-AGB) and main sequence turn-off (MSTO) stars, which are prominent in the integrated spectra of young populations. Two indices measure equivalent widths of Paschen lines originating in the atmospheres of hot stars, and are sensitive to ages up to ∼100 Myr; three indices measure the flux ratios of narrow bands surrounding molecular absorption breaks due to very cool and luminous TP-AGB stars; and the final index is a blended line also sensitive to TP-AGB stars. The TP-AGB is known to dominate the NIR flux of stellar populations between ∼100 Myr and 3 Gyr, and therefore the indices are particularly sensitive to ages in this regime. To demonstrate that the NIR indices can be used as chronometers, I compare the values measured in NGC 5102 and M32 to those in the Maraston (2005) stellar population models for a grid of ages and metallicities. The model-derived star formation histories for both galaxies are consistent with previous studies with established optical spectroscopic techniques. Moreover, in the case of NGC 5102 the indices are able to detect the presence of two distinct stellar populations with ages ∼20–40 Myr and several hundred Myr. I also address the issue of TP-AGB contribution in stellar population models, which is largely uncertain due to poorly understood processes in the evolution of TP-AGB stars, such as mass loss and convective burning. I find that the TP-AGB contribution in the Maraston (2005) models is accurate within error limits on the measured indices. Therefore, more work will be needed to place strict

limits on this important ingredient in stellar population models. The NIR indices in M32 are also examined, and model comparisons predict an SSP-equivalent age of $\sim$2.75 Gyr, consistent with optical studies. A more complicated star formation history in M32 cannot be ruled out, however, because the sensitivity of the indices declines at intermediate ages.

CONTENTS

Page

LIST OF TABLES vii

LIST OF FIGURES viii

LIST OF ABBREVIATIONS xi

LIST OF SYMBOLS xiii

Chapter

I. Introduction 1

1.1 Integrated spectroscopy of galaxies 3

1.2 Stellar population synthesis 5

1.2.1 TP-AGB stars 8

1.3 Implications for galaxy evolution 12

II. Preliminary results 15

2.1 Introduction 16

2.2 Observations and Stellar Population Models 19

2.3 Results 20

2.4 Conclusion 24

III. NGC 5102 28

3.1 Introduction 29

3.2 Spectroscopy and Data Analysis 32

3.2.1 OSIRIS 32

3.2.2 SpeX 34

3.2.3 Telluric corrections 35

3.2.4 Optical spectroscopy 39

3.3 Spectral indices and stellar population models 39
3.3.1 Definition of indices 40
3.3.2 Index uncertainty estimates 41
3.3.3 Predictions from stellar population models 45
3.3.4 Optically-derived star formation history 49
3.4 Results of Population Analysis 51
3.4.1 Single population fit 52
3.4.2 Composite population fits 53
3.4.3 TP-AGB contribution in NGC 5102 56
3.4.4 Stochasticity 59
3.5 Discussion 60
3.6 Conclusion 63
IV. M32 83
4.1 Introduction 83
4.2 Observations and data 86
4.3 Spectral indices and stellar population models 87
4.4 Results 89
4.4.1 SSP-equivalent fit 89
4.4.2 Composite population estimates 92
4.5 Discussion 94
V. Discussion 100
VI. Future Work 104
6.1 Further calibration with PSB galaxy sample 104
6.2 Application to ULIRGS 106
6.3 High Resolution Stellar Population Modeling 107
6.4 The JWST connection 108

LIST OF TABLES

2.1 Index Definitions and Values 20
3.1 Index Definitions 42
3.2 Index Values for NGC 5102 44
4.1 M32 index values and associated uncertainties 89

LIST OF FIGURES

2.1 Optical (for reference) and NIR spectra of NGC 5102 and M32 are plotted. The optical spectrum of NGC 5102 is from the Goodman High Throughput Spectrograph (Clemens et al. 2004) on the 4.1 m SOAR telescope at Cerro Pachon, Chile, while the optical spectrum of M32 was taken with the FOCAS spectrograph on the 8 m Subaru telescope at Mauna Kea, Hawaii (see Rose et al. 2005). The NIR spectra were taken with the SpeX spectrograph for this paper. The region of low atmospheric transparency is shaded. The J and H bands are shown, as we have defined no indices in the K band. The Paschen series is marked with the lower ticks to illustrate the differences between the spectra. Note the stronger Balmer lines in the optical spectrum of NGC 5102 than in M32, which is also reflected in the stronger Paschen series in the NIR spectrum of NGC 5102. 25

2.2 Wavelength regions of spectral indices for NGC 5102 (top) and M32 (bottom) smoothed to the resolution of the M05 models, with flux bands shown in red, and line regions in blue. 26

2.3 NIR spectral indices derived from the M05 models are plotted as a function of age, for four metal abundances. Thick horizontal lines denote the observed values for NGC 5102 (solid line) and for M32 (dashed line), respectively. The formal (photon statistical) error bars in the NGC 5102 and M32 indices are smaller than the thickness of the plotted lines. We note that the Paβ+ index is contaminated with other features. 27

3.1 Typical Mauna Kea atmospheric transmission at an airmass of $\sim$1.2 (upper line, right axis) in a region around the Paδ line in an A0V spectrum (lower line, left axis). Because the transmission is smooth around the line (and the instrument profile is relatively constant as well, although not pictured here), the Paδ line can initialize the convolution kernel that smooths the Vega model spectrum to match the observed telluric standard. (Figure 1 in Vacca et al. 2003, reproduced with permission). 64

3.2 Example of telluric correction using A0V star (a), and application to observed galaxy spectrum (b). 65

3.3 Optical and NIR SpeX spectra of NGC 5102 and the intermediate-age compact elliptical M32 for reference. The optical spectrum of NGC 5102 is from the Goodman High Throughput Spectrograph (Clemens et al. 2004) on the 4.1 m SOAR telescope at Cerro Pachon, Chile, while the optical spectrum of M32 was taken with the FOCAS spectrograph on the 8 m Subaru telescope at Mauna Kea, Hawaii (see Rose et al. 2005). The NIR spectra were taken with the SpeX spectrograph for this paper. The region of low atmospheric transparency is shaded. Only the J and H bands are shown because we have defined no indices in the K band. The Paschen series is marked with the lower ticks to illustrate the differences between the spectra. Note the stronger Balmer lines in the optical spectrum of NGC 5102 than in M32, which is also apparent in the stronger Paschen series in the NIR spectrum of NGC 5102. 66

3.4 From top to bottom in each plot, NGC 5102 spectrum (black), continuum-normalized intrinsic A0V spectrum (blue), and continuum-normalized telluric correction spectrum (green). The spectra have been smoothed to the resolution of the M05 models. The top plot shows the results from a normal telluric correction, the middle plot shows the effects of an under-compensated Paδ line, while the bottom plot shows the effects of over-compensation. Note the obvious features in the telluric correction in the poorly-fit cases. 67

3.5 From top to bottom: NGC 5102 spectrum for normal telluric correction, over-compensation, and under-compensation of the Paδ line in the Vega convolution kernel, respectively. 68

3.6 Percentage of TP-AGB fuel spent in C-stars as a function of metallicity in the M05 SPS models. Note the strong metallicity dependence, and the increase with age for each metallicity until $\sim$2 Gyr. (Figure 12 from M05, reproduced with permission.) 69

3.7 SEDs for M05 SSP models with $Z_{\odot}$ and Kroupa IMF. Note strong age dependence of both Paschen series and TP-AGB features. 70

3.8 Index vs. age for Maraston models at four metallicities. 71

3.9 Ca IIvs. Hδ/Fe I λ4045 index-index plot for NGC 5102 (open circle). Lines represent SSP tracks for three different metallicities. Ages in Gyr are labeled on the SSP tracks. Large print corresponds to the [Fe/H] = -0.4 model, and small print corresponds to [Fe/H] = -0.0. 72

3.10 Same as Figure 3.8. Measured values for NGC 5102 and M32 are the top and bottom horizontal lines, respectively, with thin lines showing 1σ uncertainties. 73

3.11 Five best M05 SSP fits to NGC 5102 indices that minimize $\sigma^2_{\rm fit}$. Legends detail the age, metallicities, and IMFs for the SSP models (SAL denotes Salpeter, KRO denotes Kroupa). 74

3.12 (a) DSS2 R-band image of NGC 5102; (b) Estimated SFH for nuclear region. (Reproduced with permission from S.F. Beaulieu). 75

3.13 Same as Figure 3.11, but for a composite two-SSP model fit. Legend includes mass fraction, IMF, age, and metallicity for each fit. 76

3.14 Same as Figure 3.13, but isolating the effect of the IMF on the index fitting. 77

3.15 Same as Figure 3.14 with metallicity constraints $[Z/H] \geq -0.33$. 78

3.16 Same as Figure 3.15 with CN index excluded. 79

3.17 $Z_\odot$ M05 models (Kroupa IMF) showing the dependence of the indices on the TP-AGB contribution to total light. 80

3.18 Composite model fits with varying TP-AGB contribution. 81

4.1 Best M05 model SSP fits to M32 indices. 97

4.2 Fits to $Z_\odot$ M05 models with exponentially-declining star formation rate. 98

4.3 Best M05 model composite two-SSP fits to M32 indices. 99

6.1 Region around the 1.28μm Paβ+ index showing the difference between high-resolution semi-empirical model spectra for a 1 Gyr SSP. The colored lines show the pseudo-continua (green) and the line (red). The blue horizontal lines show the continuum calculated from interpolating over the pseudo-continua. 111

LIST OF ABBREVIATIONS

AGB	Asymptotic Giant Branch
AGN	Active Galactic Nucleus/Nuclei
cE	Compact Elliptical
CMD	Color-Magnitude Diagram
DM	Dark Matter
DSS	Digital Sky Survey
EW	Equivalent Width
GC	Globular Cluster
HB	Horizontal Branch
HRD	Hertzsprung-Russell Diagram
IMF	Initial Mass Function
IP	Instrumental Profile
IR	Infrared
IRAF	Image Reduction and Analysis Facility
IRTF	Infrared Telescope Facility
ISM	Interstellar Medium
JWST	James Webb Space Telescope
M05	Maraston (2005)
MC	Magellanic Cloud
M/L	Mass-to-Light Ratio
MS	Main sequence
MSTO	Main-Sequence Turnoff

NIR	Near-Infrared
OSIRIS	Ohio State Infrared Imager/Spectrometer
PMS	Post Main-Sequence
PSB	Post-Starburst
RGB	Red Giant Branch
SB	Starburst
SDSS	Sloan Digital Sky Survey
SED	Spectral Energy Distribution
S/N	Signal-to-Noise
SFH	Star Formation History
SFR	Star Formation Rate
SP	Stellar Population
SSP	Simple Stellar Population
SXD	Short Cross-Dispersed
TP-AGB	Thermally-Pulsing Asymptotic Giant Branch
ULIRG	Ultra-Luminous Infrared Galaxy
VCR03	Vacca et al. (2003)
WFPC2	Wide-Field Planetary Camera 2
XD	Cross-Dispersed

LIST OF SYMBOLS

$M_\odot$	Solar mass
$\Psi(t)$	Star formation rate
R_e	Total effective radius
$\sigma^2_{\rm fit}$	Model fit statistic
$T_{\rm eff}$	Effective temperature
z	Redshift
Z	Metallicity
$Z_\odot$	Solar metallicity

Chapter 1

Introduction

Galaxies are luminous tracers of the large-scale structure of the universe, providing a picture of the distribution of the gravitationally-induced clumping of dark matter (DM) over cosmological timescales. The fundamental objective of the study of galaxy evolution is to understand the physical processes responsible for the variety of galaxy properties that we observe in the universe. Because galaxies are gravitationally-bound collections of stars, gas, and dust, both baryonic and DM phenomena will affect their formation and evolution. For example, a simple model of how galaxies form can be constructed by assuming that small, linear density fluctuations in the early universe cause the dissipative collapse of collisionless DM "halos" in overdense regions, with baryonic matter collapsing along with the DM and possibly experiencing shock heating (e.g., White & Rees 1978; Davis et al. 1985; Birnboim & Dekel 2003; Avila-Reese 2006, and references therein). Following this model any further, however, is difficult because several factors can influence the resulting galaxy such as angular momentum, the efficiency of gas cooling, and interaction with the background radiation (Mo et al. 2010). Also unclear is under what exact conditions stars will begin to form, and what effect they will have on the gas content due to supernovae and injection of metals into the interstellar medium. To add another level of complexity, many galaxies are believed to harbor supermassive black holes that may also play a role in evolution of the host galaxy (e.g., Kormendy & Richstone 1995), and can fuel active galactic

nuclei (AGN). It is clear that baryonic self-interactions and interactions with DM play important roles in galaxy evolution, and they must be simultaneously accounted for in models (e.g., Dekel et al. 2009; Conroy & Wechsler 2009; Kaufmann et al. 2009).

The evolution of galaxies is not only decided by secular processes, but also by interactions with other galaxies. In fact, the amalgamation of small clumps of matter into larger ones, known as hierarchical buildup, is an accepted model of galaxy assembly over cosmological timescales (e.g., White & Frenk 1991; Lacey & Cole 1994; Bromm & Yoshida 2011, and references therein). There is abounding evidence that mergers play an important role in galaxy evolution, and galaxies classified as ultra-luminous infrared galaxies (ULIRGs, e.g., Sanders et al. 1988a) are thought to be in the dissipative collapse phase of the merger of two galaxies. Because mergers of gas-rich galaxies are violent processes, they lead to energetic phenomena such as vigorous starbursts and AGN, indicating that the star formation history (SFH) and stellar mass buildup of the universe is linked to the rate at which galaxies merge, and also the dependence of that rate on redshift, galaxy type, and environment. Therefore, models must follow the large-scale DM halo clustering and merging as well as the galaxy-scale baryonic physics occurring within the halos (semi-analytic models, e.g. Baugh 2006). Because the baryonic physics is complex and computationally expensive to model, calibrations with observed galaxies are necessary to inform our understanding of galaxy formation and evolution. Hence, observational methods must exist for extracting galaxy properties such as mass, SFH, and chemical composition from observations.

In this thesis, I present an observational technique that has direct implications for studying stellar mass buildup within galaxies, and can aid in testing the predictions from hierarchical models of galaxy evolution. This technique relies on a detailed understanding of stellar evolutionary effects, and their influence on the integrated light of galaxies. The stellar content of galaxies can be deduced by comparing the emitted flux to models that predict the light output of populations of stars, a simple example being broadband colors, where red colors indicate old stars and blue colors indicate younger stars. Unfortunately, uniquely determining stellar population properties from

colors alone is difficult because the chemical composition of stars also affects color in that young metal-rich populations can have identical colors to older more metal-poor populations (the 'age-metallicity degeneracy'). Because a population's mass-to-light ratio (M/L) depends strongly on age and metallicity, this uncertainty between age and metallicity effects will prevent accurate estimates of physical properties, and must be addressed. A method for breaking this degeneracy between age and metallicity utilizes integrated spectroscopy, and because of its direct implications for the work presented in this thesis, I will now turn to a discussion of this technique.

1.1 Integrated spectroscopy of galaxies

Deconstructing integrated galaxy light into its constituent luminous components (stars, gas, and dust) is a difficult endeavor because of the many interdependent parameters that must be simultaneously accounted for. The distribution of stellar masses (i.e., the initial mass function, IMF); SFH and the related chemical enrichment history; quantity, spatial distribution and chemical properties of dust; and ionization state of the interstellar medium (ISM) will all affect the emitted light of a galaxy. Therefore, any attempt at synthesizing a galaxy spectrum must treat each of these components, which relies on a detailed understanding of stellar evolution and the physics of gas and dust. Early attempts at modeling galaxy spectra involved adding linearly weighted empirical stellar spectra to match observed galaxy spectra in a trial-and-error fashion, because sophisticated models of stellar population evolution were not yet available (e.g., Spinrad & Taylor 1971; O'Connell 1976, among many others). However, it became clear that the prohibitive number of parameters involved in this method prevented it from being a practical technique, and that the ability to synthesize stellar populations by following the theoretical evolution of stars would allow for more robust comparisons to galaxy light. Initial attempts at stellar population synthesis (SPS) involved early-type galaxies because, in contrast to spiral galaxies, their spectra are affected very little by gas and dust, and their stellar content can sometimes be

approximated by a single, old population (e.g., Tinsley & Gunn 1976), but more recent work has provided models that cover a wide range of stellar age and mass. I will discuss SPS in more detail below, but first I will discuss observational methods for determining galaxy properties in integrated light.

The vast majority of galaxy spectroscopy has been performed at optical wavelengths, for several reasons. First, ground-based observations suffer little from telluric absorption and/or emission from Earth's atmosphere, which tends to be stable over the course of a night's observing, allowing for deep, high-resolution spectroscopic studies. Second, the optical light emitted from galaxies tends to be dominated by stars on the main sequence (MS, especially in the blue part of the spectrum) and the red giant branch (RGB), whose stellar atmospheric physics is well understood compared to stars in later stages of stellar evolution. Moreover, there is a wealth of information available at optical wavelengths in the form of spectroscopic features from the hydrogen Balmer series and a multitude of metal lines. Spectroscopic indices that measure the strength of these features can yield important clues about the SFH of a galaxy. While many indices are dependent on both age and metallicity, preventing a unique description of SFH (e.g., O'Connell 1986; Worthey 1992), judicious combinations of indices when plotted against one another in two-index diagrams can resolve the degeneracy between age and metallicity (e.g., Faber et al. 1985; Rose 1985, 1994; Worthey 1994; Leonardi & Rose 2003).

In the near-infrared (NIR) region of the spectrum, however, the picture changes. In all but the youngest populations, the NIR light will be dominated by emission from evolved stars, whose evolution is difficult to model due to the complex physical processes that occur in their stellar interiors, as well as mass loss from the surface. Also, ground-based NIR observations suffer from severe atmospheric effects. Airglow emission lines from OH radicals high in Earth's atmosphere are present throughout the NIR wavelength region, and must be removed. However, the average flux of the OH lines, and their relative strengths, can vary substantially over timescales of a few minutes, which limits integration times. The transmission of the atmosphere also

depends strongly on wavelength, and there are several regions that are completely opaque. The transmission varies on short timescales as well, and thus even relatively transparent regions can fluctuate. Moreover, the thermal emission of the atmosphere increases with wavelength, and in the K band can dominate the signal from a faint object, or saturate the detector. However, over the past $\sim$20 years, improvements in instrumentation and development of observational techniques for mitigating telluric effects have allowed for NIR spectroscopic observations of star clusters and galaxies (e.g., Mouhcine et al. 2002; Silva et al. 2008).

Yet, because of these difficulties, there has not been a coordinated effort to define a set of NIR diagnostic features that can serve as chronometers for stellar populations, as there has been with optical spectroscopy. A major obstacle is that, only until the last decade or so, models of stellar population did not include detailed treatments of the NIR contribution from evolved stars, and so predictions of the evolution of spectroscopic features were not available. I will now turn to the discussion of stellar population models, and describe recent developments that have allowed for preliminary efforts to construct NIR spectroscopic chronometers.

1.2 Stellar population synthesis

Stellar population modeling is an incredibly complex endeavor because of inherent nonlinearities in stellar evolutionary timescales, uncertainties in the physics of stellar interiors, and the lack of empirical stellar spectra that span a large range of metallicities and abundance ratios. However, I will start with a basic description of SPS, which can be simply described as follows. If we assume that all the stars in a population form simultaneously with identical chemical compositions, and are distributed in mass according to an IMF, we can consult theoretical models of stellar interiors and atmospheres to follow the evolution of the population as a function of time. To translate the stellar properties into emitted light requires a detailed stellar library (i.e., a grid of stellar spectra with a large range in $T_{\rm eff}$, surface gravity, and Z) to

assign to each star in the population an associated spectrum. The spectra can then each be weighted by number and luminosity, and combined to create an integrated spectrum for the population as a whole. This provides a model for an ideal coeval population, also known as simple stellar population (SSP). A more complicated SFH can be modeled by convolving an SSP model with the star formation rate (SFR) and integrating over the time since formation.

Many groups have provided SPS models (see, e.g., Tinsley & Gunn 1976; Renzini & Buzzoni 1986; Worthey 1994; Fioc & Rocca-Volmerange 1997; Maraston 1998; Vazdekis 1999; Bruzual & Charlot 2003; Maraston 2005; Conroy et al. 2009), and I will give an overview of the methods employed in the execution of, and the outstanding problems still remaining in, stellar population modeling. To begin, we imagine our population of stars to be large enough in number that we can assume a continuous mass distribution, and then divide the population into narrow stellar mass intervals, or bins. Each mass bin will be treated separately because a star's mass determines its properties and evolution (of course, the evolution depends on chemical composition as well, but we assume all stars in the population to have identical composition). Then, for stars in each mass bin, we find the surface gravity (i.e., size) and temperature by consulting stellar evolution models that solve the basic equations of stellar structure, while accounting for overshooting in convective cores through some individual prescription. If each bin's gravity and temperature are transformed into luminosity, then it can be placed on the Hertzsprung-Russell (L vs. $T_{\rm eff}$) diagram (HRD); the collection of points on the diagram from all mass bins forms an 'isochrone', a curve that represents a snapshot of the population on the HRD at a given age. The exact morphology of the isochrone will depend on the particulars of the models, and there are many groups that provide stellar evolution tracks and isochrones[1].

Stellar evolution models can provide isochrones up to the beginning of the the early

[1]For example, the Padova tracks (Fagotto et al. 1994; Girardi et al. 2000; Salasnich et al. 2000), the Geneva tracks (e.g., Schaller et al. 1992; Charbonnel et al. 1996), and the Cassisi tracks (e.g., Cassisi et al. 1997, 2000).

asymptotic giant branch (E-AGB), which immediately follows the helium-burning horizontal branch (HB) phase, and marks the onset of H and He shell burning in stars with masses $0.8 < M/M_{\odot} < 8$[2]. The properties returned for each mass bin along the isochrone up the E-AGB are then transformed into observable spectra with a stellar library, which can consist of either empirical or synthetic spectra. Empirical libraries (e.g., STELIB, Le Borgne et al. 2003) can provide high-resolution spectra, but suffer from incomplete coverage of $T_{\rm eff}$, surface gravity (g), and metallicity for some spectral types, such as hot MS stars, which tend to have approximately solar metallicities. The alternative is to synthesize spectra from model stellar atmosphere calculations (e.g. Kurucz 1992), but these models tend to be lower resolution (e.g., BaSeL, Westera et al. 2002) because it is computationally expensive to simultaneously apply the millions of atomic and molecular lines to each spectrum. And while synthetic spectra cover a larger range in $T_{\rm eff}$, g, and Z, some spectral features fail to match those in observed stars and stellar populations (Le Borgne et al. 2003). However, empirical calibrations of synthetic spectra can improve accuracy, and such "semi-empirical" libraries are widely used in stellar population synthesis (Lejeune et al. 1997). For stars in evolutionary stages beyond the E-AGB, individual prescriptions must be applied. Namely, it becomes infeasible to match stellar spectra to model atmospheres because in later stages of evolution stars experience an unknown amount of mass-loss, sudden transitions in the nucleosynthesis occurring in the interior of the star, and convection that can redistribute fuel and bring metals to the surface.

To determine the integrated light of stars in a population up to the E-AGB, one can integrate over the IMF-weighted isochrone from the lower to upper mass limits of the model. This is known as 'isochrone synthesis' (Bruzual & Charlot 1993), and is the standard method for SPS models. However, a computational issue arises for post–main-sequence (PMS) stars because they will have very similar masses to the

[2]The evolution of massive stars requires special treatment because electron degeneracy cannot support the C-O core after the HB, and C burning occurs. I do not consider high mass stars in this thesis because they do not impact the results of my analysis.

main-sequence turnoff (MSTO), and there will be stars in different evolutionary phases with essential identical masses. Therefore, a very fine mass grid must be utilized for the integration to avoid systematic errors due to underestimating the contribution from certain PMS phases, indicating that mass is an unstable integration variable for PMS phases. This issue can be avoided by choosing to integrate instead over the available fuel for nucleosynthesis in each PMS star. This 'fuel consumption' method (Renzini & Buzzoni 1986; Buzzoni 1989; Maraston 1998) allows for a more stable treatment of PMS evolution, and is utilized in the Maraston (2005, hereafter M05) stellar population models, which I use extensively throughout this thesis. The fundamental statement of the fuel consumption theorem is that the integrated bolometric luminosity from the PMS can be calculated from the amount of fuel being burned in each evolutionary phase.

The evolutionary phase that is of most significance to this work is the thermally-pulsing asymptotic giant branch (TP-AGB), which has been notoriously difficult to include in SPS models. However, the TP-AGB can be a useful chronometer in the NIR because TP-AGB stars are very luminous, and have a strong age dependence. I will now turn to the details of the TP-AGB and their inclusion in SPS models.

1.2.1 TP-AGB stars

In the analysis presented in this thesis, the contribution from TP-AGB stars in young ($\lesssim$2 Gyr) populations plays an important role. While stars with masses $\sim 0.8 \lesssim M/M_{\odot} \lesssim 8$ will go through an AGB phase, we are concerned with intermediate mass stars, $\sim 2.5 \lesssim M/M_{\odot} \lesssim 8$ because this is the mass range in which TP-AGB stars can dominate a population's flux. The evolution of such stars after the hydrogen-burning main sequence is as follows. After core hydrogen exhaustion there are several distinct phases, each defined by activity in the core: contraction of the core on Kelvin-Helmholtz timescales ($\sim$1 Myr for a $6M_{\odot}$star) during which the core temperature increases under non-degenerate conditions; a much longer He-burning phase once the core temperature reaches $\sim 10^8$ K; and finally, when the core He is exhausted, a phase

during which He- and H-burning shells surround an inert, degenerate C-O core. As this last phase begins, the star is said to be on the E-AGB, and as the He shell moves outward towards the (inert) H shell it eventually becomes extinguished and contracts, and the H shell begins to burn efficiently through the CNO cycle. This leads to a pulsational process as the He ash from the H shell settles on the C-O core, and eventually becomes dense and hot enough to ignite in a runaway thermonuclear process that produces a large amount of energy (and hence luminosity at the stellar surface). The He-burning shell is then extinguished, and this "thermal pulse" is followed by a quiescent period (Habing & Olofsson 2003). Once this process has begun, the star is on the TP-AGB, and will undergo many pulsation cycles — resumption of H shell burning, He settling and buildup of He ash layer, He shell "flash" and extinguishing of H shell — over timescales of $\sim 10^4$ years until mass loss associated with the pulsations and/or the occurrence of a "superwind" blows off the outer envelope, leaving behind a C-O white dwarf (see, e.g., Iben & Renzini 1983; Salaris & Cassisi 2005).

This material carries with it the products of nucleosynthesis, and thus AGB stars play an important role in the chemical enrichment of the interstellar medium (e.g., Herwig 2005). The nuclear processes that take place in AGB stars consist of the CNO cycle; triple-α process; hot-bottom (or envelope) burning in which the convective envelope reaches down to the H-burning shell and alters the isotopic and elemental abundances of Ne to Si; and the synthesis of heavy elements, e.g., Sr, Y, and Zr, via the s process wherein neutron capture is slow compared to β-decay. The nuclear products of these processes can be brought to the stellar surface by the convection initiated by thermal pulsations, known as the "third dredge-up", and the surface abundances of, e.g., C and s process elements will increase over time. Each thermal pulse provides conditions for third dredge-up events, and the efficiency of this process is a subject of ongoing observational and theoretical investigations (e.g., Battinelli & Demers 2004).

Because TP-AGB stars are very cool ($T_{\rm eff} < 4000$ K) and extended, they have high NIR luminosities. They also display strong metal and molecular absorption features due to the products of nucleosynthesis, such as carbon, nitrogen, oxygen and s-process

elements, being dredged up from the interior via convection (Vassiliadis & Wood 1993). TP-AGB stars with strong TiO, VO, and H_2O features are classified as (oxygen-rich) M stars, while stars with strong CO, C_2, and CN features are (carbon-rich) C stars. A TP-AGB star becomes carbon-rich when enough carbon has been dredged up that the ratio of carbon to oxygen, C/O, is greater than one. When C/O<1, all of the carbon will be tied up in CO, and there will be no other molecular carbon features. This leads to the metallicity dependence of C-stars, namely, in TP-AGB stars with low-metallicity progenitors, there will be less oxygen, and thus fewer dredge-ups need to occur to achieve C/O>1, thus low metallicity populations will tend to have more C-stars. TP-AGB stars can also display variability on order of ∼100 days and, during the peak luminosity, can show hydrogen Brackett and Paschen emission (Lançon & Wood 2000).

These properties of TP-AGB stars have important implications for stellar populations, because the TP-AGB can dominate the NIR flux of a population at young–intermediate ages (∼100 Myr to 3 Gyr). This is due to the fact that in populations less than ∼100 Myr, evolved stars undergo core carbon burning under non-degenerate conditions and do not go through a bright AGB phase. However, after 100 Myr, stars are of low enough mass to be supported by degeneracy in the carbon core, which leads to He shell burning around the core and a bright TP-AGB phase. This sudden onset is known as the "AGB phase transition" (Renzini & Buzzoni 1986), and because of its strong age dependence, authors have realized its potential as a chronometer for stellar populations (e.g., Lançon et al. 1999). A similar phenomenon, the "RGB phase transition," occurs at ∼1 Gyr when evolved stars develop degenerate He cores and go through a bright RGB phase. At this point the RGB begins to dominate the NIR flux. These transitions indicate that the onset and duration of the influence of the TP-AGB is set by basic stellar astrophysics, and therefore SPS models have a solid foundation to build upon when including the TP-AGB.

However, the practice of including TP-AGB stars in SPS models is difficult because of large uncertainties in the exact dependence of observed properties on metallicity,

and the time spent in the pulsating phase (which directly affects the contribution from the TP-AGB as a function of population age). Much work has been done to include the TP-AGB in models, and there has been substantial recent progress (Renzini & Voli 1981; Persson et al. 1983; Frogel et al. 1990; Bressan et al. 1998; Maraston 1998; Lançon et al. 1999; Lançon & Mouhcine 2002; Maraston et al. 2001, 2006; Conroy et al. 2009). I will focus on the M05 models here, because they represent the most thorough treatment of the TP-AGB in SPS models to date, as they cover a large range in metallicity and provide low resolution spectra, which allows for the measurement of spectroscopic indices.

An issue that plagued early attempts at calculating TP-AGB evolution in populations was uncertainty in the efficiency of hydrogen burning at the bottom of the convective envelope, known as convective, or "hot bottom" burning, which can affect the amount of fuel consumed during the TP-AGB phase, and hence the lifetime. This effect causes a deviation from the standard model core mass–luminosity relation (Bloecker & Schoenberner 1991), and so requires an empirical calibration. Frogel et al. (1990) observe a sample of Magellanic Cloud (MC) clusters and, by combining clusters with similar ages to average out stochastic effects, measure the AGB contribution as a function of age and provide a benchmark for model comparison. When computing the fuel consumption in the TP-AGB phase, M05 then performs a semi-empirical calibration by adjusting the level of convective burning to match the observed TP-AGB contribution in the MC clusters. While this informs the behavior of the TP-AGB as a function of age, metallicity effects need to be accounted for. M05 notes that mass loss and total AGB fuel consumption do not vary strongly with Z, while the ratio of C to M stars is quite sensitive to Z. This is reflected in the model by the amount of fuel consumed in each type of star. The fuel consumption is then directly transformed into observables by consulting the averaged TP-AGB spectra of Lançon & Mouhcine (2002), which bin stellar spectra from the cool star library of Lançon & Wood (2000) by temperature and spectral type. The important implication of the M05 models for the study of galaxy evolution is that features due to TP-AGB stars will be prominent

in the integrated spectra of stellar population after the TP-AGB phase transition at ∼100 Myr and up to ∼3 Gyr. These features can then be used to define age-sensitive spectroscopic indices that will useful chronometers.

While the fuel consumption is calibrated with MC clusters, there is still much uncertainty in the actual spectral energy distributions, especially because the empirical spectra used to predict flux from AGB stars in models are from Galactic stars and therefore do not span a large range in Z (moreover, it is difficult to estimate the metallicity because of AGB stars' cool temperatures and preponderance of metal lines). Recent studies by Conroy et al. (2009, 2010) have attempted to place limits on the uncertainties inherent in the treatment of the TP-AGB, and determine errors in derived properties such as age and metallicity when comparing observed populations to models. It is clear that because of these uncertainties, methods for extracting SFHs from galaxies by comparing integrated NIR light to SPS models will require calibrations with objects whose properties are known a priori.

1.3 Implications for galaxy evolution

Having briefly described the present state of the TP-AGB in stellar population models, I now turn to the scientific motivation behind these efforts, and the implications for the study of galaxy evolution. There are two main motivations driving the analysis presented in this thesis: (1) a set of NIR spectroscopic indices that are sensitive to TP-AGB features would be useful for determining SFHs of galaxies, but would need to be tested against other established methods to constrain model uncertainties, and (2) accurate measurements of stellar mass from integrated light require that the contribution of the TP-AGB is correct because it can strongly affect M/L due to the high luminosities of TP-AGB stars. The importance of the latter is illustrated when considering very red galaxies observed in the early universe. The initial interpretation was that these galaxies are massive ellipticals with old stellar populations, which is inconsistent with the picture of hierarchical buildup of mass (Yan et al. 2004). However,

Tonini et al. (2010) show that the problem can be explained by mis-application of stellar population models, and that the red colors can be provided by a much less massive, younger population with appreciable TP-AGB flux. Therefore, accurate treatment of the TP-AGB is critical for interpreting galaxy light in the early universe, because the stellar populations will be young (and hence the NIR will be dominated by flux from the TP-AGB), and the inferred masses will depend strongly on the model M/L, which in turn depend on the TP-AGB contribution.

The most direct method for addressing both motivations would be to find a sample of populations with well-known SFHs and metallicities, obtain NIR spectroscopy, and use them as calibrating objects to test the reliability of SPS model predictions. Ideal objects for this would be clusters, because they can be considered SSPs, and as explained previously, there exist many MC clusters with AGB stars. However, observational obstacles prevent this line of attack. Namely, the MC clusters have surface brightnesses too low for high signal-to-noise integrated spectroscopy, and more importantly, stochastic effects within clusters would cause large variations in AGB contribution from cluster to cluster. The requirement of high surface brightness and large numbers of stars can be met by galaxy nuclei, especially those in a recent post-starburst state, which is the method I pursue here.

The organization of the thesis is as follows. In § 2, I will introduce preliminary work to develop a set of empirically-defined NIR indices that are prominent in the spectrum of NGC 5102, a blue S0 galaxy with a young nuclear post-starburst population, that can be used as chronometers. The NGC 5102 spectrum is contrasted with that of M32, which is an intermediate-age elliptical galaxy. The indices measure features due not only to TP-AGB stars, but also to hydrogen Paschen lines that originate in the atmospheres of hot stars. While there has been much discussion of using TP-AGB features as chronometers (e.g., Lançon et al. 1999), I have found no mention in the literature of utilizing the strong age dependence of Paschen lines to detect young ($\lesssim$100 Myr) populations. Because NGC 5102 is a bright, nearby galaxy it has been extensively studied in the optical, and has a well-established SFH, making it a useful

calibrating object. Applying the standard method for development of spectroscopic indices, I track the indices in SPS models as a function of age and metallicity and compare to the measured indices in the test object. In § 3, I describe the results of the calibration with NGC 5102 and attempt to place limits on the TP-AGB contribution in the M05 SPS models, finding that the models are accurate within the systematic uncertainties of the measured indices. Then, an analysis of M32 is detailed in § 4, and the SFH is found to be consistent with an SSP of $\sim$2.75 Gyr, but because the sensitivity of the TP-AGB features is declining at that age, more information cannot be extracted. In § 5, I discuss the implications of the results from the previous chapters, and in § 6, I describe possible future work.

Chapter 2

Preliminary results

Jesse Miner

Department of Physics and Astronomy, CB 3255, University of North Carolina, Chapel Hill, NC 27599

jminer@physics.unc.edu

James A. Rose

Department of Physics and Astronomy, CB 3255, University of North Carolina, Chapel Hill, NC 27599

jim@physics.unc.edu

Gerald Cecil

Department of Physics and Astronomy, CB 3255, University of North Carolina, Chapel Hill, NC 27599

cecil@physics.unc.edu

ABSTRACT

We present near infrared (NIR) IRTF/SpeX spectra of the intermediate-age galaxy M32 and the post-starburst galaxy NGC 5102. We show that features from thermally-pulsing asymptotic giant branch (TP-AGB) and main sequence turn-off (MSTO) stars yield similar ages to those derived from optical spectra. The TP-AGB can dominate the NIR flux of a coeval stellar population between ∼0.1 and ∼2 Gyr, and the strong features of (especially C-rich) TP-AGB stars are useful chronometers in integrated light studies. Likewise, the Paschen series in MSTO stars is stongly dependent on age and is an indicator of a young stellar component in integrated spectra. We define four NIR spectroscopic indices to measure the strength of absorption features from both C-rich TP-AGB stars and hydrogen features in main sequence stars, in a preliminary effort to construct a robust chronometer that probes the contributions from stars in different evolutionary phases. By comparing the values of the indices measured in M32 and NGC 5102 to those in the Maraston (2005) stellar population synthesis models for various ages and metallicities, we show that model predictions for the ages of the nuclei of M32 and NGC 5102 agree with previous results obtained from integrated optical spectroscopy and CMD analysis of the giant branches. The indices discriminate between an intermediate age population of ∼3–4 Gyr, a younger population of $\lesssim$1 Gyr, and can also detect the signatures of very young $\lesssim$100 Myr populations.

2.1 Introduction

Integrated spectroscopy of galaxies has been performed primarily in the optical because much of the (blue) optical light comes from the well-understood main sequence turnoff stars. As one pushes into the near infrared (NIR), the integrated light of a stellar population is dominated by very luminous stars in later stages of stellar evolution, such as thermally pulsing asymptotic giant branch (TP-AGB) stars. Beginning with Renzini & Voli (1981) and continuing with, e.g., Frogel et al. (1990), Bressan et al. (1998), Maraston (1998), Lançon et al. (1999), Lançon & Mouhcine (2002), it

has become clear that the unique features and high luminosity of TP-AGB stars profoundly affect the NIR integrated light of stellar populations. Specifically, for stellar populations with ages ∼100 Myr to ∼1 Gyr, the TP-AGB can contribute up to ∼60% of the K-band flux (depending on metallicity, see Maraston 2005). Strong molecular features, from CN, CO, C_2, and H_2O, in TP-AGB stellar atmospheres should appear in the integrated NIR spectrum of populations in this age range.

Unfortunately, relatively poorly understood processes such as mass loss, convective transport of heavy elements to the surface, and thermal pulsation influence the late stages of stellar evolution and thus predictions for the integrated spectrum. Furthermore, the ratio of C-rich to O-rich AGB stars in a population is known to depend strongly on metallicity, meaning that the contribution from TP-AGB stars can vary drastically not only with age but also composition (Mouhcine & Lançon 2003). However, observational work has constrained these effects on the integrated light of stellar populations with observations of Magellanic Cloud and Galactic clusters, and the predictive potential of NIR spectroscopic features has been demonstrated (e.g., Lançon et al. 1999; Mouhcine & Lançon 2002; Maraston 2005). In short, TP-AGB features should be traceable in galaxies whose NIR light is dominated by stars in the ∼100 Myr to ∼1 Gyr age range.

For example, Mouhcine et al. (2002) have detected the presence of TP-AGB stars in the NIR spectrum of a young star cluster in the galaxy NGC 7252, and have verified that the predicted features expected in a young population (∼300 Myr) are present in the NIR spectrum. This successful detection of TP-AGB features in NGC 7252 thus motivates additional NIR spectroscopy of bright, nearby galaxies with young populations to further test the use of NIR spectral indicators as chronometers. We also note that while light from the TP-AGB can dominate the NIR flux, the main sequence turn-off (MSTO) also contributes an appreciable amount to the integrated light, and hydrogen features (specifically the Paschen series) due to MSTO stars will be visible. To investigate the behavior of the TP-AGB and MSTO features as a function of both age and metallicity we consulted the Maraston (2005, hereafter M05)

stellar population synthesis models, which include a careful treatment of the TP-AGB. In this Letter we use NIR spectra of two galaxies with very different star formation histories to test if population synthesis models of TP-AGB and MSTO features can differentiate between young and intermediate-age populations.

Because its high nuclear surface brightness and proximity allow for both high SNR spectroscopy and resolved stellar photometry of the giant branch, the intermediate age compact elliptical galaxy M32 has been extensively studied. Recent work has included integrated optical spectroscopy of the nucleus and extranuclear region out to the half-light radius R_e (del Burgo et al. 2001; Worthey 2004; Rose et al. 2005; Coelho et al. 2009), and NIR imaging of the giant branches (Davidge & Jensen 2007). These studies find that the nuclear light is dominated by an approximately solar metallicity intermediate-age population ($\sim$3 – 4 Gyr). Because its stellar content has been constrained by several established age-dating techniques, M32 is ideal for testing other predictive techniques.

Likewise, the blue S0 galaxy NGC 5102 is close and bright enough for high SNR integrated spectroscopy plus resolved CMD analysis of its brightest stars. It is classified as a post-starburst (PSB) galaxy because its strong Balmer-line absorption and absence of emission indicates that star formation terminated recently. Studies by, e.g., Deharveng et al. (1997); Davidge (2008) have indicated that the nuclear region of NGC 5102 has undergone a termination of star formation within the past $\sim$10–100 Myr, after a several hundred Myr period of activity, guaranteeing that there is an appreciable young population with a mean age of a few 100 Myr. The intermediate age stars in M32 and the younger stars in NGC 5102 are a useful pairing because most of the NIR light emitted by these two galaxies comes from stars in different evolutionary stages: the younger population will be dominated by the TP-AGB and a blue MSTO, while in the intermediate age population most of the light comes from the red giant branch and an older MSTO (see Fig. 13 in M05).

In this Letter we define four age-sensitive NIR spectroscopic indices, two of which measure previously defined TP-AGB features, and two that measure Paschen series

absorption lines, and compare the observed values in M32 and NGC 5102 to predictions of the M05 stellar population models. We demonstrate that the derived ages from the NIR indices agree closely with previously published ages determined from optical spectroscopy, and thus provide evidence to support the reliability of NIR spectral signatures as a useful chronometer for galaxy evolution.

2.2 Observations and Stellar Population Models

On the nights of 12 and 13 May 2010, we observed NGC 5102 with the SpeX spectrograph on the NASA Infrared Telescope Facility (Rayner et al. 2003). The detector is a 1024×1024 Aladdin 3 InSb array. We used the short cross-dispersed (SXD) mode, with a $0\farcs8$ slit (spectral $R = 750$) aligned with the parallactic angle. We took two ABBA object/sky sequences for a total of eight on-object exposures of 120 s each. The SXD mode simultaneously covers $\lambda\lambda 0.81 - 2.4$ μm, so avoids issues such as order overlap and variable sky features that plague single-order infrared spectroscopy. Standard SpeX calibrations (arc lamps and flats) were performed after the exposures, and we observed a standard A0 V star at similar airmass to remove atmospheric absorption and calibrate fluxes. The nuclear region of M32 was observed on 10 June 2010 with the same instrumental setup, number of exposures and integration time.

Spectral extraction and atmospheric correction were performed using the Spextool package, version 3.4 (Cushing et al. 2004). See Vacca et al. (2003) for a detailed description of the telluric correction process. The final spectra of six separate orders were coadded and combined, and are displayed in Figure 2.1, along with optical spectra.

We define four spectroscopic indices (see Table 2.1): two are flux ratios of narrow bands bracketing absorption breaks (1.08μm CN, 1.77μm C_2), and two are equivalent widths of hydrogen Paschen lines (1.00μm Paδ, 1.28μm Paβ+), where the "+" reminds the reader that due to the low resolution of the models, other lines are present in the Paβ equivalent width feature. The absorption breaks arise from the cool, luminous stars on the TP-AGB, while the Paschen lines are contributed by hot main sequence

Table 2.1. Index Definitions and Values

Feature	Band 1 (μm)	Band 2 (μm)	Line (μm)	M32	NGC 5102
1.00μm Paδ	0.997–1.000	1.012–1.015	1.002–1.011	0.84 Å	2.63 Å
1.08μm CN	1.060–1.070	1.095–1.105	...	1.10	1.20
1.28μm Paβ+	1.258–1.265	1.297–1.305	1.275–1.289	1.75 Å	2.89 Å
1.77μm C_2	1.753–1.763	1.775–1.785	...	1.06	1.11

Note. — Bandpasses used to define spectral indices. The 1.00 and 1.28 μm Paschen features are equivalent widths, while the two other indices are flux ratios of narrow bands bracketing molecular absorption breaks due to TP-AGB stars. The index values for M32 and NGC 5102 are included.

turnoff stars in young populations, and thus this method probes two independent stellar phases with very different physical origins (the cool, extended atmospheres of TP-AGB stars vs. the hot atmospheres of MSTO stars). An enhanced view of the spectra of M32 and NGC 5102 in the regions of the four spectral indices is shown in Figure 2.2. To track the dependence of these four indices on age and metallicity we have measured them in the M05 simple stellar population (SSP) models, which cover a large range in both age and metal abundance, and provide an output integrated spectrum for each age and metallicity. In all cases we have used a Kroupa initial mass function and a red horizontal branch.

2.3 Results

As can be seen qualitatively in Figure 2.1, there are clear differences between both the optical and NIR spectra of the recent PSB galaxy NGC 5102 and the intermediate-age M32. In the optical the Balmer lines are much more prominent, and the Ca II K line weaker, in NGC 5102 than in M32. Likewise, the Paschen line series and the two break features due to the TP-AGB are significantly stronger in the NIR spectrum of NGC 5102 than M32. To provide a quantitative foundation to these differences

and to make a direct comparison with the predictions for spectral index behavior of the M05 models, in Figure 2.3 values for the four above-defined indices are plotted as a function of age for the M05 models, at four different metallicities, along with the observed values for NGC 5102 and M32. Due to the high SNR of the observed spectra, the formal (photon statistical) error bars for the NGC 5102 and M32 index values are actually smaller than the width of the plotted lines. Systematic errors due to, e.g., flat-fielding issues, subtraction of night sky emission lines, and removal of telluric features, clearly dominate the true uncertainties, and await a more detailed analysis.

It is readily seen that the two absorption break indices, as well as the Paβ+ index, first increase with increasing age as the TP-AGB becomes more prominent, and then decline at ages greater than $\sim$1 Gyr, as the RGB overtakes the TP-AGB as the dominant contributor in the NIR. The Paδ index behaves similarly, but with the index first rising and then falling more rapidly with age (at 100 Myr). The two galaxies are seen to have quite distinct SFHs; the large break indices and large Paschen index values in NGC 5102 argue for a young ($\lesssim$2 Gyr) population with appreciable flux from the TP-AGB, and from upper main sequence stars, while M32 shows little contribution from the TP-AGB or young stars.

Because both NGC 5102 and M32 must have had complicated SFHs and chemical enrichment histories, it is certainly an oversimplification to compare their integrated spectra to SSP model predictions. The derived ages are really an SSP-equivalent age (Serra & Trager 2007), in that the mean age derived from the indices is weighted by the contributions from the entire SFH of the galaxy, which tends to more heavily weight the younger, more luminous, populations. Nevertheless, we can demonstrate that inferences about the SFHs of these two galaxies from the NIR spectra concur with previous results obtained at optical wavelengths. In the case of M32, the low values of all four NIR indices consistently argue for an SSP-equivalent age $\gtrsim$3 Gyr, which is in accord with the ages of $\sim$4 Gyr obtained from optical spectra by Worthey (2004) and Rose et al. (2005) for the central region; Davidge & Jensen (2007) also find an

intermediate-age population in M32 based on resolved star photometry of the RGB. Coelho et al. (2009) find evidence for an old (>10 Gyr) population underlying the intermediate age population, each contributing roughly half of the optical light. The implication is that the SSP-equivalent age results from the combination of an old population, and one no older than ∼4 Gyr. In principle, for instance, the SSP-equivalent age of 4 Gyr could arise from the combination of a young, ∼1 Gyr, population superposed on the old population. However, in Rose (1994) it was found on the basis of spectral indices in the blue that any contribution from a 1 Gyr population must be very small. The NIR spectral indices for M32 plotted in Figure 2.3 certainly supports the conclusion from the optical indices that any contribution from a population as young as 1 Gyr must be small.

Turning now to NGC 5102, the most striking aspect of Figure 2.3 is the contrast between the consistently higher NIR indices in NGC 5102 and those in M32, implying that while the light of M32 is dominated by an intermediate-age population, that of NGC 5102 is dominated by a younger population in which both the TP-AGB and hot young main sequence stars make a strong contribution. The TP-AGB signature is evident in the high observed values of the 1.08μm and 1.77μm break features, while the young main sequence contribution is evident in the high value of the Paδ index at 1.00 μm and to a lesser extent the partially-contaminated Paβ+ index at 1.28 μm.

Two aspects of the behavior of the NIR indices with age and metallicity complicate their interpretation. First, as mentioned, the break indices initially rise with age at ∼100 Myr as the TP-AGB phase develops, then decline beyond ∼1 Gyr as the RGB develops. The Paschen indices behave similarly as the hydrogen lines in upper main sequence stars first strengthen and then weaken with the turnoff temperature. Thus two age solutions are possible for many index values. However, the Paδ index peaks at substantially younger ages than the other three indices, so can often lift the age degeneracy. Second, the timing and duration of the index peaks depend on metallicity. This is due in part to the strong metallicity dependence of the ratio of C-rich to O-rich AGB stars in a population: metal-poor populations will have a larger fraction

of C-rich giants than their metal-rich counterparts. For NGC 5102 we can assume approximately solar metallicity, because Davidge (2008) finds that the metallicity distribution function (MDF) of its disk RGB stars peaks at [Fe/H]$\sim$-0.1, whereas Beaulieu et al. (2010) report that the young nuclear population has [Fe/H]= 0.0. The solar metallicity models in Figure 2.3 show that each of the observed indices for NGC 5102 is consistent with an age of $\sim$300 Myr. The shape of the absorption breaks and the 1.28μm indices yield two possible ages from any measurement, but the 1.00μm Paδ feature is sufficiently distinct in age sensitivity to distinguish between a younger and more intermediate age population, and constrains the age to $\sim$300 Myr. As mentioned, recent studies of NGC 5102 report a period of star formation lasting several hundred Myr and ending within the past $\sim$100 Myr, showing that our index values are consistent with the results from established age-dating techniques.

Our measured NIR spectral indices in M32 and NGC 5102 reinforce the importance of TP-AGB constraints on galaxy ages obtained from NIR spectra, especially when combined with features that probe the MSTO. This technique is particularly useful for distinguishing intermediate age ($\sim$3-5 Gyr) galaxies from those dominated by a young ($\sim$1 Gyr) population. We can further discriminate for the presence of a very young ($\sim$100 Myr) population on the basis of the Paδ index. Hence our analysis demonstrates that NIR indices allow for a fairly complete description of age and metallicity for a range of stellar population ages that will become accessible with the large lookback times observable with the next generation IR space telescope, the *James Webb Space Telescope*. Specifically, this chronometer will aid in testing models of galaxy formation in the early universe: as a large number of high redshift galaxies are observed in the mid-IR, formation timescales can be constrained with the (restframe) NIR indices presented here. Because $z > 2$ galaxies are $\lesssim$2 Gyr old (assuming standard Λ-CDM cosmology), the TP-AGB and young main sequence turnoff will provide much of the integrated flux, and the time of their formation can be determined from the measured NIR indices.

2.4 Conclusion

We present an analysis of integrated NIR SpeX SXD spectra of the nuclear regions of M32 and NGC 5102, and show that mean ages determined from spectroscopic indices agree with previous studies, with the important result that this method can differentiate between young and intermediate-age populations. The indices probe contributions from two different stellar evolutionary phases, the TP-AGB and the MSTO, which effectively provides two independent chronometers. Galaxy ages are derived by comparing index values to those measured in M05 model SSPs, indicating an accurate treatment of the TP-AGB in the models. This method of defining NIR indices is the first step towards a robust NIR spectroscopic age-dating technique, which will be particularly useful when applied to high redshift spectroscopic surveys undertaken by the next generation of infrared observatories.

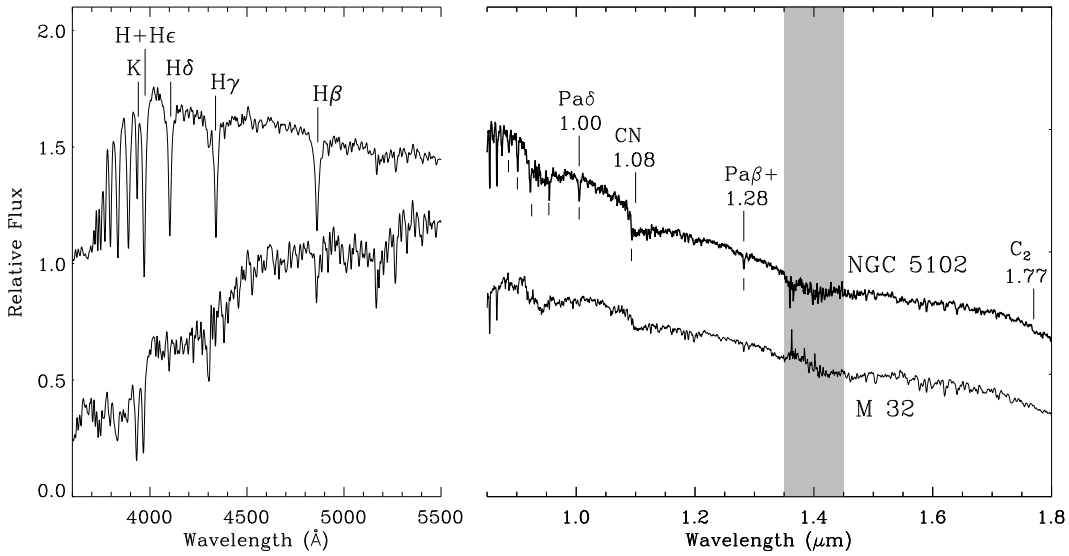

Figure 2.1 - Optical (for reference) and NIR spectra of NGC 5102 and M32 are plotted. The optical spectrum of NGC 5102 is from the Goodman High Throughput Spectrograph (Clemens et al. 2004) on the 4.1 m SOAR telescope at Cerro Pachon, Chile, while the optical spectrum of M32 was taken with the FOCAS spectrograph on the 8 m Subaru telescope at Mauna Kea, Hawaii (see Rose et al. 2005). The NIR spectra were taken with the SpeX spectrograph for this paper. The region of low atmospheric transparency is shaded. The J and H bands are shown, as we have defined no indices in the K band. The Paschen series is marked with the lower ticks to illustrate the differences between the spectra. Note the stronger Balmer lines in the optical spectrum of NGC 5102 than in M32, which is also reflected in the stronger Paschen series in the NIR spectrum of NGC 5102.

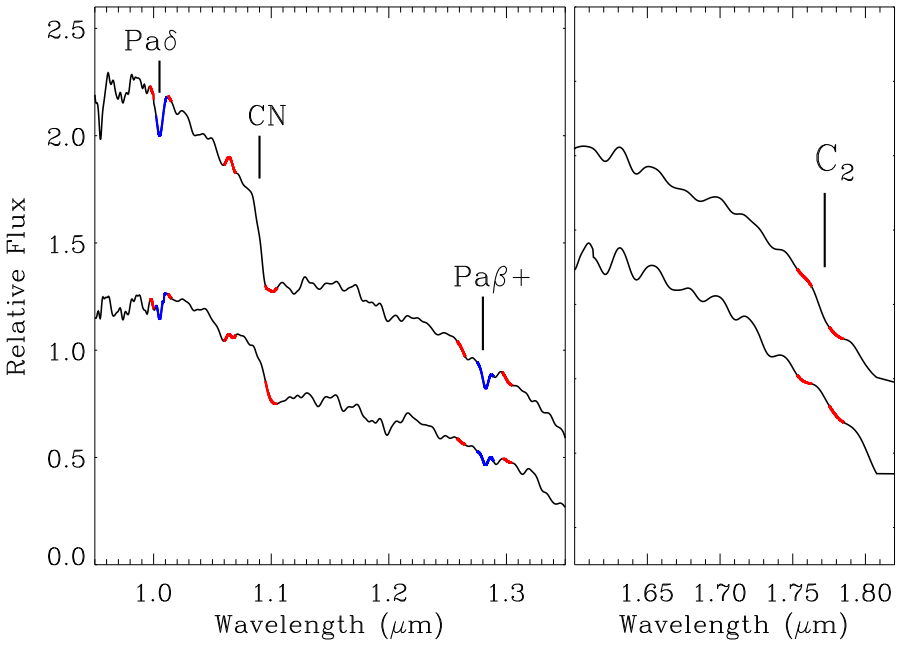

Figure 2.2 - Wavelength regions of spectral indices for NGC 5102 (top) and M32 (bottom) smoothed to the resolution of the M05 models, with flux bands shown in red, and line regions in blue.

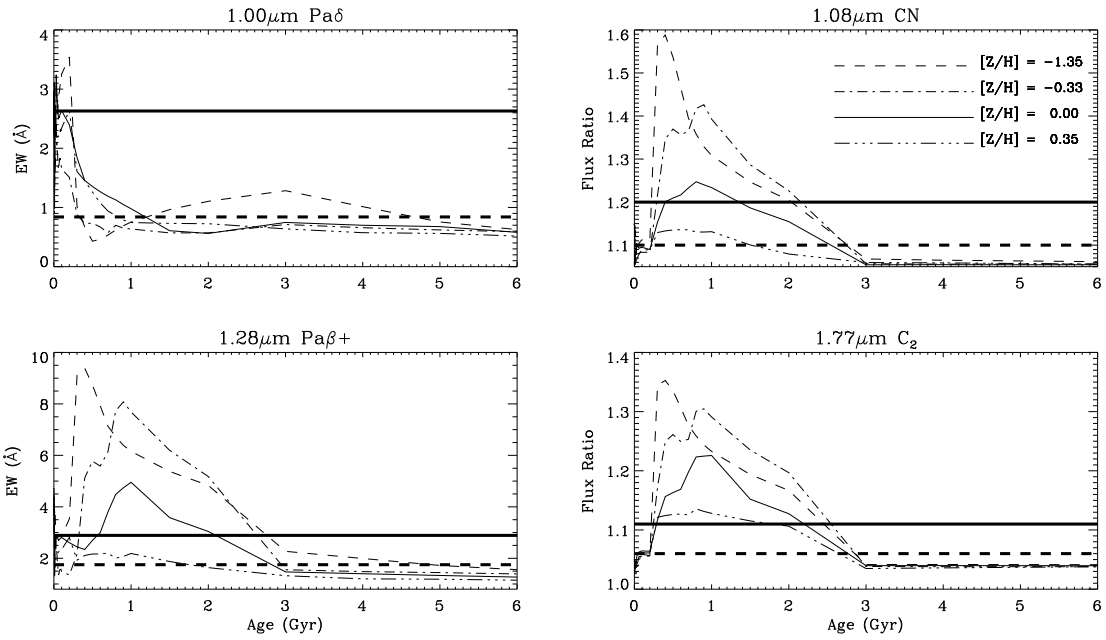

Figure 2.3 - NIR spectral indices derived from the M05 models are plotted as a function of age, for four metal abundances. Thick horizontal lines denote the observed values for NGC 5102 (solid line) and for M32 (dashed line), respectively. The formal (photon statistical) error bars in the NGC 5102 and M32 indices are smaller than the thickness of the plotted lines. We note that the Paβ+ index is contaminated with other features.

Chapter 3

NGC 5102

ABSTRACT

A near-infrared (NIR) spectroscopic study of the post-starburst galaxy NGC 5102 is used to define spectral indices that measure features due to main-sequence turnoff (MSTO) and thermally-pulsing asymptotic giant branch (TP-AGB) stars in integrated light. These indices are sensitive to populations with age $\lesssim$3 Gyr, providing chronometers that are particularly suited for measuring the stellar properties of galaxies in the early universe. Maraston (2005) stellar population models are used to track the indices as a function of population age, metallicity, and initial mass function. By comparing the observed NGC 5102 NIR indices to those measured in the Maraston (2005) models we extract NIR-derived age and metallicity estimates that are consistent with those previously established with optical studies. Specifically, we discover that the NGC 5102 indices cannot be fit well by a simple stellar population, and show that the best-fitting composite model consists of two populations with ages $\sim$20 Myr and $\sim$500 Myr. We also address the issue of total contribution by the TP-AGB in stellar population models, showing that our results for the age and metallicity of NGC 5102 are consistent with the large TP-AGB flux present in the Maraston (2005) models. The major implication of this work is that because the indices measure contributions from hot main sequence stars and cool, evolved stars, they probe timescales of populations whose light is dominated by young, massive stars up to several hundred Myr,

as well as intermediate-mass evolved stars up to ∼3 Gyr, an age regime that has been historically difficult to study with optical spectroscopy. Therefore, this technique provides a tool for studying the star formation histories of galaxies dominated by young populations, which includes local systems in post-starburst states, and galaxies in the early universe that will be accessible with the next generation of infrared observatories.

3.1 Introduction

Astronomy is now in the age of precision cosmology, in which the fundamental constants that describe the large scale expansion and evolution of the universe have been accurately determined. The study of galaxy evolution has particularly benefited from this development, because a galaxy's redshift now corresponds to a precise lookback time and distance, placing it at a well-defined time since the beginning of the universe, with an intrinsic physical size and luminosity derived from its apparent angular diameter and flux. This is in contrast to the historical dilemma of being unable to disentangle cosmological effects from galaxy evolution effects due to the uncertainty in the world model. Also, sophisticated hydrodynamical simulations can now follow the clumping of dark matter (DM) halos over cosmic time, and are able to reproduce observed large scale structure. However, due to the complexities of modeling the baryonic physics involved in galaxy evolution, there is less precision and more speculation about how and when the buildup of stellar mass in galaxies occurs. Because witnessing the formation of the first generation of stars in the early universe is implausible with current instrumentation, observational techniques that can probe the star formation history and stellar mass of more intermediate redshift galaxies are necessary. The challenge is to find observational signatures that depend strongly enough on star formation history (SFH) and metallicity (Z) to constrain the ages and masses of the stars within a galaxy. This requires the ability to follow stellar evolution over a large range of mass and Z, and to model the light output at every stage of stellar evolution in order to accurately predict the behavior of populations of stars in galaxies.

The application of stellar population models to the integrated light of galaxies has a long and fascinating history, but will not be chronicled here (see, e.g., Tinsley & Gunn 1976; Renzini & Buzzoni 1986; Worthey 1994; Fioc & Rocca-Volmerange 1997; Maraston 1998; Vazdekis 1999; Bruzual & Charlot 2003; Maraston 2005; Conroy et al. 2009). I will focus instead on the specific issue of developing stellar population diagnostics that are sensitive to the young populations found in galaxies in the early universe, to aid in the study of the stellar mass buildup of the universe. I present a near-infrared (NIR) spectroscopic technique that measures the strength of two stellar signatures found in populations younger than ∼3 Gyr: Paschen lines due to hot main-sequence turnoff (MSTO) stars, and strong molecular absorption features originating in the atmospheres of thermally pulsing asymptotic giant branch (TP-AGB) stars (see, e.g., Habing & Olofsson 2003, for a detailed description of the evolutionary characteristics of TP-AGB stars). While the use of Paschen features to detect the presence of a young population in galaxy spectra has not been addressed in the literature, the importance of the TP-AGB in interpreting galaxy light has been discussed extensively (Renzini & Voli 1981; Persson et al. 1983; Frogel et al. 1990; Bressan et al. 1998; Maraston 1998; Lançon et al. 1999; Lançon & Mouhcine 2002; Maraston et al. 2001; Maraston 2005; Maraston et al. 2006; Conroy et al. 2009). Briefly stated, in a coeval population at ∼100 Myr, stars evolving off the main sequence are of sufficiently low mass that they develop degenerate C-O cores after the He core-burning phase and go through a bright TP-AGB phase that produces enough flux to affect the integrated light of the population (e.g., Renzini & Buzzoni 1986). The large contribution continues until ∼2 Gyr, when the red giant branch (RGB) becomes the more luminous phase. Because TP-AGB stars have $T_{\rm eff} \approx 3000$ K and are extremely extended and luminous, they will emit the majority of their light in the NIR, and thus it is necessary to accurately constrain the contribution of the TP-AGB when studying the NIR properties of young populations (such as those found in early universe galaxies).

Of specific importance to galaxy evolution is the empirical characterization of stellar mass buildup over cosmic time, which depends critically on the assumed mass-to-

light ratio (M/L) of observed galaxies. In turn, the M/L depends on stellar content, because the light output per unit mass is a strong function of evolutionary phase. Therefore, the ability to measure stellar mass from integrated light, which is an essential element in describing galaxy evolution, requires accurate treatment of evolutionary phases that strongly affect the integrated M/L of a population (such as the TP-AGB and red supergiant branch). For example, Tonini et al. (2010) show that the treatment of the TP-AGB has a large impact on predictions of galaxy evolution models, and the NIR colors of observed high redshift galaxies are better fit with models containing the large TP-AGB contribution found in the Maraston (2005) models. With the TP-AGB missing, models can only approach the observed red NIR colors by incorporating an amount of old stellar mass that is unrealistic for objects in the early universe, and that directly conflicts with the picture of hierarchical mass buildup. Likewise, Maraston et al. (2006) demonstrate the strikingly different mass and age estimates of passively evolving, early-type galaxies at $z \sim 2$ when using models with and without a strong TP-AGB contribution, and show that the low M/L provided by the TP-AGB halves the required stellar mass compared to other models.

We attack this issue of measuring the properties of young populations differently and instead obtain high signal-to-noise (S/N) NIR spectroscopy of bright, nearby analogs of young galaxies in the early universe that have been well studied with established optical techniques. Here we will focus on NGC 5102, which we use to inform the development of NIR spectroscopic chronometers, and to test predictions of the TP-AGB contribution in stellar population models. NGC 5102 is a small blue galaxy in the Centaurus group at a distance of ∼3.4 Mpc (e.g., van den Bergh 1976; Pritchet 1979; Davidge 2008). It has a classical S0 morphology, but is peculiar in that it is bluer than a typical S0 and H I-rich ($M_{\rm HI} = 3 \times 10^8\ M_\odot$, van Woerden et al. 1993), suggesting that it is in a state of recent or ongoing star formation fueled by gas infall (McMillan et al. 1994). Its nuclear colors, $B-V = 0.2$ and $U-V = -0.1$, are consistent with a single burst of age of $\sim 10^8$ yr (Pritchet 1979). van Woerden et al. (1993) report weak Hα and [N II] and no NIR emission, while optical (Gallagher et al. 1975)

and ultraviolet (Rocca-Volmerange & Guiderdoni 1987) spectroscopy show a nuclear spectrum dominated by A and B stars, consistent with active star formation (SF) over the past several hundred Myr.

More recent work has involved photometry of resolved stars throughout the disk and multi-component fitting to the integrated optical spectrum. For example, Kraft et al. (2005) find that $\gtrsim$55% of stars in NGC 5102 must be younger than 3 Gyr and have $\sim Z_{\odot}$, and a 300 Myr, $0.2Z_{\odot}$secondary population is necessary to match the observed optical spectrum. A color-magnitude diagram (CMD) analysis of the nucleus by Beaulieu et al. (2010) with the *Hubble Space Telescope* Wide Field Planetary Camera 2 (WFPC2) shows extended SF over the past $\gtrsim$200 Myr and a burst at $\sim$20 Myr.

Because the SFH of NGC 5102 has been detailed, and it has been shown to contain an appreciable population of young stars in its nucleus, it can be utilized as a test object to confirm the accuracy of the chronometers detailed herein. In § 3.2 I present the NIR spectroscopy of NGC 5102 obtained with the OSIRIS and SpeX spectrographs. Definitions of the spectroscopic indices and their behavior with age and metallicity as predicted by stellar population models, are presented in § 3.3. Measured indices in NGC 5102 are compared to the corresponding model indices in § 3.4, along with an investigation into the TP-AGB contributions in the models. The implications for using these indices as chronometers, and their application to the study of galaxy evolution are discussed in § 3.5.

3.2 Spectroscopy and Data Analysis

3.2.1 OSIRIS

Preliminary observations of NGC 5102 were obtained with the Ohio State InfraRed Imager/Spectrometer (OSIRIS, Depoy et al. 1993), in cross-dispersed (XD) mode, which allows for simultaneous *JHK* coverage. OSIRIS utilizes a 256×256 HgCdTe array and covers 1-2.5 μm, although we have found that the usable wavelength range

in the cross-dispersed (XD) mode is ∼1.2–2.3 μm. Between 2008 July 17 and 2010 January 26, we had a total of nine nights during which we were able to observe NGC 5102. For each exposure on-object, a sky exposure of equal integration time was taken to subtract atmospheric OH emission lines, and subsequent to the object exposures, a telluric standard star was observed to correct for absorption due to Earth's atmosphere.

The spectral extraction was performed in the following manner. First, the spectrum was traced along the dispersion direction for each separate order and extracted using the *echelle* IRAF[3] package. The sky spectrum, using the same trace as the object frame, was then extracted. As described in Davies (2007), the sky emission levels were adjusted order-by-order to minimize residuals in the object − sky spectra. With the sky-subtracted spectra in hand, the next step is to remove the effects of telluric absorption. This can be done by observing a "telluric standard" close in time to the science object whose spectral shape is known a priori, and then, through division of the observed spectrum of the standard object by the true spectrum, obtaining the telluric absorption spectrum. In practice, this is impractical because there does not exist the large sample of NIR spectroscopic standard stars that would be necessary to guarantee that for every science target there would be a standard star within ∼0.1 airmasses (which is required due to the strong dependence of telluric absorption on airmass). However, as will be explained in detail in § 3.2.3, commonly used standard objects are A0V stars, because their relatively featureless spectrum (except for strong hydrogen absorption lines) can be considered equivalent to that of Vega, for which high-resolution synthetic model spectra exist [4] We perform the telluric corrections in this manner, using the *Xtellcor_general* routine in the Spextool IDL package (Cushing et al. 2004).

[3]IRAF is distributed by the National Optical Astronomy Observatories, which are operated by the Association of Universities for Research in Astronomy, Inc., under cooperative agreement with the National Science Foundation.

[4]Vacca et al. (2003) use a publicly-available spectrum from R. Kurkucz, http://kurucz.harvard.edu/stars.html.

Measurements of features in the spectra obtained with OSIRIS are plagued by large systematic uncertainties due to severe pixel-to-pixel variations in the detector that affect flatfielding, inconsistent telluric corrections, and inefficiencies in the re-acquisition of the target after nodding to the sky that cause several minute delays between exposures (telluric conditions vary on scales of several minutes). Severe variations in the features night to night rendered any measurements of spectral features effectively meaningless, as the systematic uncertainties were intractable. Also, the wavelength coverage of OSIRIS is quite limited, and four of the six spectroscopic features that we define in § 3.3.1 are not observable. However, the OSIRIS observations did afford an opportunity to detect the presence of (but not accurately measure) the Paβ feature at 1.28 μm as well as the C_2 feature from TP-AGB stars at 1.77 μm, and follow-up observations were conducted with the more sensitive SpeX spectrograph, as described next.

3.2.2 SpeX

NGC 5102 was observed 2010 May 12 and 13 in short cross-dispersed (SXD) mode with the NIR medium-resolution SpeX spectrograph (Rayner et al. 2003) on the NASA Infrared Telescope Facility atop Mauna Kea, HI. SpeX is equipped with a 1024×1024 Aladdin 3 InSb array. The SXD mode allows for simultaneous spectral coverage of $\lambda\lambda$0.82–2.5 μm, in six separate overlapping orders (except for a 0.06 μm gap at ∼1.8 μm). A $0\farcs8\times15''$ slit (corresponding to ∼25 pc) was placed on the nucleus at the parallactic angle, providing a spectral resolution of $R = 750$. The galaxy was at a mean airmass of ∼1.85. On 2010 May 12, two ABBA sequences of 120s exposures were taken, in which the A position is the galaxy nucleus, and the B position is sky $\sim10'$ away. The counts per pixel in the detector were well below the ∼5% nonlinearity level of ∼4000 (e.g. Rayner et al. 2004). On 2010 May 13, four ABBA sequences were obtained. On both nights, after the NGC 5102 exposures, the A0V star HD 122394, at an airmass less than 0.1 from NGC 5102, was observed in order to perform telluric corrections. Finally, the standard SpeX internal flats and arc lamp exposures were

taken for instrument calibrations. We also observed the elliptical galaxy M32 on 2010 Jun 09 and 10, using the same instrumental setup and integration times. A more detailed description can be found in § 4.

The extraction of spectra was performed with the Spextool IDL package, version 3.4 (Cushing et al. 2004), which automatically performs nonlinearity corrections (Vacca et al. 2003). Each of the six orders was extracted with a user-defined aperture after direct subtraction of a sky frame. The flatfielding and wavelength solution was performed automatically using the standard SpeX calibration frames. After each individual frame was extracted, all of the spectra were combined order-by-order. Because of variations in atmospheric throughput, the absolute flux levels can vary by several percent, and each spectrum was flux-normalized to a specific order to compensate (the order used for normalization is chosen interactively). Finally, the normalized spectra were co-added order-by-order. The resulting S/N per pixel in the co-added spectra was between ∼50 and ∼100.

I then extracted the telluric standard star spectrum in the same manner. With the combined object spectrum and the observed telluric star spectrum in hand, the next step is to remove the absorption due to Earth's atmosphere.

3.2.3 Telluric corrections

The standard technique for removing atmospheric effects in optical light involves observing spectrophotometric standards at several values of airmass once, or a few times, per night. This technique relies on the assumption that the telluric attenuation is a smooth function of both wavelength and airmass, and does not vary appreciably throughout the night. Once the atmospheric absorption has been removed, a separate solution for the instrumental response is obtained. In the NIR, however, this method is no longer applicable because the atmospheric transmission depends strongly on wavelength, and can vary over timescales of several minutes, requiring that telluric corrections be made with standard objects close to the science target both in the sky and in time. Also, telluric absorption and the instrumental response can no longer

be disentangled and must be simultaneously corrected for. As mentioned in § 3.2.1, the telluric absorption can be precisely defined by observing an object whose intrinsic spectrum is known a priori. However, a large catalog of NIR spectrophotometric standards does not exist, and astronomers have instead relied on the similarity between stars of the same spectral type. For example, Maiolino et al. (1996) developed a method of telluric correction utilizing G2V stars as standards, and a high-resolution solar spectrum as the reference spectrum. Assuming the G2V star's spectrum is identical to the Sun's, the division of the solar spectrum (after a shift to match the velocity of the telluric star) by the observed standard will provide a "correction" spectrum that can be applied to the science target. However, Vacca et al. (2003, hereafter VCR03) point out that this method has two major disadvantages: first, bright G2V stars are relatively rare, which makes it unlikely that there will be a telluric standard star close enough in airmass to the science object, and second, the many metal lines in G2 dwarfs vary enough from star to star that the resulting correction spectrum will suffer from artifacts in the line regions.

A more advantageous method of correcting for telluric absorption utilizes A0V stars, and suffers less from the aforementioned issues with G2 dwarfs. Because they are intrinsically brighter, there are more accessible A0V stars in the sky to be used as standards, and it is likely that an A0V star will be within $\sim$0.1 airmass of the science target. More importantly, because A0V stars have $T_{\rm eff} \approx 10^4$ K, their NIR spectra are effectively featureless except for strong Paschen (Pa) and Brackett (Br) hydrogen absorption lines, and if recessional velocity and line broadening due to rotation and/or surface gravity are accounted for, then a spectrum of the nearby, bright A0V star Vega can be used to represent the intrinsic spectrum.

Following VCR03, I will detail the steps necessary to perform such a correction using the A0V/Vega method. First, we begin by defining the observed spectrum of an object as the product of the intrinsic spectrum, the telluric transmission, and the instrumental throughput, all convolved with the instrumental profile (IP), which smooths the final spectrum to the instrumental resolution. This product can be

thought of as the intrinsic spectrum convolved with the IP, or in other words, a spectrum obtained with the instrument above the atmosphere, multiplied by the overall telluric and instrumental response function (i.e., the telluric absorption spectrum convolved with the IP, and multiplied by the throughput). on the ground. Therefore, if the telluric spectrum and instrumental throughput can be estimated, then the intrinsic object spectrum can be recovered through simple multiplication of the observed spectrum by the 'telluric correction' spectrum, defined by VCR03 to be the inverse of the telluric+instrument spectrum. Finding the telluric correction spectrum is not trivial without knowing the intrinsic object spectrum and the IP, but if we assume that telluric absorption is stable for small changes in airmass and over timescales less than several minutes, a separate reference star whose intrinsic spectrum *is* known (i.e., the A0V standard) can be observed to characterize the telluric absorption and instrumental response function.

For the A0V method, immediately preceding or following exposures on target, a telluric standard with similar airmass is observed. If the simplest assumption is made that the intrinsic A0V spectrum is identical to the Vega spectrum, then the telluric correction spectrum can be found directly. While this would be a reasonable assumption if the A0V spectrum consisted of only a featureless continuum unattenuated by dust, because there are strong hydrogen absorption features, any differences in the line profiles due to rotational broadening (A stars can have rotational velocities of $\sim$300 km/s, e.g., Abt & Morrell 1995) and surface gravity between the observed A0V star and Vega must be accounted for. In practice, we then consider the intrinsic A0V spectrum to be the Vega model spectrum convolved with a kernel that accounts for these line-broadening effects and the instrumental profile, and then recover the intrinsic spectrum of the target (convolved with the IP).

Considering that the only quantity not directly observed or known a priori is the convolution kernel, the observer must somehow estimate the amount of line broadening, and adjust for any line strength variations in the telluric standard star with respect to the synthetic Vega model spectrum. This can be accomplished by finding

an absorption line that is in a wavelength region where the telluric transmission varies slowly, and where the instrumental throughput is relatively constant. Fortunately for infrared spectroscopists the telluric extinction, A0V stellar atmospheres, and the SpeX instrument have all conspired to allow the region around the Paδ λ1.005μm line to fit these criteria. As seen in Figure 3.1, the atmospheric transmission around Paδ is $\sim$100%, and thus the line in the observed telluric standard should be pristine, assuming photometric conditions. *Xtellcor*, the telluric correction program in the Spextool package, allows the user to interactively select the Paδ line in the observed telluric standard in order to calculate the kernel to be applied to the Vega spectrum that best fits the recessional velocity and line profile of the A0V star (after reddening the model to match the colors).

The program then applies the kernel to the entire Vega spectrum. At this point, assuming that the convolved Vega spectrum perfectly matches the intrinsic spectrum, we could find the telluric correction spectrum. In practice, however, not every line will be well fit by the convolved model spectrum, and user adjustment of individual lines is necessary. As will be explained in detail later, this process of optimizing the fits interactively will have a critical impact on measurements of features in our galaxy spectra. Once the user is satisfied that the residuals from the line fitting process have been minimized, the multiplication of the observed science target by the telluric correction spectrum is performed. The separate orders are then merged, which is also done interactively with the Spextool package.

To summarize the A0V telluric correction method, a standard star is observed close in airmass and time to the science target, and a Vega model spectrum is convolved to match the telluric star. The ratio of convolved Vega spectrum (which represents the intrinsic A0V spectrum) to observed spectrum will then produce a telluric correction spectrum. The individual steps are preformed in Spextool as follows:

1. A0V spectrum normalized in the region of Paδ;
2. Shifting, scaling, and reddening of Vega model to match A0V star;
3. Convolution of Vega spectrum with kernel derived from normalized Paδ region;

4. Individual scaling of hydrogen lines in Vega model to match A0V lines.

Figure 3.2 shows an example of a telluric correction spectrum using an A0V star, and its application to an observed galaxy spectrum (6th order of SpeX SXD mode). The convolved Vega spectrum and observed A0V spectrum, and their ratio, are displayed in Figure 3.2(a), while the observed and corrected spectra of NGC 5102 are shown in Figure 3.2(b).

3.2.4 Optical spectroscopy

On the night of 2010 February 17, we observed NGC 5102 with the Goodman High Throughput Spectrograph (Clemens et al. 2004) on the 4.1 m SOAR telescope at Cerro Pachon, Chile. The Goodman Spectrograph is an all-refracting optics imaging spectrograph mounted at one of the Nasmyth foci, and utilizes a volume phase holographic (VPH) grating as the dispersing element. The spectra are imaged onto a 4k $\times$ 4k Fairchild 486 back-illuminated CCD. For our observations the spectra were binned by 2 pixels in the dispersion direction and by 4 pixels along the slit. We took three exposures of 180 s with a $1\farcs03$ slit, at a median airmass of 1.01. With the 600 lines/mm VPH grating the binned pixels sample the spectrum at 1.6Å/pix at a resolution of 4.5Å, and cover the spectral range $\lambda\lambda$3490–6160Å. Wavelength calibration was performed with a HgCuAr lamp. The flux-calibrated optical spectrum of NGC 5102 is shown in Figure 3.3.

3.3 Spectral indices and stellar population models

In order to develop a technique for measuring stellar population properties in galaxies, spectroscopic indices need to be defined whose dependence on population age and metallicity can be estimated. By examining the NIR spectrum of the young nucleus of NGC 5102, and comparing it to the spectrum of a galaxy with a more intermediate-age population, we will identify spectral features that are unique to the young population. Stellar population synthesis models will then be necessary to describe the behavior of

these features with population age and metallicity, and to determine their suitability for use as chronometers. We will also estimate the systematic uncertainty in the measured NGC 5102 indices due to the telluric correction process. Finally, an analysis of the SFH of NGC 5102 from optical spectroscopy is presented to establish a benchmark for comparison to our NIR results.

3.3.1 Definition of indices

The final telluric-corrected spectrum of NGC 5102 is shown in Figure 3.3 along with the spectrum of the intermediate-age compact elliptical galaxy M32 for comparison. Optical spectra are also included to illustrate the relative strengths of Balmer and metal lines. I have labeled features of interest that will be discussed in detail in the following sections, and that show the striking difference between the young, several hundred Myr population of NGC 5102 and M32, whose mean nuclear age is $\sim$3 Gyr. The tick marks show the Paschen series in NGC 5102, which, like the Balmer series, is more prominent than in M32. In fact, it is clear that all of the labeled features are more prominent in the NGC 5102 spectrum, indicating that they are sensitive to young stars (here defined to be $\lesssim$3 Gyr). Also notable is the lack of emission in both spectra, which suggests that neither galaxy is currently undergoing appreciable star formation, and both are thus in post-starburst (PSB) states: NGC 5102 is a recent PSB with star formation declining $\sim$20–100 Myr ago, while M32 has been quiescent for $\sim$3 Gyr (e.g. del Burgo et al. 2001; Worthey 2004; Rose et al. 2005; Coelho et al. 2009). It is clear that because these features can distinguish between young and intermediate-age populations, they will be useful diagnostics for stellar population analysis, but before they can be applied to the study of galaxy properties their dependence on properties such as SFH and metallicity must be understood.

We note that the features labeled in Figure 3.3 have quite different stellar origins: the two Paschen lines (Paϵ, Paδ) are due to hot main-sequence turnoff (MSTO) stars while the three molecular features (TiO, CN, and C_2) are absorption breaks arising from the cool, extended atmospheres of thermally-pulsing asymptotic giant branch

(TP-AGB) stars. The Paβ+ feature is a special case, because while it measures the strength of the Paβ line, when the spectrum is smoothed to the resolution of the models, other lines will be present in the index (which, as we will discuss in § 3.3.3, are likely due to TP-AGB stars). To quantify these features, I have defined spectroscopic indices that measure their strengths. Equivalent widths (EW) measure the Paschen line indices, using the standard definition:

$$EW = \frac{\int_{\lambda_1}^{\lambda_2}(C_\lambda - F_\lambda)d\lambda}{\int_{\lambda_1}^{\lambda_2} C_\lambda d\lambda} \tag{3.1}$$

where F_λ is the line flux and C_λ is the continuum level. However, it should be noted that the regions around the Paschen lines in integrated NIR galaxy spectra will be contaminated by absorption from evolved stars, so a true continuum is not available. Instead, a pseudo-continuum is defined by interpolating over narrow bands just beyond the line wings. The TP-AGB features are absorption breaks and therefore can be described by flux ratios of narrow bands bracketing the breaks. Table 3.1 lists the bandpasses that define each index.

3.3.2 Index uncertainty estimates

The NIR spectra of NGC 5102 obtained with SpeX have high S/N, and therefore the uncertainty associated with the index measurements is dominated by systematics, not photon statistics. While this would be the case in general for high S/N data, ground-based NIR spectroscopy produces especially troublesome systematic errors due to the telluric correction process. Specifically, the A0V/Vega method described in § 3.2.3 can lead to the following errors in the extracted spectrum. First, any changes in telluric conditions between the object exposures and the telluric star exposures will result in an imperfect correction. Second, the convolution kernel that smooths the synthetic Vega spectrum to match the line profiles of the observed A0V star will never produce a perfect fit[5], and thus user adjustment of line strengths is required. How-

[5]However, VCR03 note that the most severe discrepancies are in the higher-order Paschen and Brackett series lines, which do not affect our analysis here.

Table 3.1. Index Definitions

Feature	Band 1 (μm)	Band 2 (μm)	Line (μm)
0.92μm TiO	0.8900–0.8970	0.9270–0.9340	...
0.95μm Paϵ	0.9510–0.9525	0.9575–0.9585	0.9530–0.9570
1.00μm Paδ	0.9970–1.0000	1.0120–1.0150	1.0020–1.0110
1.08μm CN	1.0600–1.0700	1.0950–1.1050	...
1.28μm Paβ+	1.2580–1.2650	1.2965–1.3050	1.2750–1.2890
1.77μm C_2	1.7530–1.7630	1.7750–1.7850	...

Note. — Bandpasses used to define spectral indices. The Paschen indices are equivalent widths, where Bands 1 and 2 are used to define the pseudo-continuum around the absorption line, while the TP-AGB indices are flux ratios of narrow bands bracketing molecular absorption breaks.

ever, this interactive and necessarily subjective adjustment can introduce systematic uncertainty into the corrected spectrum around the line regions if the lines are over- or under-compensated. In *Xtellcor*, the user is able to see the final telluric correction spectrum and therefore can detect any obviously discrepant fits, but there may still be variations in the line profiles in multiple extractions of the same observed spectrum. In the specific case of the indices we have defined here, because NGC 5102 has a recessional velocity of only $\sim$450 km/s, its Paschen line features sit atop the Paschen lines in the A0V telluric star (albeit slightly shifted), requiring special care to minimize the effects of inaccurate line fitting.

Figure 3.4 illustrates the impact that a poor fit to the A0V telluric star can have on the corrected spectrum of the science object. The top plot shows a normal fit to

the Paδ line, wherein the Vega spectrum was accurately convolved to match the line profile. Note the smooth appearance of the telluric correction spectrum in the line region, contrasted by the telluric spectra of the bottom two plots, which suffer from under- and over-compensation, respectively. The under- and over-compensation of the line is greatly exaggerated to illustrate its effect on the line strength in the science target. If the line is under-compensated in the convolved Vega spectrum, then the telluric correction spectrum (which is the ratio of model to observed) will have an artificial emission feature, and because of the slight velocity offset between NGC 5102 and the standard star, the corrected spectrum can display a P-Cygni-type profile (see Figure 3.5). Likewise, over-compensation will artificially deepen the observed line in the object spectrum.

While these extreme examples show that poor fits can be detected in the telluric correction spectrum, even small variations in the convolution kernel applied to the synthetic Vega spectrum will introduce artifacts into the corrected object spectrum. To quantify this effect, we have performed multiple telluric corrections on the sky-subtracted and co-added NGC 5102 spectra. By making small, but not visibly erroneous, adjustments to the line strengths during the telluric correction process, we can estimate the amount of scatter expected in the resulting index measurements in the galaxy spectrum[6]. It is clear that the systematic uncertainties in the Paschen indices will be substantially larger than those in the TP-AGB features, since the TP-AGB features do not coincide with A0V hydrogen lines, with one exception. Paγ sits at the base of the break in the 1.08μm CN feature; the blueward passband avoids the line itself, while the redward passband sits on the wing of Paγ. Because of the slight redshift of NGC 5102, the actual passband is pushed off of the line wing, and thus the index measurement will not be particularly affected by poor fits to the A0V Paγ line.

After each iteration of the telluric correction process is performed, the resulting

[6]It can be assumed that each telluric correction was performed with equal care, and the difference in the interactive adjustments to individual line strengths between corrections were unbiased. The reader is again directed to VCR03 for a detailed description of the *Xtellcor* user interface.

Table 3.2. Index Values for NGC 5102

Index	Value	σ
0.92μm TiO	1.136	0.005
0.95μm Paϵ	1.8 Å	0.4 Å
1.00μm Paδ	2.8 Å	0.3 Å
1.08μm CN	1.210	0.013
1.28μm Paβ+	4.0 Å	0.4 Å
1.77μm C_2	1.114	0.005

Note. — Index values and corresponding best estimate of uncertainty for NGC 5102.

telluric-corrected spectrum is then resampled to the sampling of the M05 models to allow for direct comparison between galaxy and model indices. Because the sampling of the models is much coarser than the SpeX spectra, the resampling effectively smooths the galaxy spectra to the low resolution of the models. The resampling is particularly important at wavelengths greater than 1.00μm, where the model sampling is 50Å per resolution element, which limits the number of model data points in the Paδ and Paβ line region to 3. Table 3.2 lists the measured values for each index in NGC 5102, and the associated uncertainty estimates, which are defined to be the standard deviation in the measured indices for several iterations of the telluric correction procedure. It is clear that the Paschen indices suffer much more from systematic uncertainty, which is to be expected due to the large systematic errors introduced during the A0V line-fitting process. As will be described in § 3.3.3, comparisons with indices from stellar population models must account for the disparity in uncertainties.

3.3.3 Predictions from stellar population models

Now that six indices have been determined from inspection of the NIR spectra of NGC 5102, we turn to stellar population synthesis (SPS) models to characterize the dependence of the indices on properties such as age, metallicity and initial mass function (IMF). Because NGC 5102 has been studied extensively using established optical techniques and its SFH and metallicity are known, we can test the predictions of the SPS models against these established results from previous work.

In general, determining the stellar content of galaxies is difficult due to the non-linear nature of the masses, luminosities, and timescales of evolutionary phases of stars, as they range over many orders of magnitude. However, at any given epoch in a coeval population, stars in certain evolutionary phases will tend to dominate the light output and provide age-sensitive signatures that can be detected in integrated light. For example, the blue light of young populations is dominated by bright MSTO stars, which has allowed for the development of accurate optical spectroscopic techniques because we understand MS stellar atmospheres and evolution well. This picture changes, however, in the NIR where evolved stars are the predominant light source. Specifically, TP-AGB stars can dominate the flux in populations with age $\sim$0.1–3 Gyr (Maraston 1998), whereas the RGB becomes the dominant source at $>$3 Gyr. For modeling, this is problematic because the advanced stages of stellar evolution are plagued by uncertainties due to mass loss, partial mixing, and abrupt changes in nucleosynthesis. Whereas the transformation from intrinsic stellar parameters to observed spectra is straightforward for main sequence and RGB stars, phases later than the RGB require individual prescriptions based on observational calibrations. This is significant because models of the light output of stellar populations must simultaneously account for stars in all phases of evolution, as well as the associated uncertainties (which can be large, especially in the treatment of evolved stars).

The process by which SPS models provide an integrated spectral energy distribution (SED) for a population given its IMF, metallicity (Z), and SFH is as follows. First, theoretical stellar evolution models describe the temperatures and surface grav-

ities as a function of stellar mass for a coeval population at a given age and metallicity. The result is an 'isochrone', a snapshot of the distribution of model stars in the Hertzsprung-Russell (L–$T_{\rm eff}$) diagram. These theoretical stellar properties are then converted into observable spectra, through either empirical or theoretical stellar libraries. Empirical libraries can provide high resolution spectra, but for the early-type main sequence stars needed to model young populations, are necessarily based on local $\sim Z_{\odot}$ stars. Synthetic model spectra tend to be lower resolution, but cover a large range in Z for all spectral types.

This theoretical treatment of stellar evolution, known as 'isochrone synthesis' (e.g., Bruzual & Charlot 1993, 2003), is only possible for stages through the early AGB (Maraston 2005), because the complex physical processes occurring in more evolved stars are difficult to model and tie to observed spectra. Therefore, the isochrone synthesis method requires individual prescriptions for including later stages of stellar evolution. For the Maraston (2005, hereafter M05) SPS models, which we use for our analysis here, the method by which the contributions from post main-sequence (PMS) stars are included in a population's integrated spectrum is known as the 'fuel consumption' method (Renzini & Buzzoni 1986; Buzzoni 1989; Maraston 1998), where the 'fuel' is the amount of H and He available to produce energy in PMS stars. In effect, the fuel consumption method integrates over the fuel available to PMS stars instead of attempting to add up contributions from mass bins along an isochrone. Because the PMS stars in a population will be within a few percent of the turnoff mass, integrating over mass bins requires tiny mass intervals, and would introduce systematic uncertainties into the integrated light. The fuel therefore is a more stable variable of integration, because it varies smoothly throughout PMS evolution.

In this work, we examine NIR spectroscopic features sensitive to young populations, and are therefore concerned with the details by which the fuel consumption method includes the contribution of TP-AGB stars, because the TP-AGB can dominate the NIR flux of a population between ∼100 Myr to ∼3 Gyr (Renzini & Voli 1981; Bressan et al. 1998; Maraston 1998; Lançon et al. 1999; Lançon & Mouhcine 2002). Most

importantly, the metallicity of a population will affect the ratio of C-rich to O-rich TP-AGB stars (classified as C stars and M stars, respectively) because increasing metallicity causes a decrease in the ratio of C to M stars. This is due to the convective "dredge-up" of material to the surface in TP-AGB stars: in metal-poor stars oxygen is less abundant and therefore a smaller amount of carbon must be dredged up to achieve C/O>1, whereupon all of the oxygen will be bound to carbon in CO and the residual carbon will combine with other elements to form, e.g., CH, CN, or C_2.

Therefore, the amount of fuel consumed by C and M stars will vary with metallicity. The M05 prescription, using the scaling of Renzini & Voli (1981) calibrated on Magellanic Cloud (MC) globular clusters (GCs), is shown in Figure 3.6, where it is assumed that luminosity corresponds directly to fuel consumed. Two trends are evident: as expected, with increasing metallicity the fraction of fuel consumed in C stars decreases, and at a given Z the fraction increases as the population evolves and carbon is dredged up from the interior. It should be noted that the total amount of TP-AGB fuel consumption does not depend strongly on Z (Maraston et al. 2001).

Following the consumption of fuel is only the first step towards characterizing the flux from PMS stars; the light output must be tied to a spectroscopic library of evolved star spectra. To include spectra of TP-AGB stars, M05 uses the empirical library of Lançon & Mouhcine (2002), where individual stellar spectra of C- and O-rich stars in the Milky Way and MCs from Lançon & Wood (2000) are combined and binned according to spectral classification (i.e., C-rich, O-rich, or intermediate) and $T_{\rm eff}$. As the TP-AGB evolves, the fuel consumed by each spectral type (C and M) is converted into an emitted flux, and the appropriate spectrum from Lançon & Mouhcine (2002) is included in the model SED.

Figure 3.7 shows NIR SEDs from the M05 models with $Z_\odot$ and Kroupa (2001) IMF (power law IMF with exponent 1.3 for $0.1 \leq M/M_\odot \leq 0.5$, and 2.3 for $M/M_\odot \geq 0.5$, which gives a higher fraction of massive stars compared to a Saltpeter power law of 2.3). The time evolution of the spectroscopic features identified in § 3.3.1 is striking. For example, the 100 Myr population displays a strong Paschen series and Ca II triplet

at 0.85μm, while these features fade by 300 Myr and are very weak after 1 Gyr. The strong absorption breaks due to TP-AGB stars are prominent only from 300 Myr until 2 Gyr. Figure 3.7(a) shows the relative fluxes, while Figure 3.7(b) shows K-normalized spectra, to reproduce actual observed spectroscopic comparisons similar to Figure 3.3, and it is clear that there is an age-index degeneracy in that the $\sim$300 Myr model is almost identical to the $\sim$2 Gyr model. In § 3.4, I will describe a method to break this degeneracy with the Paschen indices, but it is worth noting that the TP-AGB features will be prominent in populations up to $\sim$3 Gyr, except for the very youngest ages ($\lesssim$ 100 Myr).

Having defined indices using the NGC 5102 spectrum, we can now investigate how these indices are predicted to behave with age and Z. Figure 3.8 shows each index as a function of age for four different metallicities (the four metallicities for which full models are available). As expected, the TP-AGB indices increase rapidly at $\sim$100 Myr, and decline beyond 2-3 Gyr. The metallicity dependence is seen in both the strength of the indices and the age at which they peak: the lower metallicity models have larger index values and peak earlier, which can be explained by the larger fraction of C stars. The Paϵ and Paδ indices also behave as expected, because hot MSTO stars will dominate a very young (<100 Myr) population's flux, and will decline rapidly as the MSTO cools and contributes less NIR light. The Paβ+ index tracks the TP-AGB features, suggesting that the unknown features within the index are originating in TP-AGB stars.

By comparing the measured index values in NGC 5102 to M05 model spectra, we can test whether the inferred star formation history of NGC 5102 from fitting the NIR indices is consistent with results obtained with optical imaging and spectroscopy. In the next section, I detail the fitting process, and discuss the effects of systematic uncertainty on the final results.

3.3.4 Optically-derived star formation history

We recall that recent optical studies have indicated the SFH of NGC 5102 consists of relatively constant SF over the past several hundred Myr with a recent ∼20 Myr burst, as evidenced by Figure 3.12, from the analysis by Beaulieu et al. (2010). Figure 3.12(a) shows a Digital Sky Survey (DSS) R-band image of NGC 5102 with overlaid fields observed by Beaulieu et al. (2010), while Figure 3.12(b) shows the CMD-derived star formation rate (SFR) of the nuclear region (labeled F1 in Figure 3.12(a)). This agrees well with optical spectroscopic studies of NGC 5102, which show that SSPs provide poor fits to optical features, and that composite populations are necessary to match the integrated spectrum (see § 3.1).

To perform an independent estimate of the SFH of NGC 5102, we use the optical spectrum obtained with the Goodman Spectrograph to measure two spectral indices defined in Rose (1985, 1994), Ca II and Hδ/Fe I λ4045. In Figure 3.9, the two indices are plotted against each other for SSP models with varying metallicities (see Leonardi & Rose 2003), along with the indices measured in NGC 5102. Before interpreting the location of NGC 5102 on the diagram, we will discuss the behavior of the indices with population age. The Ca II index is defined to be the ratio of the residual intensities in the Ca II H + Hϵ and Ca II K lines. It is relatively constant in cool stars because Hϵ is very weak and the ratio of Ca II H to K will not vary appreciably. The index decreases, however, as temperatures approach those of F and A stars and the Balmer lines become stronger. Hϵ begins to dominate the Ca II H line and therefore the residual intensity declines. As temperatures become even hotter towards O stars, the Balmer lines fade as hydrogen becomes ionized, and the index again increases. The Hδ/Fe I λ4045 index is also defined as the ratio of line intensities, and is sensitive to spectral type. Its behavior with population age is similar to the Ca II index because it depends on Balmer line strength, and so decreases from late- to early-type stars, and increases again for very early type stars as Hδ recedes.

Both indices depend on metallicity as well, illustrated in Figure 3.9. For example, if we follow the solar metallicity model from 1 Gyr to younger ages, we find that both

indices are decreasing until reaching a minimum at just under 400 Myr. The track then returns towards higher index values at younger ages, but offset from the descending track. The behavior of the indices can be explained by the fact that in an SSP, the MSTO is dominating the blue optical light, and because the indices are sensitive to spectral type, they are effectively measuring the spectral type of the MSTO. The morphology of the sub-solar metallicity model tracks is similar, but the gap between the descending and ascending lines is narrowing with decreasing metallicity, causing a degeneracy between SSP models with MSTO spectral types earlier or later than ∼A. The open circle shows the value for NGC 5102, and it is evident that it is not consistent with any of the SSP model tracks plotted in the diagram. However, it could be consistent with a track at a metallicity intermediate to the [Fe/H] = −0.4 and [Fe/H] = −1.7 models that would intersect NGC 5102 at ∼800 Myr, but such a low metallicity would be inconsistent with prior constraints placed on the nuclear composition of NGC 5102 by, e.g., Beaulieu et al. (2010). If we rule out a very metal-poor SSP model, then we see that a composite stellar population is necessary to reproduce the NGC 5102 indices. For example, a combination of ∼40 Myr and ∼800 Myr [Fe/H]= −0.4 populations would provide a reasonable fit. Of course, we cannot uniquely determine the SFH of NGC 5102 with this analysis because many model combinations can be constructed to provide a reasonable fit to NGC 5102, but the result indicates that the two-index diagram is consistent with previous studies showing that star formation has occurred in two distinct regimes: a young population with an age of several hundreds of Myr, and a recent burst.

With these results from established optical techniques providing a consistent model for the SFH of NGC 5102, we now turn to the an analysis of the NIR spectroscopic indices, and investigate the accuracy of predictions based solely on comparisons with stellar population models in the NIR.

3.4 Results of Population Analysis

It is evident from a visual inspection of Figure 3.3 that the optical and NIR spectrum of NGC 5102, whose nucleus is dominated by a young population, is strikingly different from that of the intermediate-age elliptical galaxy M32, and in § 3.3.1 we have quantified these differences by defining six spectroscopic indices that are prominent in the NIR spectrum of NGC 5102. We now turn to a quantitative analysis of the SFH of NGC 5102 by comparing its NIR indices to those measured in the M05 SPS models. In general, deriving a SFH from integrated spectra is difficult due to the many degeneracies in the indices with age, metallicity, and IMF, it is common practice, as a simplified approach, to derive an SSP-equivalent age and metallicity that approximately (but not exactly) represents a light-weighted mean age and metallicity for the galaxy (Serra & Trager 2007). Hence, we begin our analysis by finding the SSP model that best fits the NGC 5102 indices, and comparing the derived SSP-equivalent age and metallicity to results from previous optical analyses. Once that comparison is made, we next assess whether a more complete SFH can be derived from the NIR spectrum of NGC 5102. Such a case is made if a more complex stellar population model than a single SSP results in a significantly better fit to the observed spectral indices. We adopt the simplest prescription for an extended SFH, namely, a two-SSP composite model. We again compare the best-fitting solution from the NIR spectroscopy to that derived from optical data. In short, we use the high S/N NIR spectrum of NGC 5102 as a test case for extracting a reliable SFH from NIR spectroscopy. Finally, we examine the extent to which our NIR data for NGC 5102 can be used to constrain the contribution of the TP-AGB to the integrated NIR light, which is still a controversial issue in stellar population modeling due to the substantial uncertainties surrounding the lifetimes and metallicity dependence of TP-AGB stars. This question has important implications for the study of galaxy evolution because the TP-AGB contribution has a large effect on the assumed M/L ratio, and thus galaxy masses derived from NIR luminosities will depend critically on the accuracy of the

TP-AGB contribution in stellar population models.

3.4.1 Single population fit

Figure 3.10 shows the model indices as a function of age, with the measured index values for NGC 5102 (and M32 for comparison to a galaxy with an older PSB age) shown with horizontal lines. Estimates of the $\pm 1\sigma$ systematic uncertainties on the index values are shown as thin lines bracketing the measured value. Because every index value is larger in NGC 5102 than M32, it is clear that the indices are sensitive to young populations, as expected. Moreover, the Paϵ and Paδ indices are elevated, which breaks the degeneracy inherent in the TP-AGB features. Namely, because of the "bell-curve" shape of the TP-AGB indices with age, a single value can correspond to two significantly different ages (as can be verified in Figure 3.7(b) by noting the similarity of features in the 300 Myr and 2 Gyr models), but the presence of the Paschen lines indicates the younger age.

While we see that the NIR indices measured in NGC 5102 are qualitatively consistent with young model SSPs, we must define a quantitative diagnostic for goodness of fit between model and galaxy indices. The systematic uncertainties present in the measured indices must be accounted for, and therefore the statistic we use to measure goodness of fit will weight the similarity between each model and galaxy index by the uncertainty in the galaxy index measurement. We define the fitting statistic as

$$\sigma^2_{\rm fit} = \frac{1}{N-1}\sum_{i=1}^{6}\frac{(I_{{\rm mod},i} - I_{{\rm gal},i})^2}{\sigma^2_{{\rm gal},i}}, \tag{3.2}$$

where $I_{{\rm mod},i}$ and $I_{{\rm gal},i}$ are the i^{th} index value for the model and galaxy, respectively, $\sigma_{{\rm gal},i}$ is the estimated uncertainty of the galaxy index, and N is the number of indices in the fit. Each term in the sum is the square of the deviation from a perfect fit in units of the uncertainty on the galaxy index. This ensures that the larger systematic uncertainties in the Paschen indices are appropriately accounted for in the fitting process.

The fits are performed by finding the models whose index values minimized $\sigma^2_{\rm fit}$; the parameters allowed to vary are age and metallicity, while the IMFs are considered separately. Figure 3.11 shows the results of the single population fits, with the deviation of each model index from the NGC 5102 value plotted in units of the index uncertainty. We have shown the five best fits to illustrate the variation of ages that have similar goodness-of-fit measurements. Both the Kroupa and Salpeter IMF fits have ages ranging from 0.3–2 Gyr, all with similar values of $\sigma^2_{\rm fit}$ and identical metallicities ($Z_\odot$). It is clear that a single population cannot consistently produce index values comparable to those measured in NGC 5102, as evidenced by the large variations in the best-fitting parameters. Considering our prior knowledge of the SFH of NGC 5102, this result is not surprising because the light from NGC 5102 is coming from a recent burst and an underlying population with more extended SF. In the NIR, this leads to strong Pa features (from the burst) and strong TP-AGB features (from the young stars in the underlying population). A single SSP will not be able to simultaneously provide such features because the timescales are quite different: the Pa features are strong for ages $\lesssim$100 Myr, while the TP-AGB features are prominent for older SSP ages. Therefore the next step will be to investigate whether a composite population can significantly improve the $\sigma^2_{\rm fit}$ statistic in the fits by representing the burst and the underlying young population with separate SSPs.

3.4.2 Composite population fits

Guided by the results presented in § 3.3.4, and the poor fitting achieved with the SSP fits, we will instead compare the measured indices to a composite population consisting of two SSPs: one that characterizes the recent burst, and another that characterizes the extended SF over the past several hundred Myr. The adjustable model parameters in the fit for both populations are age, metallicity, IMF, and fraction of total mass. The "burst" population's age can range from 0.01 Gyr to 0.07 Gyr, whereas the underlying young population is allowed to vary between 0.075 Gyr and 1 Gyr, although the exact age limits have no effect on the resulting best-fitting models.

In both models, metallicity is allowed to range over $-1.35 < [Z/Z_{\odot}] < 0.00$, and the IMF either Kroupa or Salpeter. The results of this fit can be seen in Figure 3.13. Note the improvement in $\sigma^2_{\rm fit}$ compared to the SSP model fit.

The first three best fits shown in Figure 3.13 are similar in that each consists of 20 Myr and ∼300–400 Myr populations, with minor variations in metallicity, IMF, and fraction. I have also included Figures 3.14(a) and (b), which reproduce the composite population fitting with a fixed IMF, to isolate its effect on the resulting best-fitting model parameters. It can be seen that both IMF fits return the same best-fitting composite model, while the other fits differ only slightly in age and mass fraction. There are two striking results that deserve discussion. First, the metallicity of the older population is $[Z/H] = -1.35$ for all of the fits, which is puzzling because such an extremely metal-poor population is likely unphysical, given our prior knowledge from studies of NGC 5102. Second, the mass fraction of the burst ranges from 70–80%, which also disagrees with previous results that place the fraction closer to 40–50% (Beaulieu et al. 2010). With this in mind, I repeat the composite population fits restricting the metallicity to $[Z/H] \geq -0.33$. The results are shown in Figure 3.15, and while $\sigma^2_{\rm fit}$ increases slightly from ∼3.3 to ∼4.0, the resulting SFHs are more realistic. Namely, both IMF fits return mass fractions ∼50% with metallicities of the burst population solar (Kroupa) and sub-solar (Salpeter), and a consistently sub-solar young population. These metallicities agree well with Davidge (2008), who finds that the stellar metallicity distribution function in the central regions of NGC 5102 peaks at [Fe/H]∼-0.5. Also, Beaulieu et al. (2010) note that the most recently formed stars will have metallicities similar to the interstellar medium, which is approximately solar (e.g., Chandar et al. 2004; Tremonti et al. 2004).

In general, these results are consistent with the estimates of SFH from previous studies, and indicate that the NIR indices I have defined can accurately measure contributions from both recent bursts ($\lesssim$100 Myr) and young ($\gtrsim$100 Myr) populations. However, there are several details of the model fitting results that warrant further discussion. First, all of the composite fits display the same pattern of scatter in the

indices. Namely, the strengths of Paδ and CN indices are systematically smaller than the NGC 5102 value, while the C_2 feature is consistently elevated. The source of these discrepancies will not be easily pinpointed because several sources of uncertainty, none of which are easily constrained, affect the model fitting. We will, however, attempt to estimate the source of uncertainty most likely to dominate.

First, the complicated SFH of NGC 5102 cannot be perfectly described by a two-SSP model, and even under the assumption of perfect models there will be errors in the model fits. We have addressed this issue by performing SSP and composite fits with $Z_\odot$ M05 models that allow for exponentially-declining SFRs ($\Psi(t) \propto e^{-t/\tau}$) by adjusting the allowing the e-folding time, τ. Thus, the SFH would be represented by a burst population with small τ, and a population with a large τ to represent constant, extended SF. These fits returned similar best-fitting models to the composite SSP models, in that they consisted of a $\sim$20 Myr burst with several hundred Myr population and returned similar values of $\sigma^2_{\rm fit}$, indicating that failure to match the precise SFH is likely not the dominant source of discrepancy.

Second, the systematic uncertainties due to inaccurate fits to the A0V telluric standard may have been underestimated, leading to unrealistic index values in NGC 5102. This would be surprising, particularly because the Paδ line is in a wavelength region unaffected by telluric absorption (as detailed in § 3.3.2), and therefore should be fit accurately. Likewise, the CN index passbands avoid the majority of the Paγ line, and poor fitting will not affect the measured index value. However, we can't rule out the possibility that minor systematic errors introduced in the spectral extraction and telluric processes have affected the index measurements.

Another possible source of uncertainty in the fitting is of course the models themselves, and as discussed in § 3.3.3, one important ingredient in creating model SEDS is the stellar library used to construct the final spectrum. The M05 models use a model atmosphere spectroscopic library for stellar spectra up to the early AGB, and while there are issues with matching observed spectra in the metal lines of cool stars, the hydrogen series lines should be unaffected by this issue (or by non-solar abundance

ratios). Therefore, the source of the mismatch in the Paδ line is particularly difficult to determine.

The discrepancy in the model predictions of CN is less surprising, because the contribution of TP-AGB stars and their exact spectroscopic features is still quite uncertain due to weak constraints on the age and metallicity dependence (see, e.g., Conroy et al. 2009). And while the presence of TP-AGB stars in young populations has been confirmed through NIR photometry, a careful study of the individual spectroscopic features in galaxy spectra has not been undertaken[7]. Therefore, it is impossible to pinpoint the exact source of error, but it is likely that uncertainties in modeling the complex nature of the TP-AGB dominate. Because the CN index is consistently the most difficult to fit, I perform the composite model fits excluding the CN index, shown in Figure 3.16, to estimate the extent to which the CN index is driving the fitting results. The exclusion of CN has little effect on the best fits, though there is a difference between the two IMFs, with the Kroupa model returning a young population of 800 My and the Salpeter fit 500 Myr. This suggests that the extreme deviation of the CN index in the fits is not having a strong and systematic effect on the inferred SFH of NGC 5102.

3.4.3 TP-AGB contribution in NGC 5102

Because of the complexities involved in constraining the contributions of TP-AGB stars to the integrated light of stellar populations, there has been much discussion in the literature about the relative merits of different SPS models and their treatment of the lifetimes and luminosities of TP-AGB stars. Of particular interest are the results of Kriek et al. (2010) that suggest the large TP-AGB contribution in the M05 models prevents simultaneous fitting of the optical and NIR SED of a composite PSB galaxy, concluding that the M05 models provide too much TP-AGB flux, and that a smaller

[7]However, Lançon et al. (1999) define spectroscopic indices in model spectra, while Mouhcine & Lançon (2002) find spectroscopic evidence of TP-AGB stars in an NGC 7252 cluster.

TP-AGB contribution is necessary for a statistically robust SED fit. Interestingly, we find that in the case of NGC 5102 the TP-AGB features in the M05 models provide estimates of age and metallicity that agree with previous studies. If the TP-AGB contributions were indeed exaggerated, we would expect the results of our model fitting to result in inaccurate predictions. Because the conclusions of Kriek et al. (2010) and this work seem to be at odds, we will investigate the role that TP-AGB stars play in deriving best-fit models for NGC 5102. Specifically, by adjusting the TP-AGB contribution in the model SEDs and repeating the fits to NGC 5102 indices, we can quantify the effect the TP-AGB has on our conclusions.

Figure 3.17 plots the index vs. age for $Z_{\odot}$, Kroupa IMF M05 models as the bolometric contribution to the integrated light from TP-AGB stars is varied (Maraston, private communication). As expected, decreasing the contribution causes the TP-AGB indices to decrease, as the breaks weaken in integrated light due to the fractional increase in light from other phases. Likewise, the Paδ and Paϵ indices show the reverse behavior, due to the fractional MSTO light increasing as the TP-AGB decreases, while the Paβ+ behavior is more complex. Recalling that the Paβ+ index is blended with other features, we note that at ages less than a few hundred Myr the Paβ line itself dominates the Paβ+ index and the index displays a similar trend to the other Pa lines, while at more intermediate ages it is evident that the strength of the index is reflecting TP-AGB contribution. It can be seen then that the magnitude and behavior with age of all of the indices is affected by the total TP-AGB contribution, which will be reflected in derived SFHs.

To quantify the effect of varying the TP-AGB contribution, I have repeated the analysis from § 3.4.2 in which a two-SSP composite model was used to estimate the SFH of NGC 5102, but using the reduced TP-AGB models. The analysis is limited in that I only have access to the individual SEDs of the TP-AGB for the solar metallicity model, but the conclusions can still provide important constraints. Figure 3.18 shows the results of the two-model fits for models with TP-AGB contribution at 100%, 67%, 50%, and 33% of the normal M05 level. The model of the burst was kept at metallicity

$[Z/Z_{\odot}] = -0.33$ but allowed to vary in age (the TP-AGB makes no contribution to the model SED at $\sim$20 Myr). This is to ensure that the effects of varying the TP-AGB will only affect the young population, and thus will be responsible for any systematic deviations in the best-fitting parameters from the normal models.

Decreasing the TP-AGB contribution causes several changes in the fits, the most significant of which is the increase in the goodness-of-fit statistic $\sigma^2_{\rm fit}$. As the TP-AGB flux declines, it becomes more difficult to find a combination of models that match the measured NGC 5102 indices, and the best-fitting parameters deviate from the original fit. In fact, the parameters illustrate an important degeneracy in the NIR indices: for populations $\lesssim$1 Gyr the strength of TP-AGB features can be enhanced both by increasing the age or increasing the total TP-AGB contribution, while the reverse is true for $\gtrsim$1 Gyr due to the "bell-curve" shape of the index vs. age plots. For example, as seen in Figure 3.18, the best-fitting models consist of a larger fraction of light coming from the underlying young population, and the ages are slightly closer to 1 Gyr, which partially makes up for the decreased TP-AGB flux. This reinforces the importance of using well-studied galaxies as test objects, because model degeneracies can only be constrained with independent measurements, and will otherwise remain an obstacle for applications to distant galaxies. It must also be noted that a fundamental bias has been introduced in that I am performing this analysis with $Z_{\odot}$ models, while previous studies, as well as our initial results herein, indicate that the young population has a sub-solar metallicity. The sub-solar models have much stronger TP-AGB features, and so $Z_{\odot}$ models will already require older and/or more massive populations to achieve the same index values. Thus, we can conclude that the TP-AGB contribution does significantly affect the fit, and it is unlikely that their contribution in the M05 models is over-represented by a factor of two or three. However, with the evidence provided by the $Z_{\odot}$ models, we cannot conclusively reject the possibility that the TP-AGB is enhanced by a modest amount in the M05 models. To test the TP-AGB contribution in a rigorous and statistically significant way requires a sample of galaxies that span the $\sim$100 Myr to 3 Gyr age range, which will allow for the disentangling of age and

metallicity effects.

3.4.4 Stochasticity

Because TP-AGB stars are short-lived and luminous, comparisons of a population's flux to that of a model with a continuous mass distribution becomes susceptible to stochastic effects at low population masses (Santos & Frogel 1997). Lançon & Mouhcine (2000) find that at 2.2μm, the minimum population mass to keep stochastic luminosity fluctuations to $\leq$10% to be 6×10^5 $M_\odot$at 1 Gyr, while at 0.55μm the minimum mass is 6×10^3. At 200 Myr, the 2.2μm minimum mass is 1×10^6, and the 0.55μm mass is 1×10^4. Therefore, because stochastic effects worsen with increasing wavelength, the minimum mass in the J-band, where the majority of our indices reside, will be $\sim10^5$ $M_\odot$in this intermediate-age range. To quantify the possible effect that stochasticity can have on our results, we have estimated the amount of mass observed in our galaxy spectra. A J-band image of NGC 5102 from the 2MASS Large Galaxy Atlas (Jarrett et al. 2003) was obtained via the NASA/IPAC Infrared Science Archive[8]. As described in § 3.2.2, we used a $0\farcs8\times15''$slit centered on the galaxy nucleus, and by integrating the flux in the J-band image within the slit we can estimate the stellar mass as follows.

First, we transformed the counts within a slit centered on the galaxy centroid to a physical flux using the provided zero-point magnitude and the flux calibration of Cohen et al. (2003). From the estimated distance to NGC 5102 of 3.37 pc provided by the NASA/IPAC Extragalactic Database (NED[9]), we then calculated an emitted power. Next, we consulted the best-fitting M05 SED found for NGC 5102 in § 3.4.2, which is normalized to 1 $M_\odot$. The J-band luminosity of the model SED is determined by multiplying the SED by the 2MASS J filter transmission function, and the mass in the slit is found by dividing the calculated NGC 5102 J-band luminosity by the

[8]http://irsa.ipac.caltech.edu/applications/2MASS/LGA/

[9]http://ned.ipac.caltech.edu/

normalized model luminosity. Performing these calculations returns an estimated stellar mass of $\sim 3 \times 10^5$ $M_\odot$.

This suggests that stochasticity may affect the estimated TP-AGB contribution, and hence the predictions from model fits, on the $\sim$10% level. However, discrepancies of $\sim$10% in the TP-AGB will not appreciably alter the results presented here. For observations of non-local galaxies, this effect will be negligible, as similar slit widths will sample a larger total stellar mass.

3.5 Discussion

The nearby, blue S0 galaxy NGC 5102 is used here to test the accuracy of chronometers that measure the strength of NIR features due to MSTO and TP-AGB stars. Because its nucleus contains both a recent burst and an underlying young (<1 Gyr) population, NGC 5102 is a useful test galaxy, as these chronometers are particularly sensitive to young populations. By finding the composite M05 stellar population models that best fit the NGC 5102 indices, we see that the model-derived ages and metallicities agree with estimates from previous optical studies. However, a full characterization of the associated uncertainties is still needed because the results depend critically on NIR spectroscopic measurements and models of TP-AGB evolution, both of which suffer from systematic uncertainties that are difficult to constrain.

We note that there have been few detailed studies of NIR spectroscopic diagnostics for the study of stellar populations (see, e.g., Silva et al. 2008; Lyubenova et al. 2010; Riffel et al. 2011), mostly due to the lack of spectroscopic stellar libraries, and the large uncertainties associated with the duration, spectroscopic output, and metallicity dependence of later stages of stellar evolution. Calibrations on nearby galaxies are then vital for testing any NIR spectroscopic age-dating techniques, and as we have detailed above, can provide important constraints on the contributions from evolved stars to integrated population light.

We find that the NIR indices we have defined can probe two interesting timescales:

recent bursts ($\lesssim$100 Myr) are traced with the Paschen lines, while young populations up to $\sim$2–3 Gyr will display strong TP-AGB features. This is an important distinction from optical spectroscopic techniques, which struggle to determine whether the SFHs of galaxies with intermediate SSP-equivalent ages ($\sim$3 Gyr) are due to an intermediate post-burst population, or a composite population consisting of both young and old stars whose integrated spectra blend to appear intermediate-age (Maraston & Thomas 2000; De Propris 2000; Rose et al. 2005). The NIR indices, being sensitive to only young stars, can place limits on the contribution from a young population[10]. The fits to NGC 5102 indices also indicate that the model predictions are consistent with independent optical techniques, implying that the TP-AGB contributions in the M05 models are accurate within the associated systematic uncertainties, and therefore models missing an appreciable TP-AGB flux will be unable to reproduce the large index values observed in young populations. Derived SFHs will then have critical systematic errors that will lead to incorrect stellar mass estimates, as M/L depends strongly on SFH.

This is particularly significant because the ability to constrain SFH of young populations is vital to our understanding of galaxies at $z \gtrsim 2$ whose light will be dominated by young stars. The age of the universe in this redshift regime is at most a few Gyr, and the cosmic star formation rate density is peaking before the decline to present-day values (see, e.g Lilly et al. 1996; Madau et al. 1996; Steidel et al. 1999). Measurements of stellar mass in this epoch are critical to providing empirical constraints on the integrated star formation rate of the early universe because the specific processes that initiate and regulate star formation are not well understood and must be empirically calibrated (see Baugh 2006, for a review of galaxy evolution models). An issue for which the TP-AGB contribution is particularly relevant is the presence of luminous, red galaxies observed in the early universe (e.g., Yan et al. 2004; Conselice et al. 2007; Messias et al. 2010) that are not reproduced in models of hierarchical struc-

[10]In § 4, we apply this method to the intermediate-age compact elliptical galaxy M32, and show that there is little contribution from a young population.

ture formation. However, as Tonini et al. (2010) point out, rather than interpreting K-bright high-redshift galaxies as massive 'red and dead' analogs to local ellipticals, the IR colors can be reproduced with models of young, less massive populations with appreciable TP-AGB flux, which is consistent with the hierarchical buildup of stellar mass. Hence, the calibration of the TP-AGB contribution has direct implications for empirical estimates of the stellar mass buildup over cosmic time.

Having discussed the observational constraints that can be placed on TP-AGB emission in the M05 SPS models with the NGC 5102 indices, we now turn to the spectroscopic indices themselves, and their potential use as a galaxy chronometer. As seen in Figure 3.13, there are systematic trends in the model fits, with indices either consistently over- or under-represented, indicating uncertainties due to telluric corrections and/or model spectra inaccuracies. However, it is impossible to estimate the dominant source of uncertainty in the index fits with the NGC 5102 data alone, and further work will be necessary to place limits on each error source. A spectroscopic sample of galaxies with PSB ages up to several Gyr will be necessary to populate the NIR index vs. age plots and provide a statistically meaningful calibration on the model predictions. Optical spectroscopic diagnostics could then be used to calibrate the NIR indices in a model-independent manner. Such a sample will permit the disentanglement of observational and model uncertainties. Specifically, the errors introduced by telluric correction would be reduced substantially by observing galaxies with recessional velocities $\gtrsim$1000 km/s, where the galaxy's Paschen lines are pushed beyond those in the telluric standard to avoid the systematic uncertainties due to Paschen line overlap described in § 3.3.2. It is also essential that galaxies with $\sim$1 Gyr populations are studied, because this is where the expected peak in TP-AGB contribution occurs, and will allow for a meaningful test of treatment of the TP-AGB in the M05 models.

3.6 Conclusion

We investigate the use of NIR indices as chronometers sensitive to young stellar populations, and test M05 model predictions with the PSB galaxy NGC 5102. We show that TP-AGB contribution in the models is consistent with the strength of TP-AGB features in NGC 5102 within uncertainty limits. Our indices have the potential to be powerful chronometers that can be applied to high-redshift galaxies to empirically constrain the integrated stellar mass buildup in the early universe, as well as local galaxies dominated by young populations. Further observations will necessary to place limits on the contributions from systematic uncertainties due to both observational and model sources.

This research has made use of the NASA/ IPAC Infrared Science Archive, which is operated by the Jet Propulsion Laboratory, California Institute of Technology, under contract with the National Aeronautics and Space Administration.

This publication makes use of data products from the Two Micron All Sky Survey, which is a joint project of the University of Massachusetts and the Infrared Processing and Analysis Center/California Institute of Technology, funded by the National Aeronautics and Space Administration and the National Science Foundation.

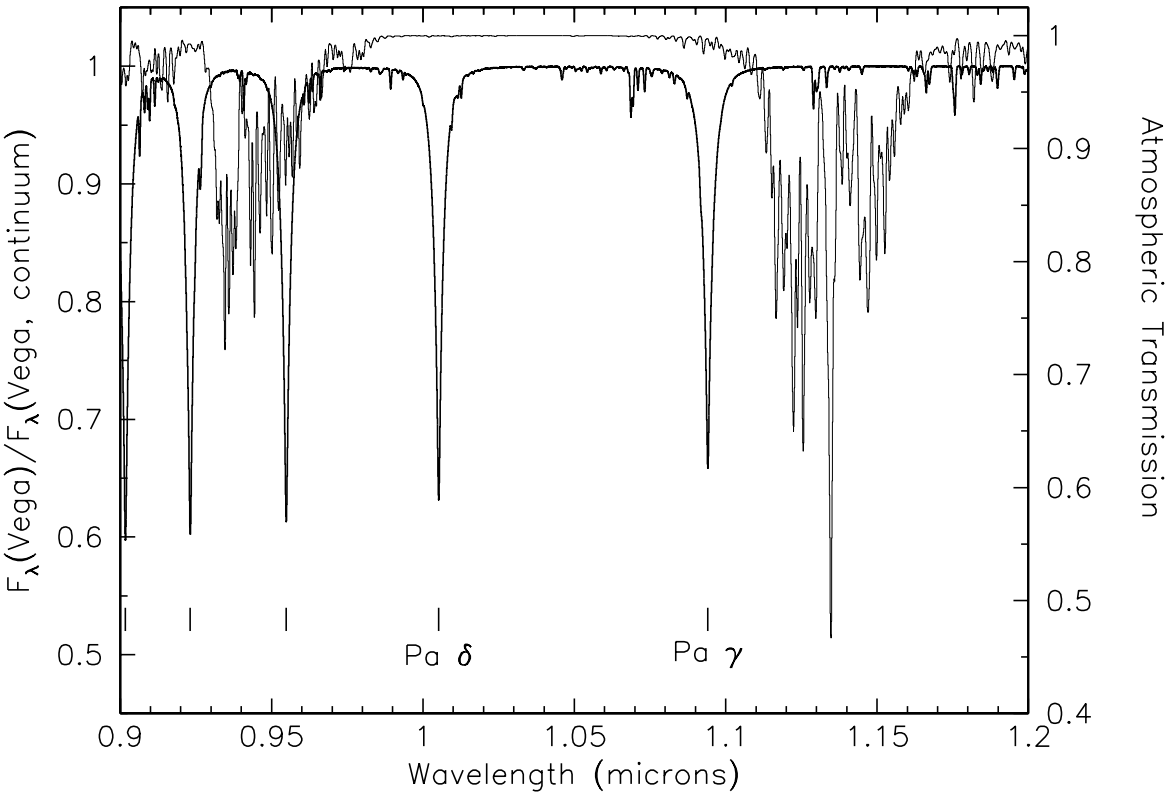

Figure 3.1 - Typical Mauna Kea atmospheric transmission at an airmass of ∼1.2 (upper line, right axis) in a region around the Paδ line in an A0V spectrum (lower line, left axis). Because the transmission is smooth around the line (and the instrument profile is relatively constant as well, although not pictured here), the Paδ line can initialize the convolution kernel that smooths the Vega model spectrum to match the observed telluric standard. (Figure 1 in Vacca et al. 2003, reproduced with permission).

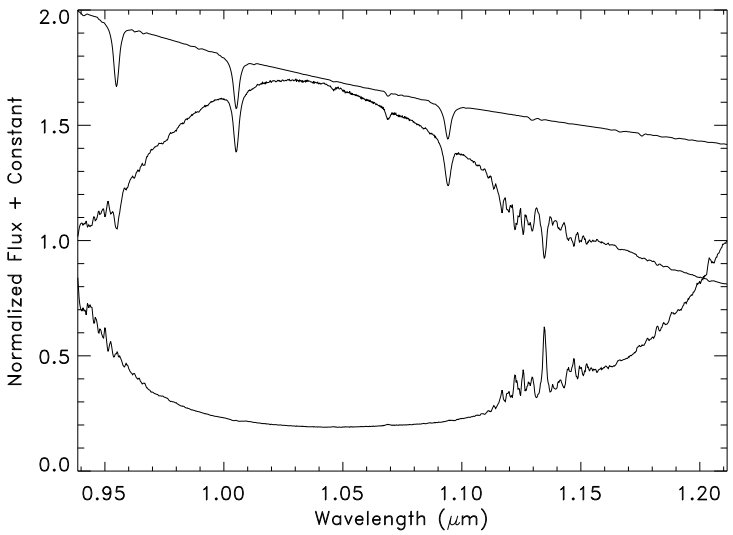

(a) From top to bottom: Convolved Vega model, observed A0V star, telluric correction spectrum (ratio of model and observed).

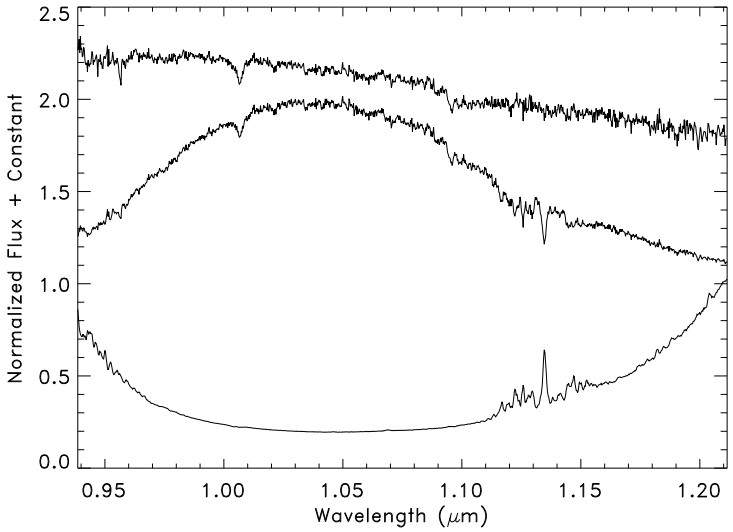

(b) From top to bottom: Telluric-corrected NGC 5102 spectrum, observed galaxy spectrum, telluric correction spectrum used.

Figure 3.2 - Example of telluric correction using A0V star (a), and application to observed galaxy spectrum (b).

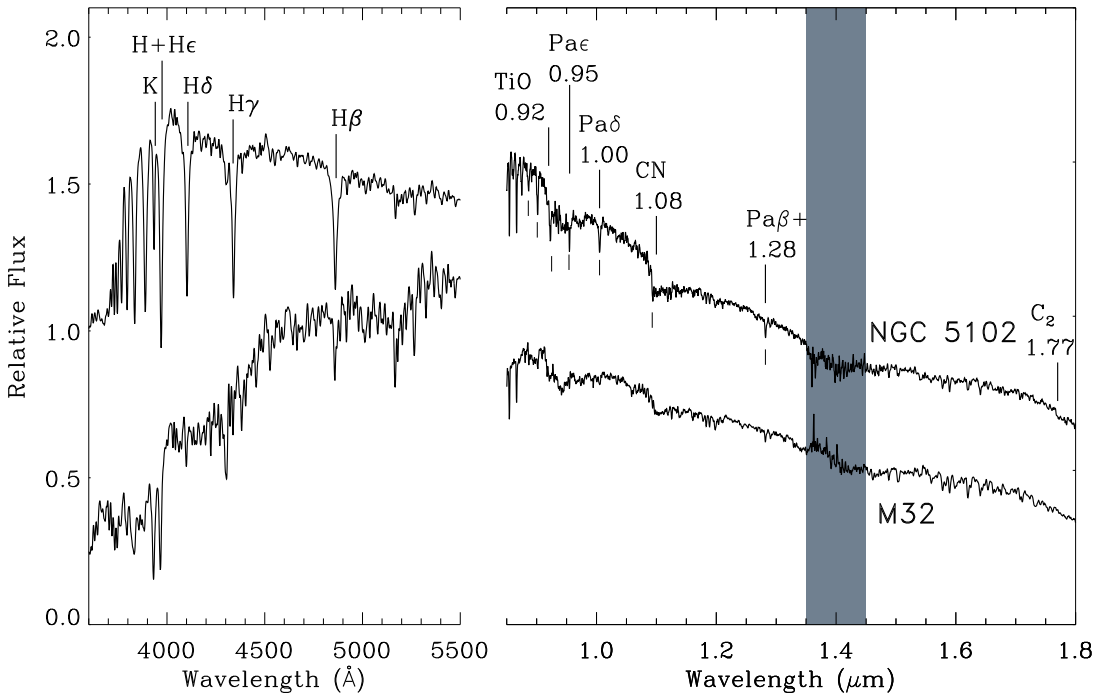

Figure 3.3 - Optical and NIR SpeX spectra of NGC 5102 and the intermediate-age compact elliptical M32 for reference. The optical spectrum of NGC 5102 is from the Goodman High Throughput Spectrograph (Clemens et al. 2004) on the 4.1 m SOAR telescope at Cerro Pachon, Chile, while the optical spectrum of M32 was taken with the FOCAS spectrograph on the 8 m Subaru telescope at Mauna Kea, Hawaii (see Rose et al. 2005). The NIR spectra were taken with the SpeX spectrograph for this paper. The region of low atmospheric transparency is shaded. Only the J and H bands are shown because we have defined no indices in the K band. The Paschen series is marked with the lower ticks to illustrate the differences between the spectra. Note the stronger Balmer lines in the optical spectrum of NGC 5102 than in M32, which is also apparent in the stronger Paschen series in the NIR spectrum of NGC 5102.

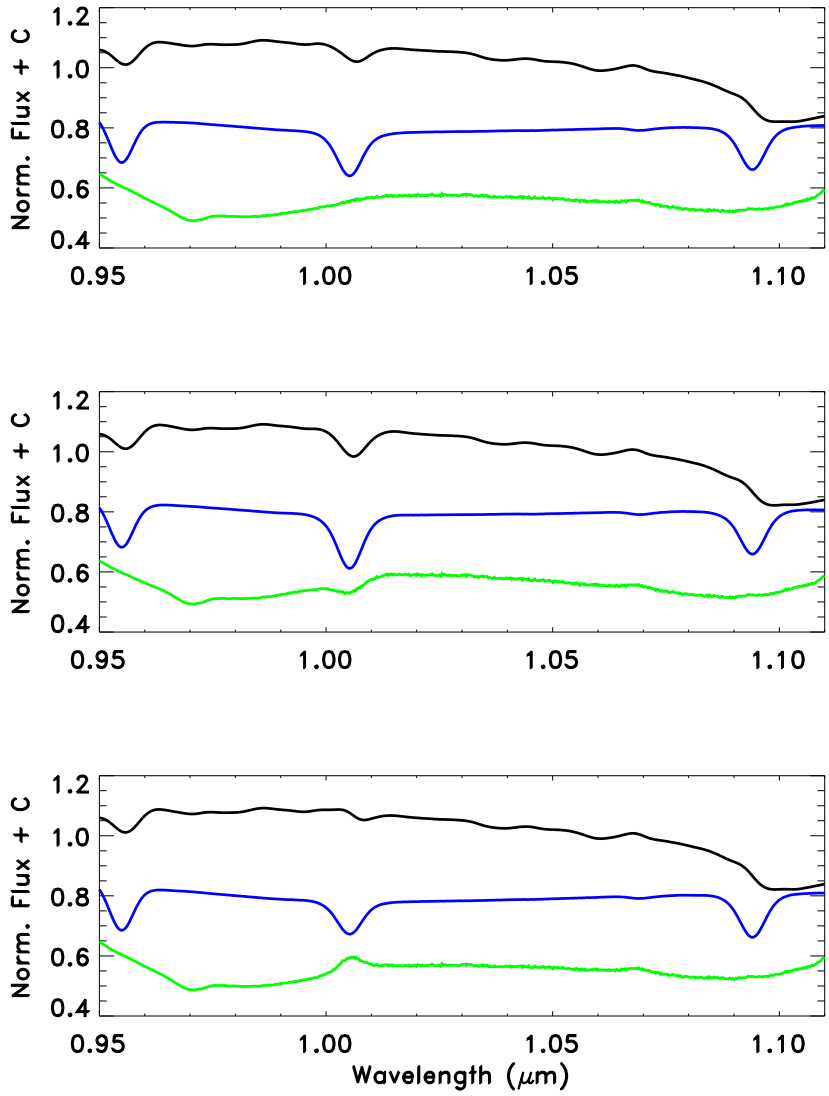

Figure 3.4 - From top to bottom in each plot, NGC 5102 spectrum (black), continuum-normalized intrinsic A0V spectrum (blue), and continuum-normalized telluric correction spectrum (green). The spectra have been smoothed to the resolution of the M05 models. The top plot shows the results from a normal telluric correction, the middle plot shows the effects of an under-compensated Paδ line, while the bottom plot shows the effects of over-compensation. Note the obvious features in the telluric correction in the poorly-fit cases.

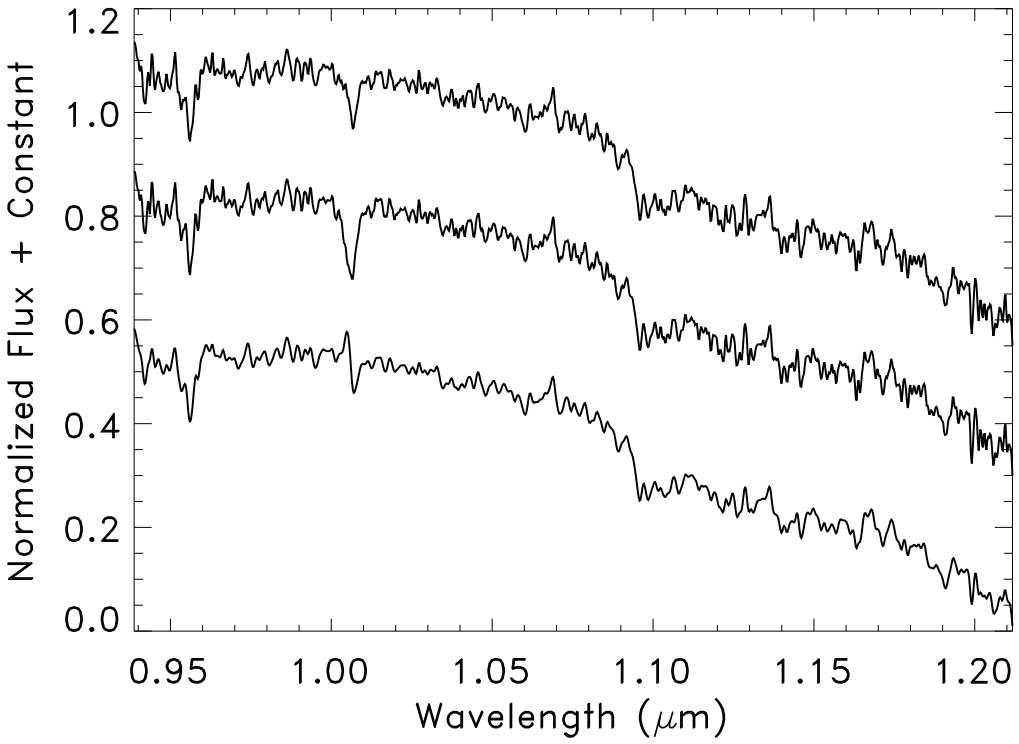

Figure 3.5 - From top to bottom: NGC 5102 spectrum for normal telluric correction, over-compensation, and under-compensation of the Paδ line in the Vega convolution kernel, respectively.

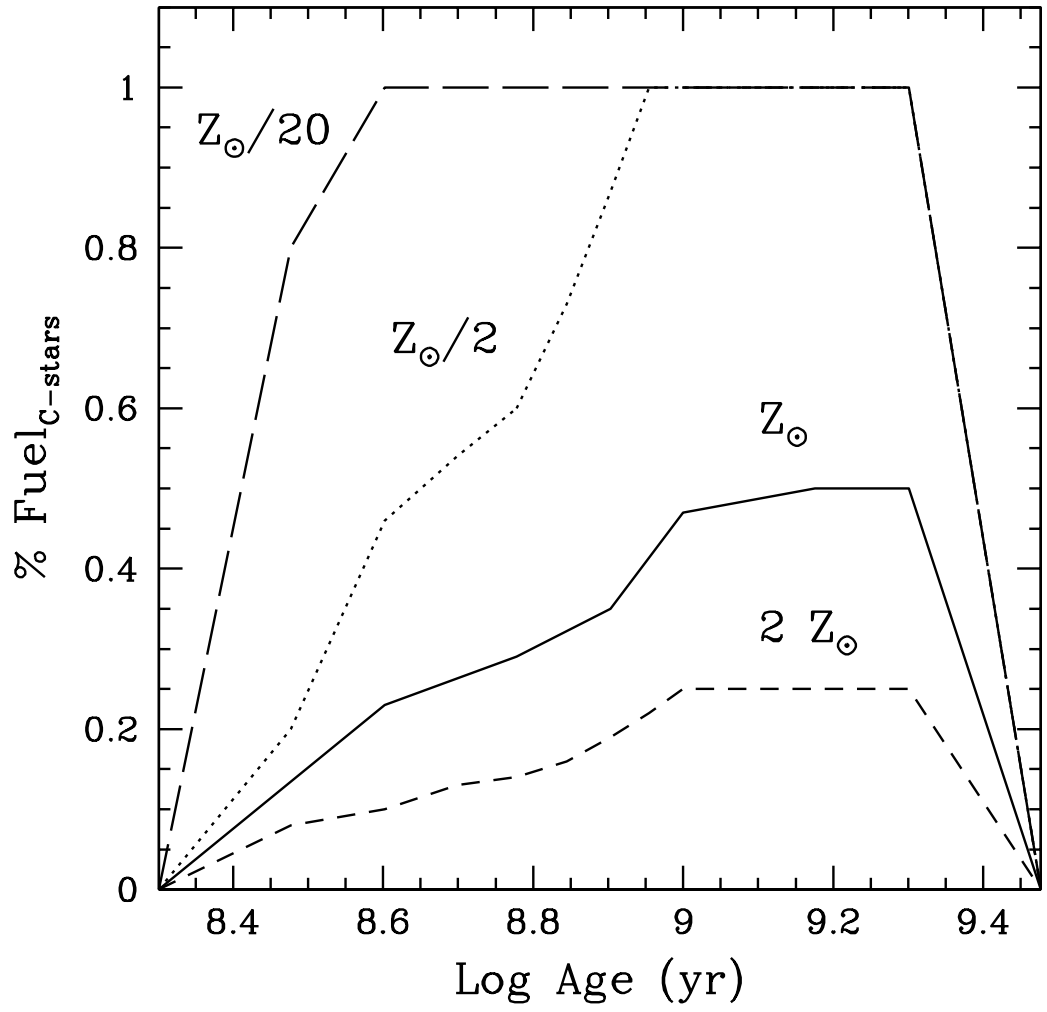

Figure 3.6 - Percentage of TP-AGB fuel spent in C-stars as a function of metallicity in the M05 SPS models. Note the strong metallicity dependence, and the increase with age for each metallicity until ∼2 Gyr. (Figure 12 from M05, reproduced with permission.)

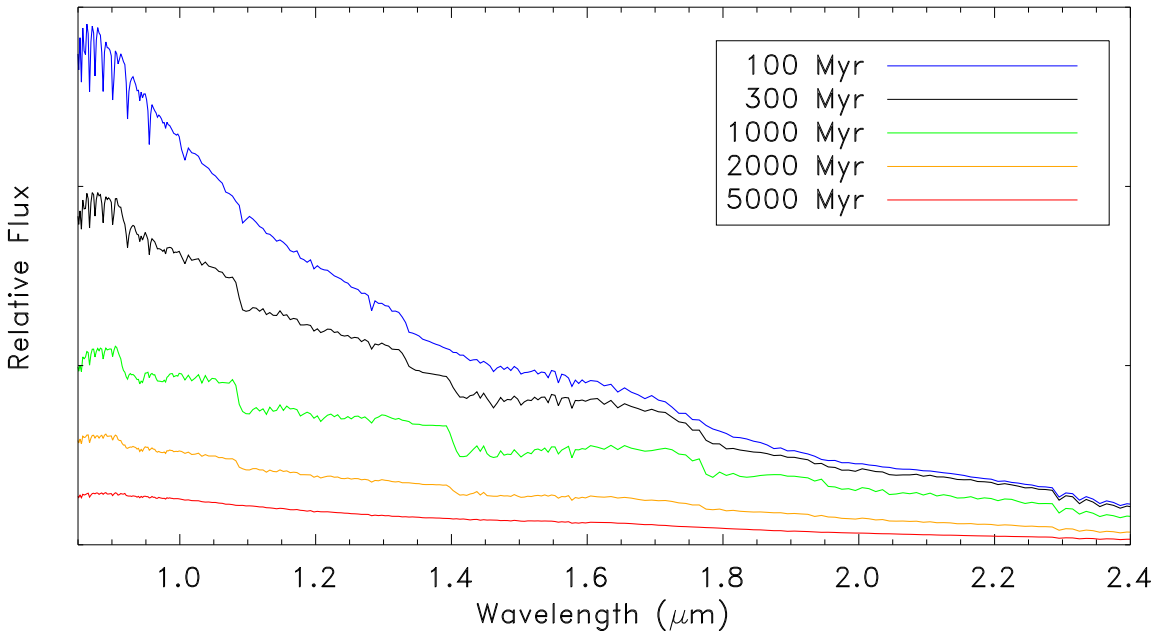

(a) Relative flux levels.

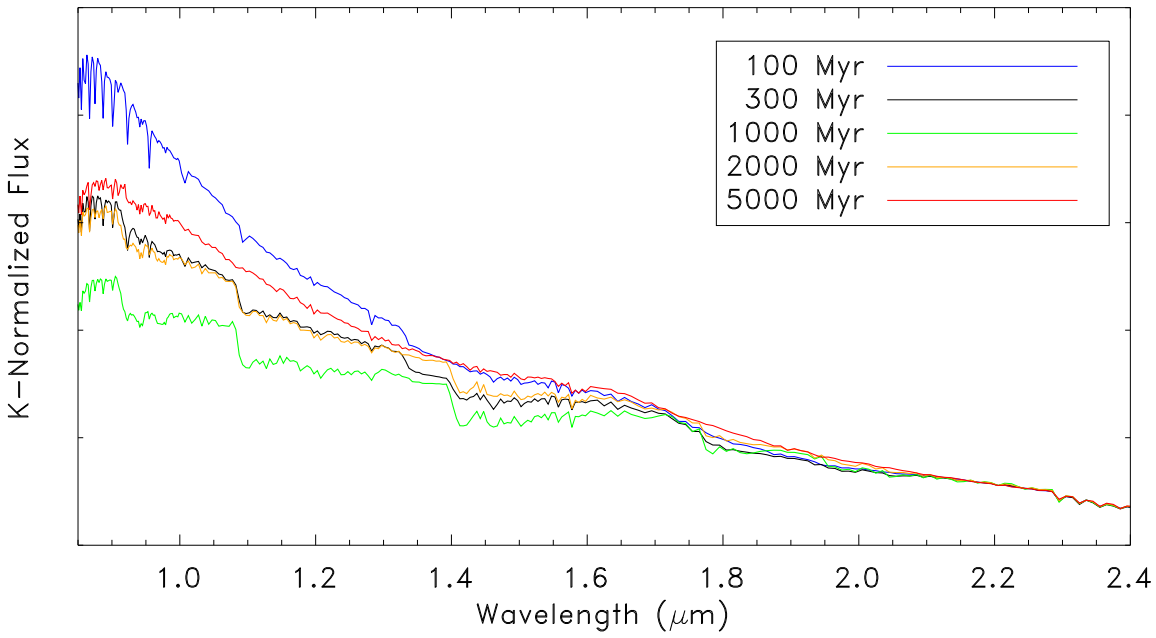

(b) Flux normalized to total K-band.

Figure 3.7 - SEDs for M05 SSP models with $Z_{\odot}$ and Kroupa IMF. Note strong age dependence of both Paschen series and TP-AGB features.

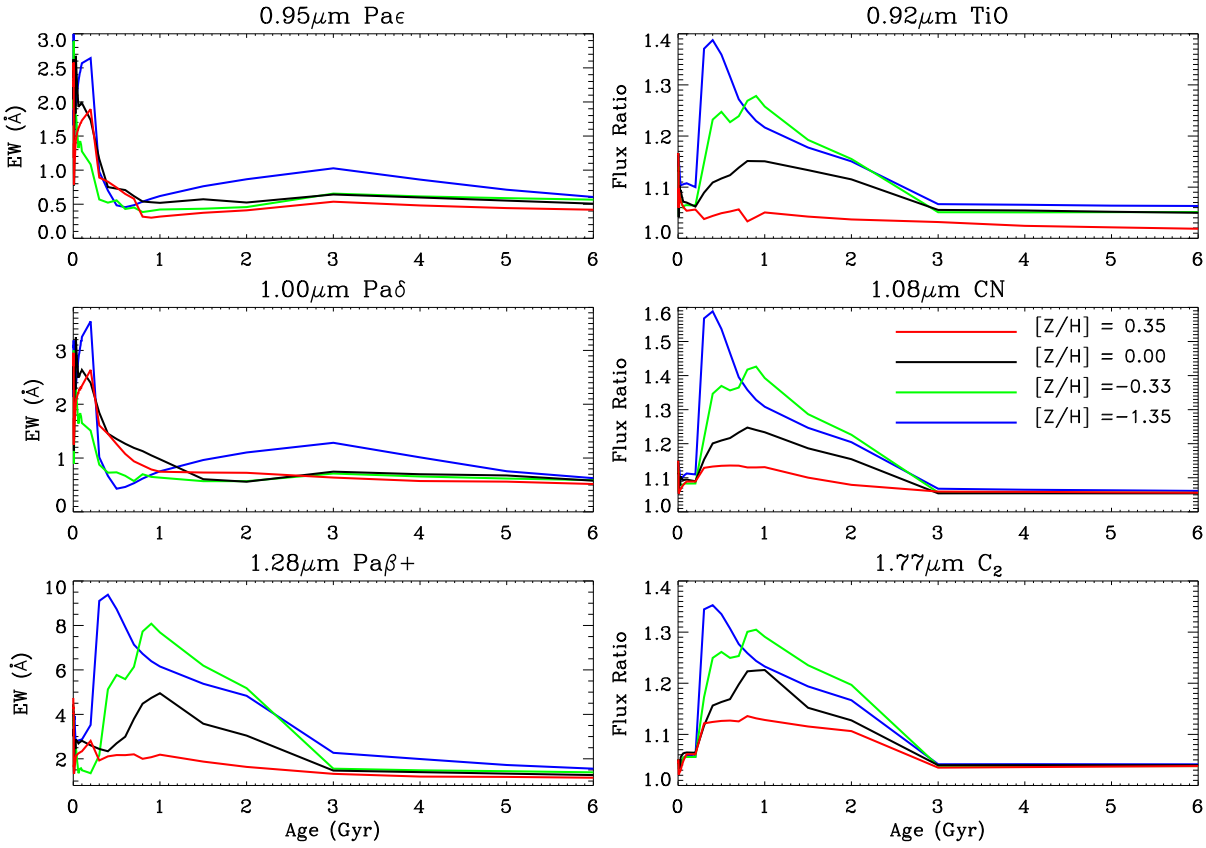

Figure 3.8 - Index vs. age for Maraston models at four metallicities.

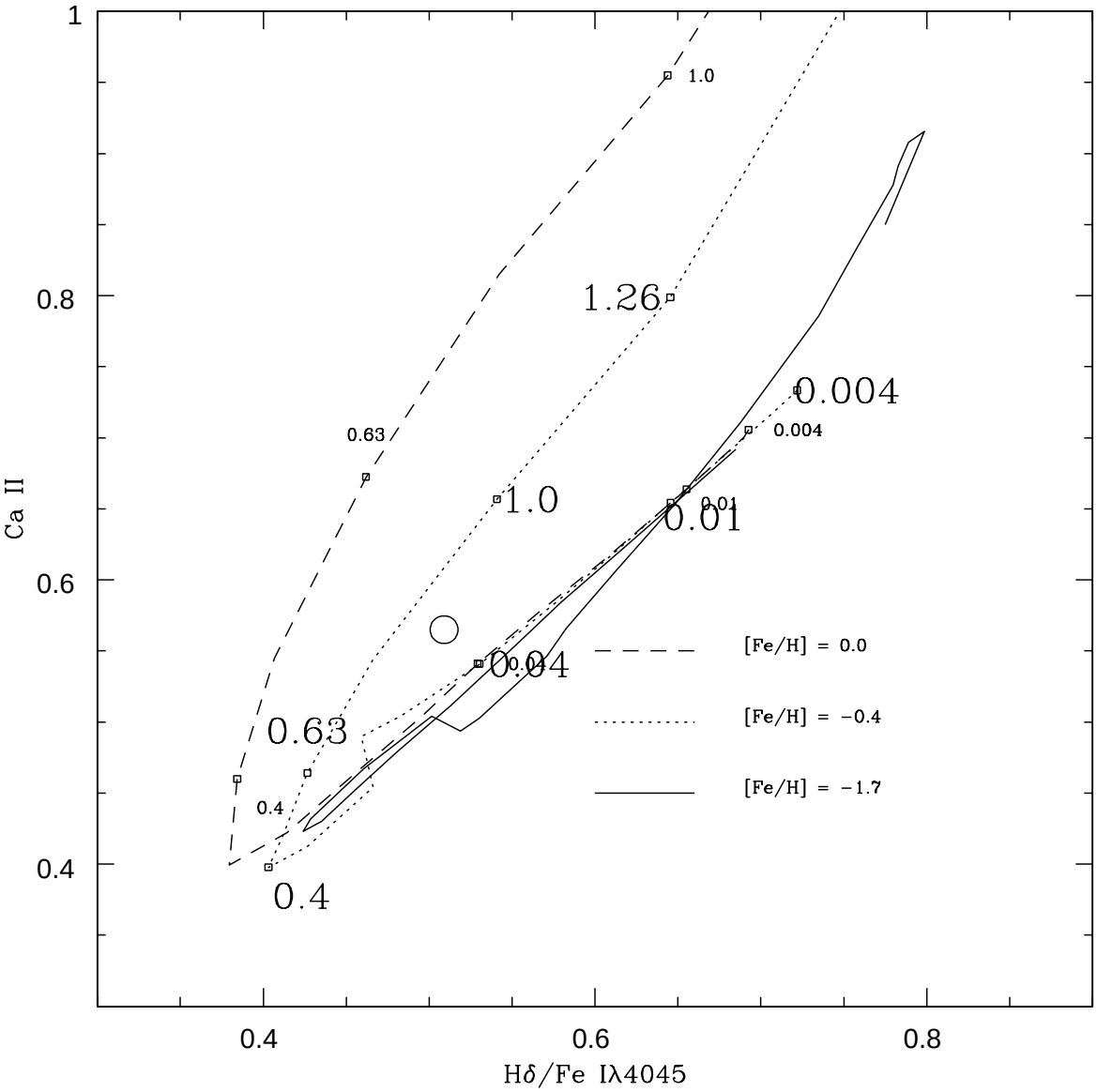

Figure 3.9 - Ca II vs. Hδ/Fe I λ4045 index-index plot for NGC 5102 (open circle). Lines represent SSP tracks for three different metallicities. Ages in Gyr are labeled on the SSP tracks. Large print corresponds to the [Fe/H] = -0.4 model, and small print corresponds to [Fe/H] = -0.0.

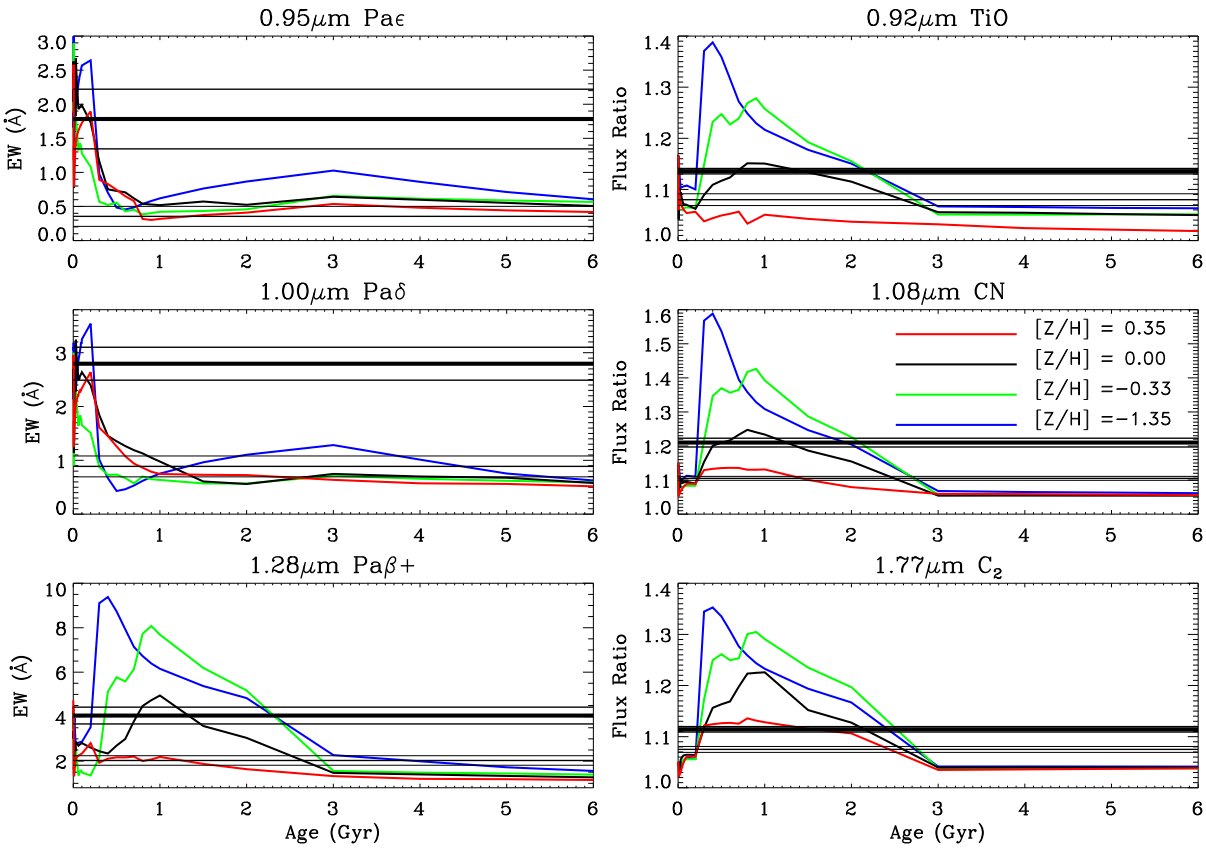

Figure 3.10 - Same as Figure 3.8. Measured values for NGC 5102 and M32 are the top and bottom horizontal lines, respectively, with thin lines showing 1σ uncertainties.

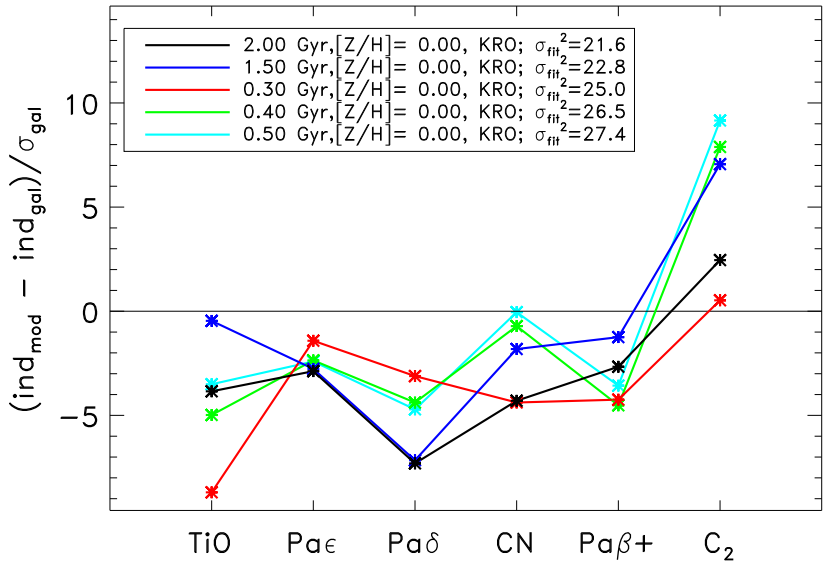

(a) Kroupa IMF.

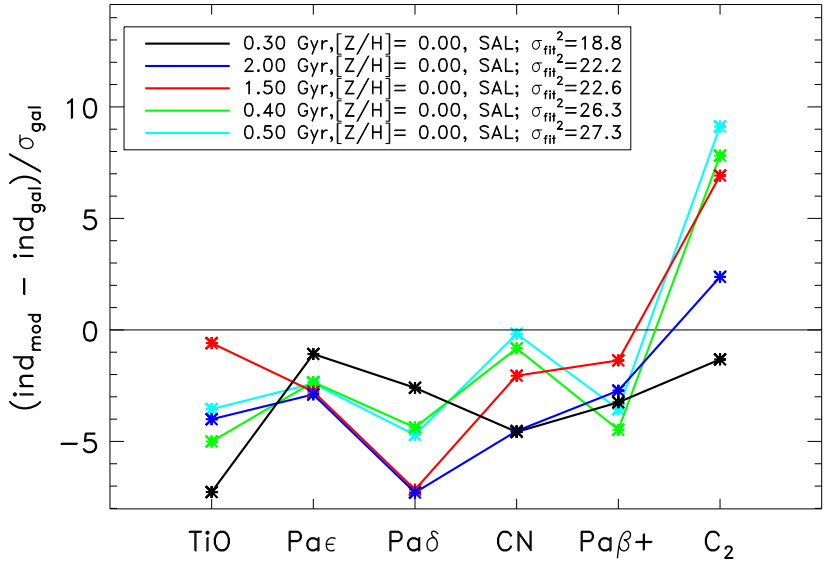

(b) Salpeter IMF.

Figure 3.11 - Five best M05 SSP fits to NGC 5102 indices that minimize $\sigma^2_{\rm fit}$. Legends detail the age, metallicities, and IMFs for the SSP models (SAL denotes Salpeter, KRO denotes Kroupa).

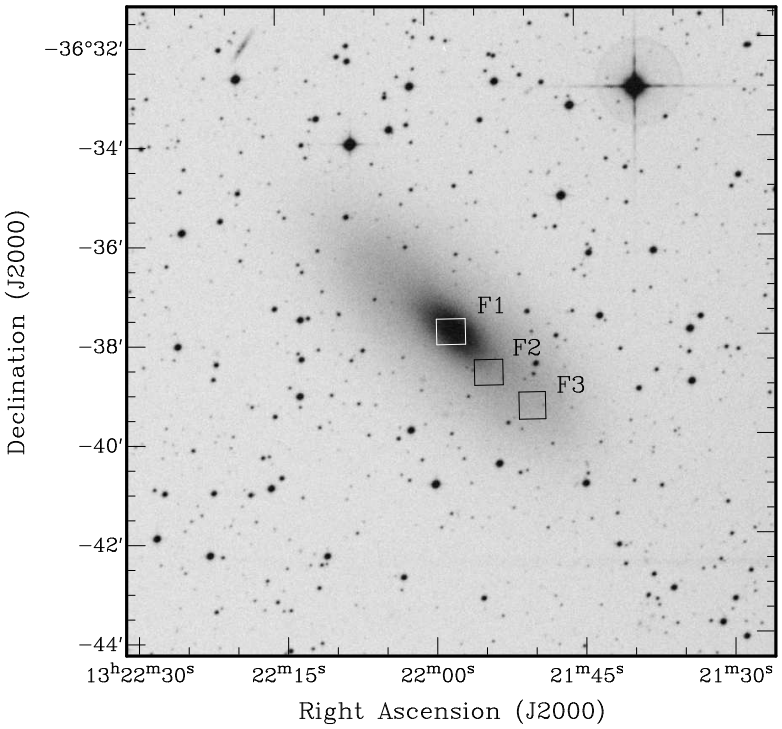

(a) Figure 1 from Beaulieu et al. (2010).

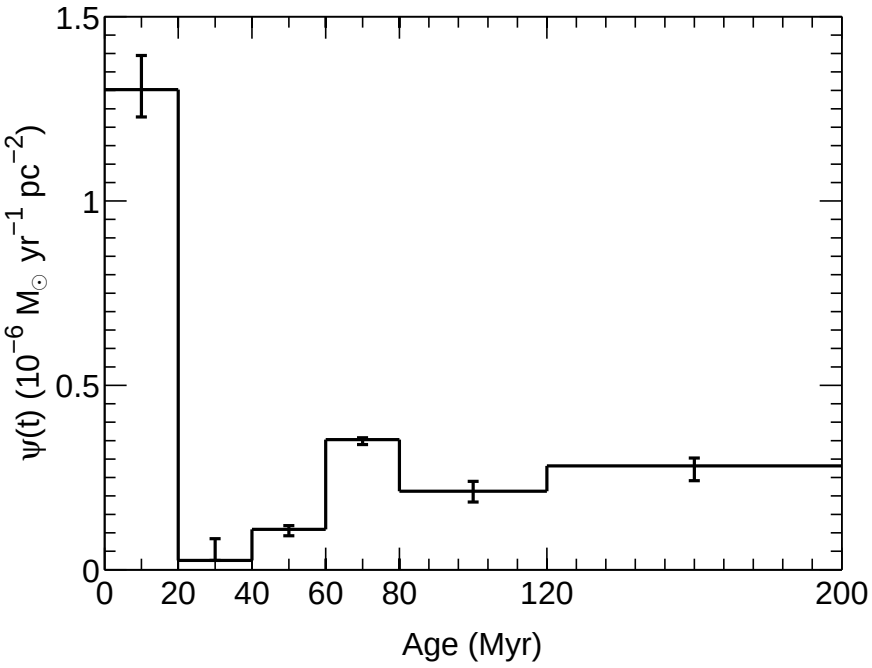

(b) Figure 11 from Beaulieu et al. (2010), showing SFH for field F1.

Figure 3.12 - (a) DSS2 R-band image of NGC 5102; (b) Estimated SFH for nuclear region. (Reproduced with permission from S.F. Beaulieu).

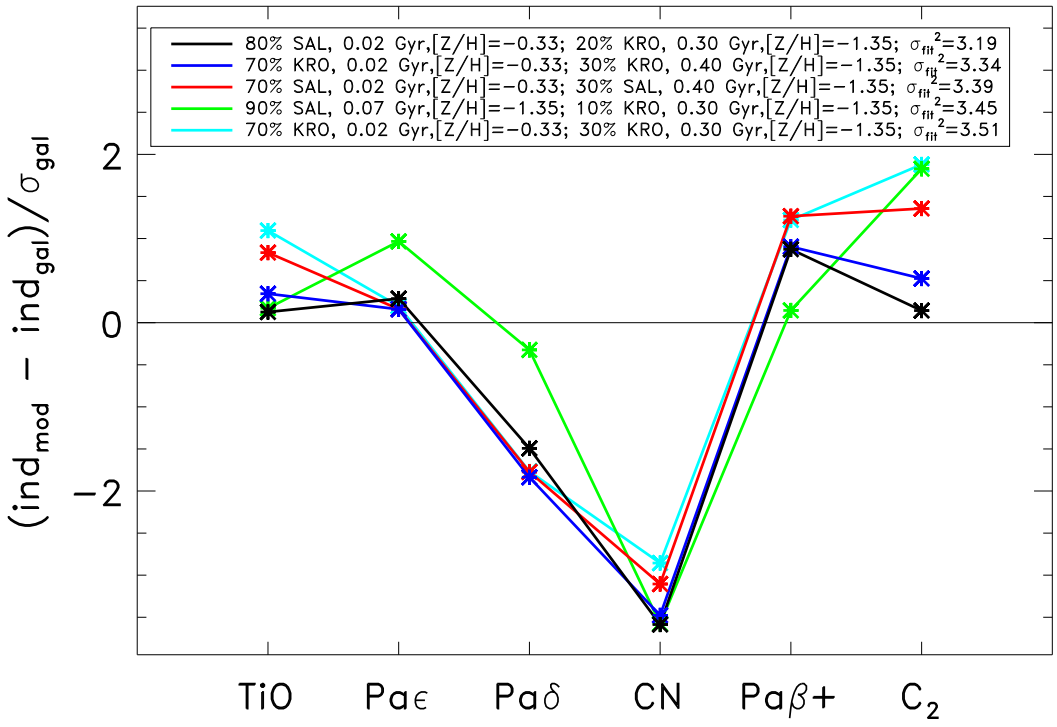

Figure 3.13 - Same as Figure 3.11, but for a composite two-SSP model fit. Legend includes mass fraction, IMF, age, and metallicity for each fit.

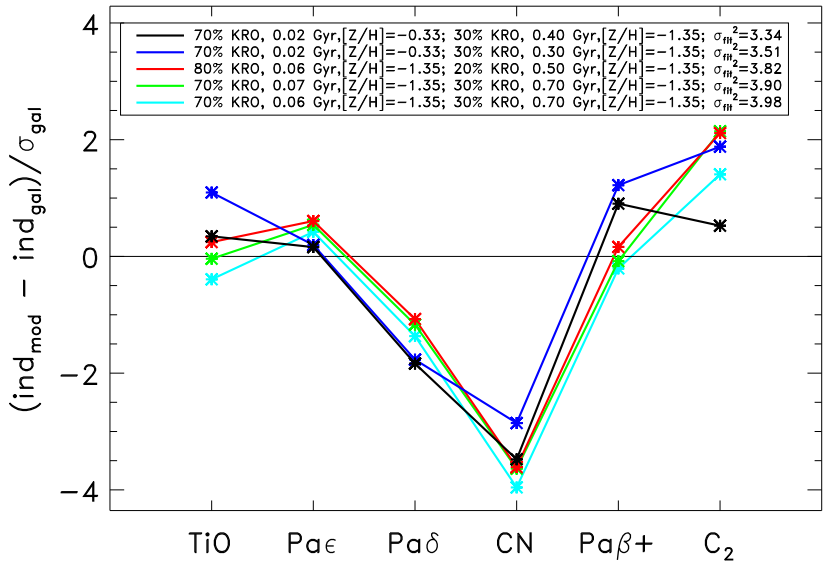

(a) Composite fit with Kroupa IMF.

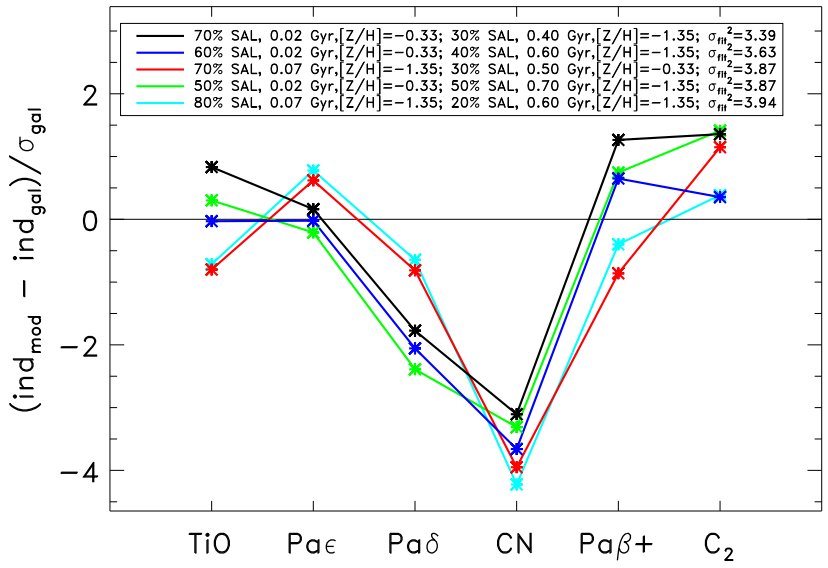

(b) Composite fit with Salpeter IMF.

Figure 3.14 - Same as Figure 3.13, but isolating the effect of the IMF on the index fitting.

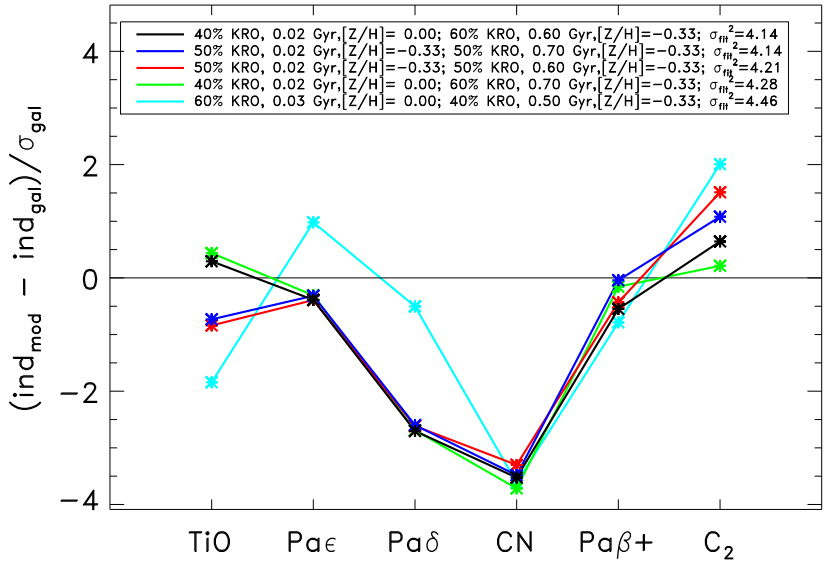

(a) Composite fit with Kroupa IMF.

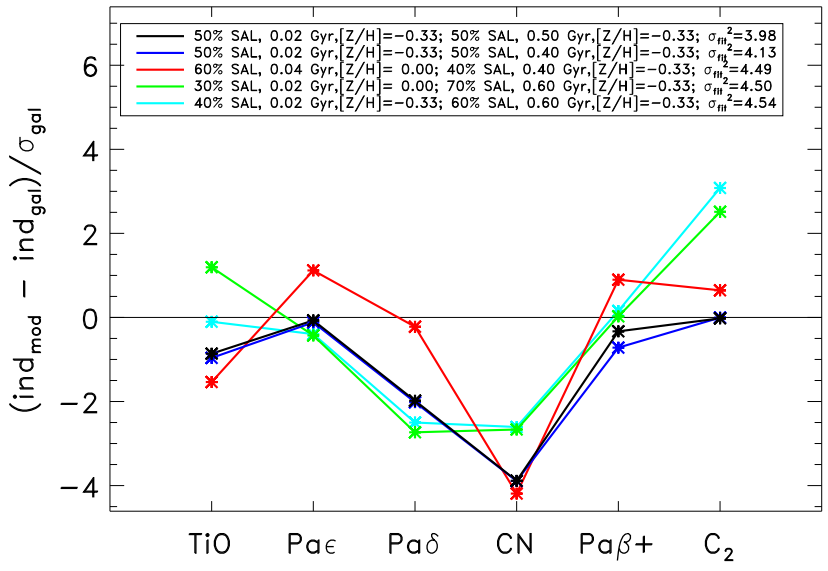

(b) Composite fit with Salpeter IMF.

Figure 3.15 - Same as Figure 3.14 with metallicity constraints $[Z/H] \geq -0.33$.

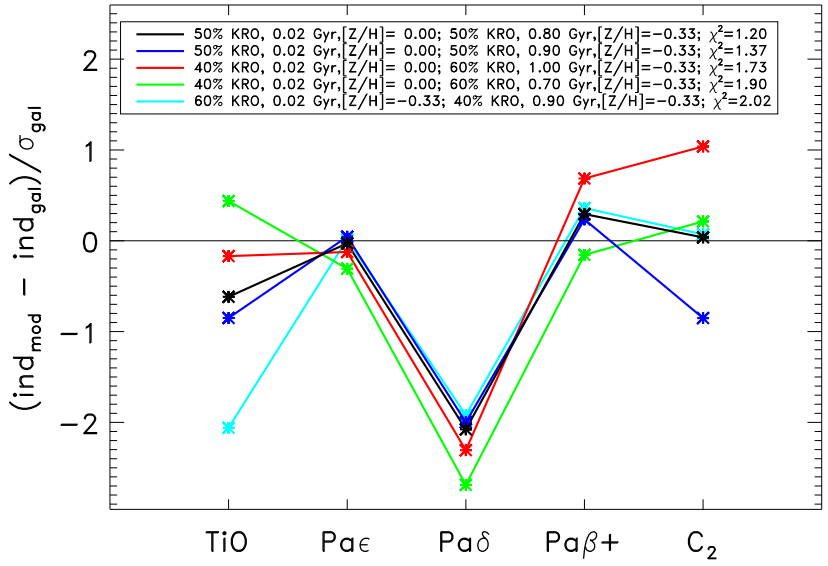

(a) Composite fit with Kroupa IMF.

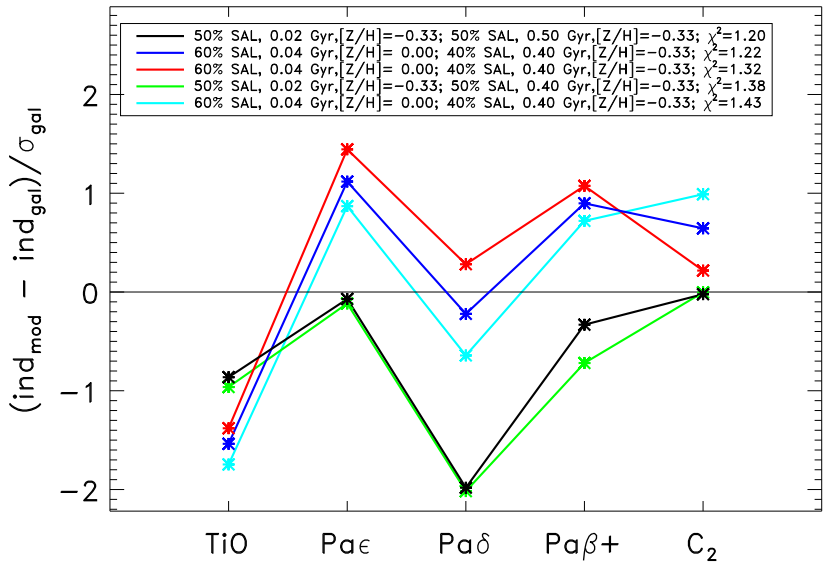

(b) Composite fit with Salpeter IMF.

Figure 3.16 - Same as Figure 3.15 with CN index excluded.

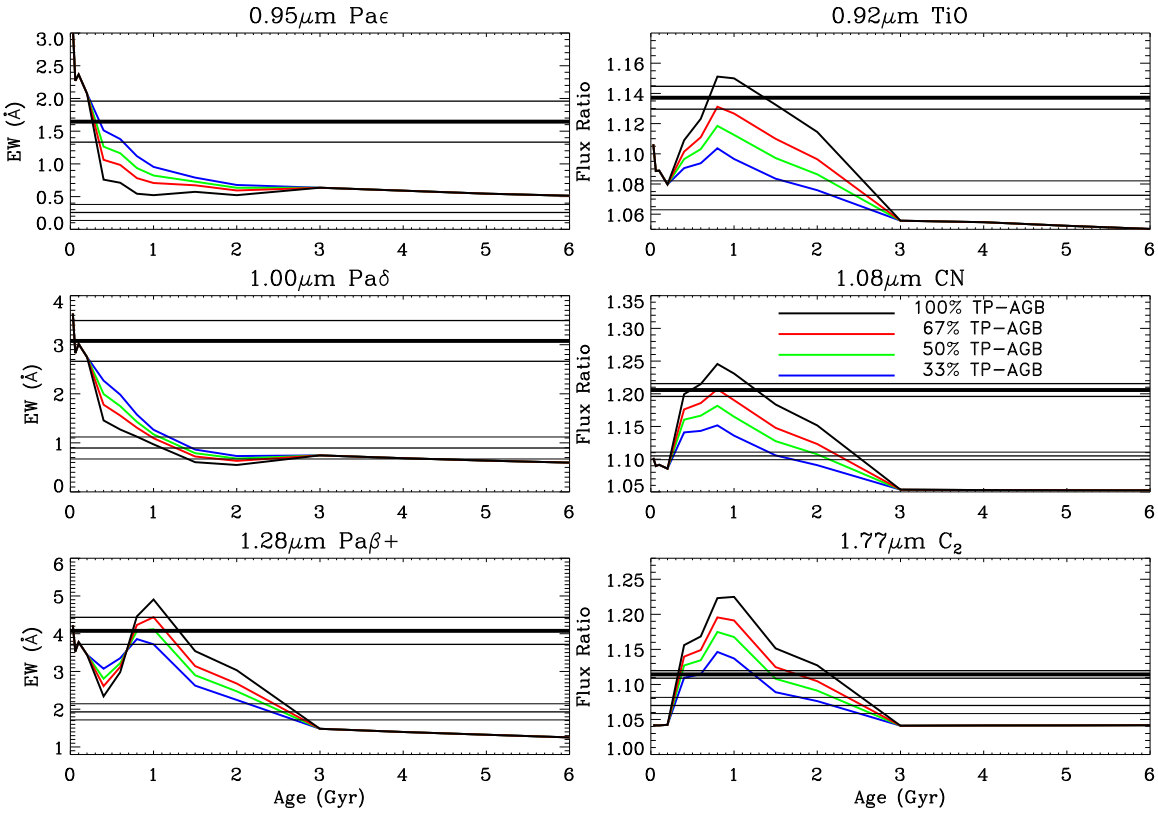

Figure 3.17 - $Z_{\odot}$ M05 models (Kroupa IMF) showing the dependence of the indices on the TP-AGB contribution to total light.

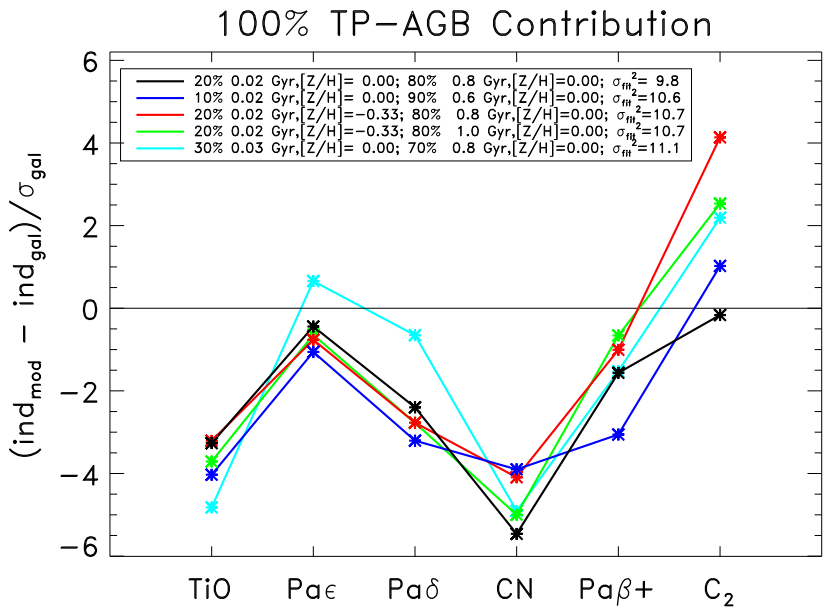

(a)

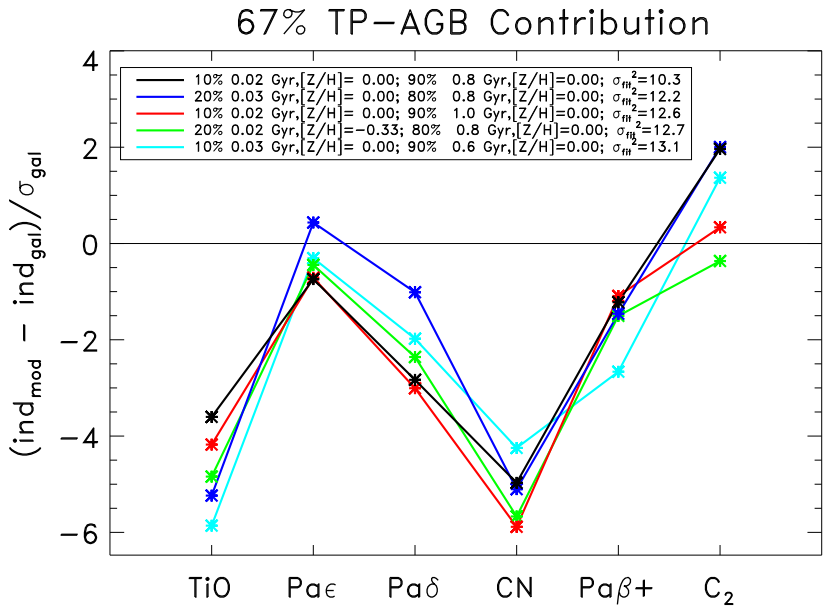

(b)

Figure 3.18 - Composite model fits with varying TP-AGB contribution.

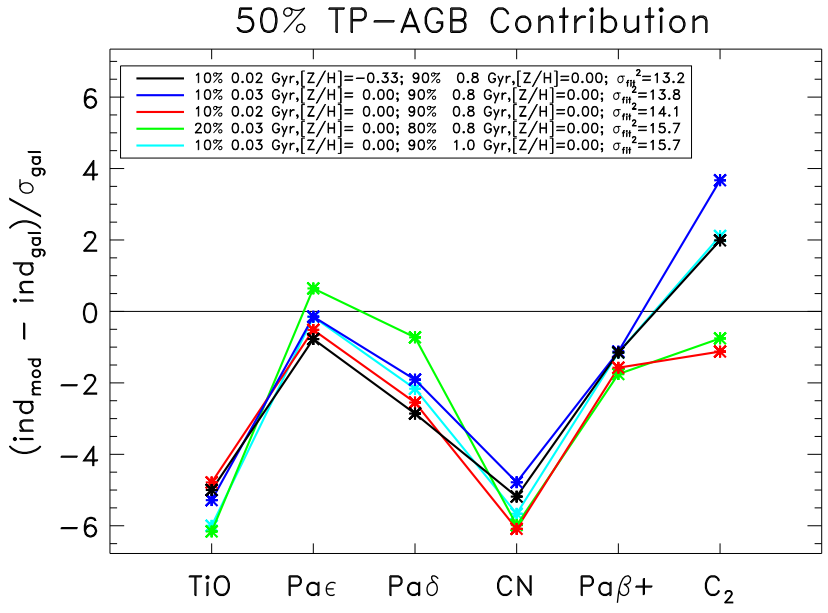
50% TP−AGB Contribution
10% 0.02 Gyr,[Z/H]=−0.33; 90% 0.8 Gyr,[Z/H]=0.00; σfit²=13.2
10% 0.03 Gyr,[Z/H]= 0.00; 90% 0.8 Gyr,[Z/H]=0.00; σfit²=13.8
10% 0.02 Gyr,[Z/H]= 0.00; 90% 0.8 Gyr,[Z/H]=0.00; σfit²=14.1
20% 0.03 Gyr,[Z/H]= 0.00; 80% 0.8 Gyr,[Z/H]=0.00; σfit²=15.7
10% 0.03 Gyr,[Z/H]= 0.00; 90% 1.0 Gyr,[Z/H]=0.00; σfit²=15.7
(ind_mod − ind_gal)/σ_gal
6
4
2
0
−2
−4
−6
TiO
Paϵ
Paδ
CN
Paβ+
C2

(b)

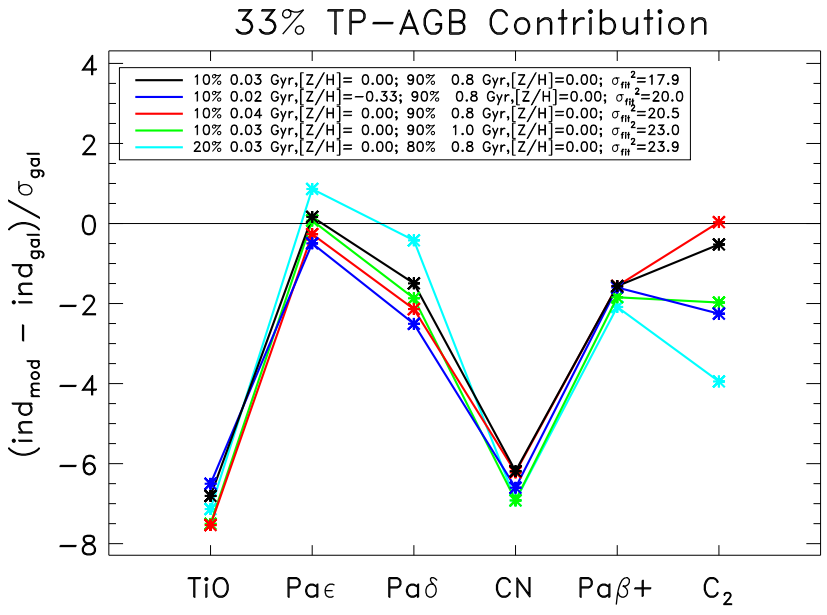
33% TP−AGB Contribution
10% 0.03 Gyr,[Z/H]= 0.00; 90% 0.8 Gyr,[Z/H]=0.00; σfit²=17.9
10% 0.02 Gyr,[Z/H]=−0.33; 90% 0.8 Gyr,[Z/H]=0.00; σfit²=20.0
10% 0.04 Gyr,[Z/H]= 0.00; 90% 0.8 Gyr,[Z/H]=0.00; σfit²=20.5
10% 0.03 Gyr,[Z/H]= 0.00; 90% 1.0 Gyr,[Z/H]=0.00; σfit²=23.0
20% 0.03 Gyr,[Z/H]= 0.00; 80% 0.8 Gyr,[Z/H]=0.00; σfit²=23.9
(ind_mod − ind_gal)/σ_gal
4
2
0
−2
−4
−6
−8
TiO
Paϵ
Paδ
CN
Paβ+
C2

(c)

Chapter 4

M32

ABSTRACT

We present near-infrared (NIR) IRTF/SpeX spectra of the nuclear region of the nearby compact elliptical galaxy M32, which displays an integrated optical spectrum consistent with an intermediate-age ∼3 Gyr stellar population. Because there has historically been uncertainty about the contribution from hot stars in M32, it is not clear whether the star formation history is consistent with a single burst ∼3 Gyr ago, or an underlying old population with low levels of recent star formation. We measure six NIR spectroscopic indices that are sensitive to both main-sequence turnoff and asymptotic giant branch stars in an attempt to characterize the star formation history of M32 and place limits on the mass fraction contained in hot stars. We find that the SFH of M32 is consistent with both a single ∼2.75 Gyr old burst of solar metallicity and an exponentially-declining star formation rate of 2.75 Gyr with an e-folding time of 100 Myr. The difficulties in using this technique for studying intermediate-age populations is discussed, and we detail possible degeneracies between star formation history parameters that can affect predictions of galaxy properties.

4.1 Introduction

The peculiar compact elliptical (cE) galaxy M32 is a nearby companion of the Andromeda galaxy, and has been extensively studied due do its close proximity, high

surface brightness, and bright nucleus. Because it can be studied both with integrated spectroscopy and photometry of resolved stars, it is an ideal testing ground for spectroscopic techniques that measure stellar population properties. Its compact nature and history of interactions with M31, however, place it in a rare taxonomy, making it a poor representative of early type galaxies in general. While typical 'red and dead' ellipticals have old stellar populations, integrated spectroscopic studies show that the star formation history (SFH) of M32 is unique in that it has an intermediate-age nucleus ($\sim$3–4 Gyr) with approximately solar metallicity and abundance ratios, and radial age and metallicity gradients that conspire to produce an overall flat color gradient (O'Connell 1980; Rose 1994; del Burgo et al. 2001; Schiavon et al. 2004; Worthey 2004; Rose et al. 2005; Coelho et al. 2009). These results are derived by measuring age- and metallicity-dependent spectroscopic indices and comparing the measured values to models of simple stellar populations (SSPs) (e.g., Rose 1985, 1994; Worthey 1994). However, a particular SSP-equivalent age and metallicity (Serra & Trager 2007) can correspond to not only an intrinsic coeval population, but also to a composite population whose spectrum has contributions from stars with a variety of ages and metallicities. In the case of M32, its intermediate SSP-equivalent age could be the result of a $\sim$3–4 Gyr post-burst population, or the combination of an underlying ancient (>10 Gyr) population and a "contaminating" small population of hot stars (Maraston & Thomas 2000; De Propris 2000).

Recent work has investigated the possibility of composite populations by testing assumptions about the relative contributions from young, intermediate, and ancient populations. Rose et al. (2005) place constraints on the contribution from a hot-star population by examining the Ca II index, defined to be the ratio of the residual intensities in the Ca II H + Hϵ and Ca II K lines, which is relatively constant in cool stars but declines as temperatures approach those of F and A stars. By subtracting a hot stellar spectrum from the M32 spectrum in varying amounts, they conclude that no more than $\sim$3% of the light at 4000Å is due to hot star contamination. In another recent integrated optical spectroscopic analysis of M32, Coelho et al. (2009) conclude

that (depending on the model used), the fractional contribution to the nuclear light at 5000Å is ∼1/4 to 1/3 ancient (>10 Gyr) and ∼1/4 to 1/2 intermediate-age (between 1 and 10 Gyr), also noting that there is evidence of a population younger than ∼1 Gyr contributing up to 30% of the light. Their derived metallicity of the nuclear region, also dependent on the model used for the fitting, ranges from $-0.63 < [Z/Z_{\odot}] < 0.47$, whereas the peak of the metallicity distribution function is reported to be slightly sub-solar. Outside of the nuclear region, Coelho et al. (2009) report that the model fits also show evidence of contribution from a $[Z/Z_{\odot}] < -1.0$ population, interesting due to the fact that the most extensive photometric analysis of resolved stars in M32 (Grillmair et al. 1996) did not identify such a population.

Other investigators have gauged the necessity of a young population in explaining the intermediate-age spectrum of M32 by searching for sources of blue light such as post-AGB stars and hot horizontal branch (HB) stars. For example, while Burstein et al. (1988) show that M32 has the weakest UV upturn (i.e., UV-to-optical flux ratio) in their sample of early-type galaxies, Brown et al. (2000) detect individual hot HB stars in the nuclear region. In fact, Coelho et al. (2009) suggest that the cause of the model fits requiring young metal-poor populations could be due to contamination by these hot HB stars, which are not present in the models. However, because of the aforementioned limit placed on hot stars by the Ca II index (Schiavon et al. 2004; Rose et al. 2005), there is still uncertainty about whether a composite population is necessary to account for the integrated spectrum of M32, or whether a single, old population with hot HB stars is sufficient. We address this issue by analyzing the near-infrared (NIR) spectrum of M32, using spectroscopic indices that are particularly sensitive to young stars (see § 3).

Integrated NIR spectroscopy may seem like an unlikely method for detecting the presence of hot stars, but the NIR flux can have an appreciable contribution from main-sequence turnoff (MSTO) stars in a very young (<100 Myr) population, as evidenced by the detection of Paschen absorption lines in galaxy spectra (e.g., Miner et al. 2011). Between ∼100 Myr and 3 Gyr the thermally-pulsing asymptotic giant

branch (TP-AGB) will emit up to ∼60% of light in the K-band (Maraston 1998), providing a handle on a young population (here defined to be between ∼100 Myr and ∼1 Gyr). Therefore, if the nucleus of M32 contains either a pure intermediate-age population or a composite population that includes young stars, spectroscopic signatures in the NIR can be used to discriminate between the two scenarios. In fact, Davidge (1990) obtained H and K spectroscopy ($\lambda\lambda 1.6 - 2.4 \mu$m) of the M32 nucleus, detecting a large contribution from late M giants and a small number of C-rich stars, and finding that ∼50% of the K-band light originates from AGB stars. This leads to the conclusion that an intermediate-age population is present, but Davidge was unable to place constraints on the size and age of the population due to large uncertainties in models describing the lifetimes and spectral output of AGB stars.

In § 3, I defined six spectral indices that measure features due to both MSTO and TP-AGB stars and that depend strongly on age and metallicity, and demonstrated that inferences about the SFH from model comparisons are reliable in the case of the young PSB galaxy NGC 5102. Herein, I will measure the NIR indices in M32 and perform fits to both single SSP and composite models in order to determine the contribution, if any, from a young population. In § 4.2, I briefly describe the observations of M32 performed with the SpeX spectrograph, and I present the index measurements in § 4.3. Model fits to the indices are performed in § 4.4, and the implications for the nuclear stellar content in M32 are discussed in § 4.5

4.2 Observations and data

On the nights 2010 June 09 and 10, we observed M32 with the SpeX spectrograph on the NASA Infrared Telescope Facility (Rayner et al. 2003), which utilizes a 1024×1024 Aladdin 3 InSb array. We used the short cross-dispersed (SXD) mode, with a $0\farcs8$ slit (spectral $R = 750$) aligned with the parallactic angle, and took two ABBA object/sky sequences for a total of eight on-object exposures of 120 s each. The mean airmass was ∼1.35. Because the SXD mode simultaneously covers $\lambda\lambda 0.81 - 2.4$ μm in

six separate orders, issues such as order overlap and variable sky features that plague single-order infrared spectroscopy are avoided. On both nights, one ABBA sequence was obtained, where the A position is on the object and the B position is a sky exposure, followed by the A0V star HD 1561, at an airmass less than 0.1 from M32, which is used to perform telluric corrections. Standard SpeX calibrations (arc lamps and flats) were performed after the exposures.

Spectral extraction and telluric corrections were performed using the Spextool package, version 3.4 (Cushing et al. 2004). See Vacca et al. (2003) and § 3.2.3 for a detailed description of the telluric correction process. The final spectra were coadded order-by-order and merged, and are displayed in Figure 3.3, along with optical spectra. Also displayed is the spectrum of the blue S0 galaxy NGC 5102 to emphasize the striking difference between young and intermediate populations both in the optical and NIR. For example, in the optical, NGC 5102 shows strong Balmer absorption, while M32 has little Balmer absorption and a Ca II index close to unity. Likewise, in the NIR all six of the features we have defined are stronger in NGC 5102 than M32, indicating that these features are sensitive to the young populations known to contribute to the NGC 5102 nuclear spectrum.

4.3 Spectral indices and stellar population models

By examining the features present in the NIR spectra of NGC 5102 and M32, we have defined six indices, as described in § 3.3: two Paschen line indices (Paδ and Paϵ) are measured as equivalent widths, three indices measure the flux ratio of narrow bands surrounding absorption breaks due to TP-AGB stars, and a blended index (Paβ+) also tracks the TP-AGB contribution. To examine the expected behavior of these indices as a function of age and metallicity in a stellar population, we track each index in the Maraston (2005, hereafter M05) stellar population synthesis (SPS) models, which provide spectral energy distributions (SEDs) for SSPs at different ages, metallicities, and assuming two initial mass functions (IMFs, Kroupa or Salpeter). Figure 3.8 shows

the indices vs. age for four metallicities, and the following conclusions can be made. First, the indices rise and fall over different timescales. The Paschen lines decline within ∼100 Myr, while the TP-AGB indices are increasing at that age, peaking at ∼1 Gyr (depending on metallicity), and declining by ∼3 Gyr. Second, the TP-AGB indices show a striking dependence on metallicity in that decreasing metallicity causes an increase in the index value, due to the metallicity dependence of the ratio of C-rich to O-rich AGB stars. In metal-poor stars the original oxygen abundance is lower than in metal-rich stars, and therefore less carbon has to be dredged up from the shell-burning region during the TP-AGB phase for the C/O ratio to become greater than unity (Renzini & Voli 1981). This is significant because the TP-AGB features we are measuring originate in the atmospheres of C-rich stars, and their abundance directly affects the features present in integrated light.

In Figure 3.10, the measured index values of M32 are overlaid on the M05 model index vs. age plot along with NGC 5102 for comparison to a young population, with the estimated uncertainty in each index also shown. The galaxy spectrum is degraded to the sampling of the models before the indices are measured to avoid any discrepancies due to sampling differences between observed and model spectra. Because the sampling is much coarser in the models, this effectively smooths the observed galaxy spectrum to the low resolution of the model. The M32 indices are all much lower than those of NGC 5102, which is expected, since M32 is more intermediate-age and lacks a large contribution from a young population. However, the M32 TP-AGB features are not consistent with a pure intermediate (>3 Gyr) population, as they are slightly elevated above the flat index values seen in intermediate and old models. Visual inspection of Figure 3.10 indicates that the SSP-equivalent age is consistent with slightly younger than 3 Gyr. I will discuss the implications of this in the next section, and perform a similar analysis to that in § 3 for NGC 5102.

As described in § 3.3.2, there are large systematic uncertainties associated with the NIR indices, especially the Paschen lines, because the telluric correction method utilizes A0V stars, which themselves have strong Paschen absorption. Any errors in the

Table 4.1. M32 index values and associated uncertainties

Index	Value	σ
0.92μm TiO	1.080	0.012
0.95μm Paϵ	0.36 Å	0.15 Å
1.00μm Paδ	0.89 Å	0.20 Å
1.08μm CN	1.105	0.006
1.28μm Paβ+	2.0 Å	0.2 Å
1.77μm C_2	1.075	0.006

fitting of the A0V telluric star line profiles with a convolved synthetic Vega spectrum will directly affect the strength of the Paschen lines in the object spectrum after multiplication by the telluric correction spectrum, assuming its recessional velocity does not push the object lines beyond those of the telluric standard. The recessional velocity of M32 is ~ -200 km/s, and this error will be present. I am able to estimate $\pm 1\sigma$ systematic uncertainties due to this effect by characterizing the variation in the measured indices for multiple iterations of the telluric correction process. Because of the brightness of the M32 nucleus, statistical errors will be negligible in comparison to the systematic uncertainties. Table 4.1 lists the measured indices for M32 and their associated uncertainties.

4.4 Results

4.4.1 SSP-equivalent fit

Similar to the analysis presented in § 3.4, I will find the M05 SSP models that best fit the M32 indices in order to gauge the statistical likelihood of the spectrum consisting solely of a coeval population, using the same $\sigma^2_{\rm fit}$ statistic to measure goodness of fit.

I allow the models to vary in $[Z/H]$ from -0.33 to 0.35 and in age from 10 Myr to 15 Gyr. I treat IMF separately, performing a fit for the Kroupa and Salpeter models.

The M32 index values are visually consistent with an SSP-equivalent age slightly younger than the 3 Gyr M05 models. However, the M05 models have a coarse age resolution above 1 Gyr, and SEDs are only available for 2 Gyr and 3 Gyr, neither of which appear to fit the M32 indices well in Figure 3.8. To increase the possible SSP ages available for the fitting process, I have interpolated the M05 SEDs in age, and the fits allow for 2.25, 2.50, and 2.75 Gyr ages. Because the index strength is slowly and smoothly varying beyond $\sim$1 Gyr, the interpolation will be minimally affected by non-linear stellar evolution effects. Specifically, between 2 and 3 Gyr the Paschen indices are relatively constant, and the TP-AGB features are slowly declining as the RGB contribution is increasing, and therefore the interpolation will not introduce any significant uncertainty into the fitting process. The results of the single SSP fit with the interpolated ages are shown in Figure 4.1, where the five best model fits are plotted for each available IMF (Kroupa and Salpeter).

The best-fitting SSPs for both IMFs return $\sigma^2_{\rm fit} = 3.4$ for $Z_\odot$ models with ages of 2.50 and 2.75 Gyr, for Salpeter and Kroupa IMF, respectively. Comparing this $\sigma^2_{\rm fit}$ to that of the single SSP fit for NGC 5102 ($\sim$20), we see that the statistical significance of the M32 SSP-equivalent age is much greater. Hence, there is less motivation to apply a composite model to disentangle the contributions from multiple populations, although because we have prior measurements of the SFH of M32 from integrated optical spectroscopy, the results from such a fit can provide a useful gauge of the application of NIR indices to an intermediate age composite population. In fact, the SSP-equivalent age of M32 from optical spectroscopy is also $\sim$3 Gyr, indicating that the NIR results are sensitive to the same stellar content[11], and that the indices can be useful chronometers up to at least 3 Gyr. It is not clear, however, what the precise significance of the $\sigma^2_{\rm fit}$ statistic is, because while it is much improved from the extreme

[11]This is in contrast to the NIR indices in NGC 5102, which, unlike integrated optical spectroscopy, are sensitive to the TP-AGB as well.

example of the NGC 5102 single SSP fit, the value deviates enough from unity that it would not be considered a robust result in a formal χ^2 analysis. Our uncertainties are dominated by systematics, and therefore the fitting statistic is not a formal χ^2, but the comparison can provide a useful zero-point because we define $\sigma^2_{\rm fit}$ in a similar manner. The significance of this comparison will be discussed in § 4.5.

A thorough assessment of Figure 4.1 requires consideration of the nature of the indices and their associated uncertainties, and the uncertainties inherent in the models themselves. Because the NIR indices are sensitive to features prominent in populations less than ∼3 Gyr, their predictive ability is greatly reduced when applied to old populations. With little variation at old ages, the indices only provide lower limits on age. In other words, index values consistent with ages greater than 3 Gyr rule out the presence of a young population, but cannot provide accurate age estimates. However, M32 is a noteworthy case because its SSP-equivalent age is slightly less than 3 Gyr, indicating that the contribution from TP-AGB stars is still detectable, and that the NIR indices can be used to differentiate between young and intermediate-age populations.

The systematic uncertainties in the index measurements will also play a decisive role in the best fit and must be considered. The significantly larger errors on the Paschen EW indices compared to the TP-AGB flux ratios will affect the tolerance of deviations within the fitting process, because the small errors on the TP-AGB indices will require the model indices to be within a few per cent to return a fit with small enough $\sigma^2_{\rm fit}$ to be considered robust. The Paschen indices, on the other hand, have fractional uncertainties on order ∼10% and thus allow for much more variation in the fitting process. Specific to M32, because the measured Paschen indices are consistent with the minimum model values that remain constant at ages above ∼1 Gyr, they do not provide useful information about the SSP-equivalent M32 age. This illustrates an advantage of the combination of Paschen and TP-AGB features, because small Paschen index values alone only provide lower limits on age, but combined with elevated TP-AGB indices can constrain the age to be within ∼1–3 Gyr. The magnitude of the

TP-AGB indices can then indicate a more precise age (this of course depends on the assumption of accurate TP-AGB treatment in the models, which will be addressed below).

We can consider the M32 SSP-equivalent age of ∼2.75 Gyr to be a statistically significant result considering uncertainties on the measured indices, and the unknown model errors. The fact that the NIR result is consistent with optical spectroscopic studies indicates the model treatment of the NIR light of intermediate-age populations is accurate within uncertainty limits. Next, the possibility of a composite population in M32 is considered, and compared to the results from the single SSP fit.

4.4.2 Composite population estimates

Exponentially-declining SFH

In § 4.1, I have detailed previous investigations into the contribution from hot stars in M32, which can either be young, massive main-sequence stars or stars in a blue horizontal branch of an older population. The results are consistent with a small contribution of order a few per cent of the optical light from one, or both, of these sources. In order to place limits on such a population using the NIR indices described above, I will perform fits with two composite SFH models: an exponentially-declining star formation rate that provides young stars from ongoing formation, and a two-SSP model that will place limits on contribution from a recent burst.

Unlike the case of NGC 5102, whose nuclear light is dominated by recent SF, the spectroscopic features in M32 can be affected by extended SF. Star formation over ∼100 Myr can be approximated well by a single burst, but at 3 Gyr since the onset of extended star formation, recently-formed stars will contribute to the integrated light. Therefore, if the nuclear SFH of M32 is not represented by an SSP, then we would expect the spectroscopic features to reflect the presence of stars at various ages. A simplifying assumption is that the SF has been declining exponentially since an initial burst ($\Psi(t) \propto e^{-t/\tau}$), where the time constant, τ, describes the severity of the

decline; large values of τ correspond to approximately constant SF while lower values represent bursts. The M05 SPS models provide models with exponentially declining SF for values of $0.1 \leq \tau/\mathrm{Gyr} \leq 20$ at $Z_{\odot}$, and I have repeated the model fitting procedure allowing the models to range over all ages and values of τ. The resulting fits are displayed in Figure 4.2.

The fits to the exponentially declining models produce smaller values of σ^2_{fit} than the SSP fits, with the best-fitting models for both IMFs 2.75 Gyr with $\tau = 0.10$ Gyr, corresponding to a rapidly declining burst. These results indicate that the NIR indices are consistent with an extended burst, but this interpretation relies on the assumption that the models are free of systematic error, which we know not to be the case, especially in the NIR where the light is dominated by evolved stars. It is certainly plausible that the nucleus has experienced a SFH more complicated than a single coeval burst, but because of the systematic errors on the measured indices, it is unclear whether the improvement in σ^2_{fit} with the exponentially-declining models is physically significant. Furthermore, because optical spectroscopy has revealed that only a small percentage of the flux is coming from hot stars, there is an upper limit on the amount of recent star formation, and thus models with large values of τ would not be consistent with this picture of an intermediate-age population with a "frosting" of hot stars. Examination of Figure 4.2 also illustrates an important degeneracy in the indices between age and SFH. Namely, older models with larger τ values have similar index values to younger models with smaller τ. This is not surprising, because the NIR indices are sensitive to young populations, and both scenarios provide an appreciable flux from young stars. Note that the second-best fit in the Kroupa IMF model is a 13 Gyr population with slowly declining SF, and its indices are almost indistinguishable from the other models within $\sim 1\sigma$. This illustrates a serious limitation to the application of NIR indices to intermediate and old populations, and must be addressed by either consulting other methods that are sensitive to older stars (e.g., Silva et al. 2008), or calibrations with a large sample of intermediate-age populations to measure indices in a model-independent manner.

Two-SSP composite population

I next perform fitting with two SSP models, allowed to vary in age (0.1–15 Gyr) and metallicity ($-0.33 \leq [Z/H] \leq 0.35$), treating each IMF separately. The results of the composite fits are presented in Figure 4.3, including the associated $\sigma^2_{\rm fit}$ of the fits.

The best-fitting models consist of a 5% (by mass, corresponding to ∼25% of J-band light) contribution from a young ∼600 Myr $Z_\odot$ population and an underlying old, sub-solar population. With $\sigma^2_{\rm fit}$ ∼1, the fit statistics are much improved from the single SSP fit indicating that the two-SSP model is able to fit each index reasonably well within uncertainty limits. However, the physical plausibility of such a composite model is questionable when considering what is known from optical spectroscopy. If 5% of the mass is in a young ∼600 Myr population with the rest of the mass in an underlying ancient population, then the young stars would emit ∼50% of the light at λ4000Å, and the optical spectrum would look quite different than that displayed in Figure 3.3. Also, as described in § 4.1, Schiavon et al. (2004) and Rose et al. (2005) show that the Ca II index limits the amount of hot star emission to ∼3%. Therefore, the assumption of a two-SSP population is inconsistent with optical results, but the values of $\sigma^2_{\rm fit}$ imply a good fit. This is likely due to the fact that the Paschen indices provide no age information aside from a lower limit of ∼100 Myr, while the TP-AGB indices are only slightly elevated compared to old populations. In effect, we are attempting to fit a multi-parameter model to a system constrained only by the three redundant TP-AGB indices, which themselves have very little dynamic range compared to the baseline values for old populations. Caution is obviously necessary, then, when assuming a SFH for the model fits. The significance of this finding will be addressed in § 4.5.

4.5 Discussion

M32 is a particularly useful galaxy for testing the NIR method presented here because the spectral indices measure contributions from young stars, and the M32

nucleus is just slightly below the age at which the indices lose their sensitivity. By comparing the measured NIR indices of M32 to those of SPS models, I address two distinct motivations: (1) improve understanding of the nuclear SFH of M32 and attempt to place limits on contributions from a young population; (2) evaluate the feasibility of the NIR index method for studying intermediate age populations that do not show strong TP-AGB features.

The first item is a consequence of the ongoing difficulty in explaining the integrated optical spectroscopy of M32, which is consistent with an SSP-equivalent age of $\sim$3 Gyr, but may have a more complicated SFH. The presence of a small number of hot stars would change the nature of the underlying population, and so placing limits on the contribution from hot stars would allow for a more precise description of the SFH of M32. In effect, the driving question is whether there was a true burst $\sim$3 Gyr ago, or whether a small amount of recent star formation is contaminating the light from a classical 'red and dead' old population. I have found an SSP-equivalent age of 2.75 Gyr, which is consistent with the results from optical spectroscopy. The fitting statistics are difficult to interpret due to the fact that the uncertainties are dominated by systematics, both in the measured indices and in the models, but the SSP fit can be considered reasonably good within error limits. We do, however, consider composite populations to investigate whether a complex SFH provides more robust fits. The M05 models with $\Psi(t) \propto e^{-t/\tau}$ slightly improves the fitting statistics, although the best fitting model of 2.75 Gyr with $\tau = 10$ Myr is effectively identical to the SSP-equivalent model. These fits did, however, introduce a degeneracy in that the indices for a single burst are very similar to populations with extended star formation, because both scenarios provide an appreciable amount of mass in young stars. This hints at the difficulty of measuring properties of an intermediate-age population with methods that are most sensitive to young stars.

From the two-SSP model it is also evident that the fitting statistics may not detect the application of an unphysical SFH, which suggests that extreme caution must be used when interpreting results from NIR indices. The best-fitting models predicted

young populations with mass fractions of ∼5%, which is not consistent with optical spectroscopy. This particular issue is likely due to the fact that the measured index values in M32 are quite weak (compared to, say, the young populations dominating NGC 5102), and thus close to the minimum values that the indices settle into at ages greater than 3 Gyr. In fact, this leads to a degeneracy similar to that encountered in the optical. Namely, a galaxy with weak, but non-zero, contribution from young stars can be modeled by many combinations of populations with differing ages and mass fractions. It is also a reminder of the difficulty in uniquely determining SFH from analysis of integrated light.

Therefore, it is evident that the uncertainties in the NIR indices coupled with their low measured values in M32 prevent any strong statements about the SFH of M32. It is certain that because of the slightly elevated TP-AGB features (compared to their constant values at ages >3 Gyr) there is some contribution from a young population, but the indices cannot uniquely determine whether it is more consistent with a burst or with extended star formation. In the age regime of ∼3 Gyr, the indices have lost much of their sensitivity, suggesting an upper age limit to the types of populations this method can effectively study. Other NIR indices may be more sensitive to old stars (such as the CO bandheads at 2.30 μm), and further investigation into diagnostic features will be necessary to construct a robust age-dating method that can be applied to a wider variety of SFHs.

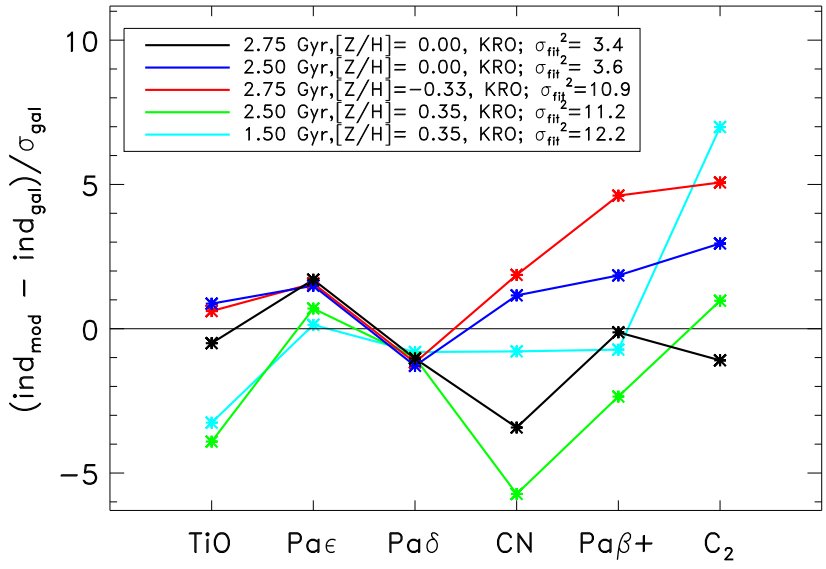

(d) Best SSP fits with Kroupa IMF.

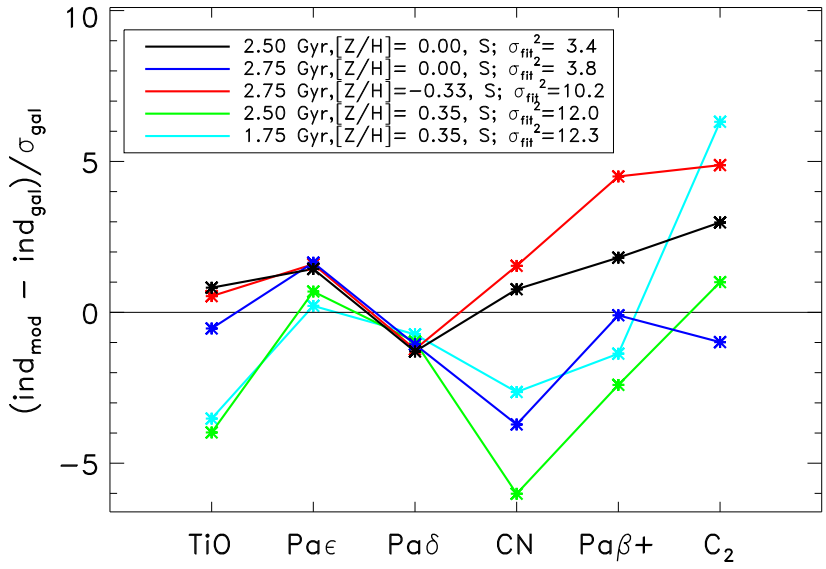

(e) Best SSP fits with Salpeter IMF.

Figure 4.1 - Best M05 model SSP fits to M32 indices.

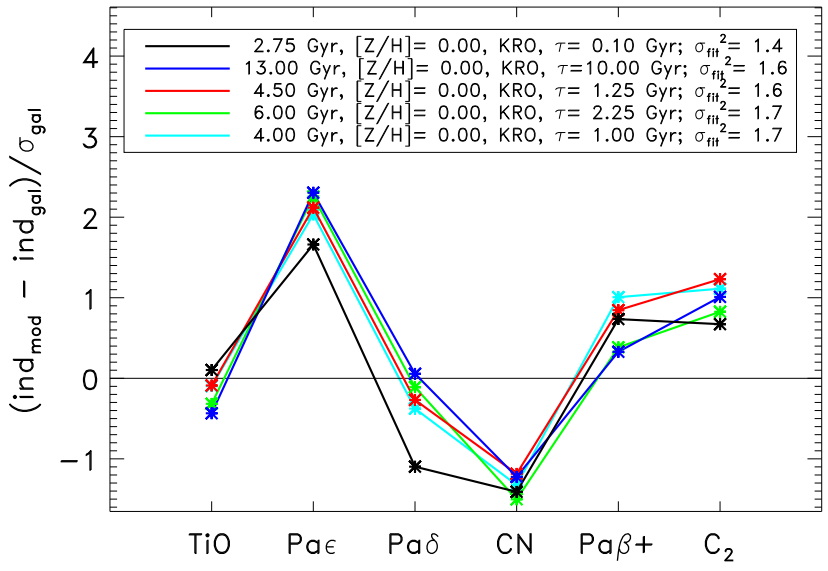

(a) Exponentially declining SFR with Kroupa IMF.

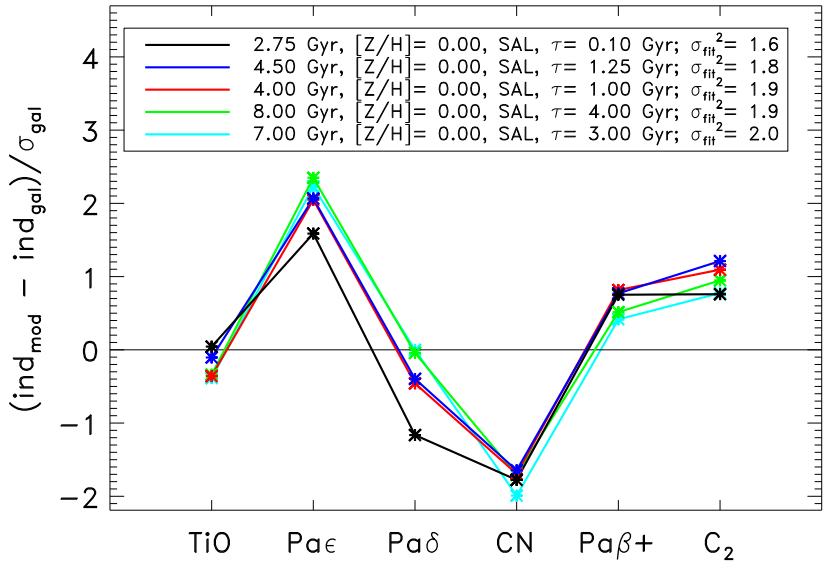

(b) Exponentially declining SFR with Salpeter IMF.

Figure 4.2 - Fits to $Z_{\odot}$ M05 models with exponentially-declining star formation rate.

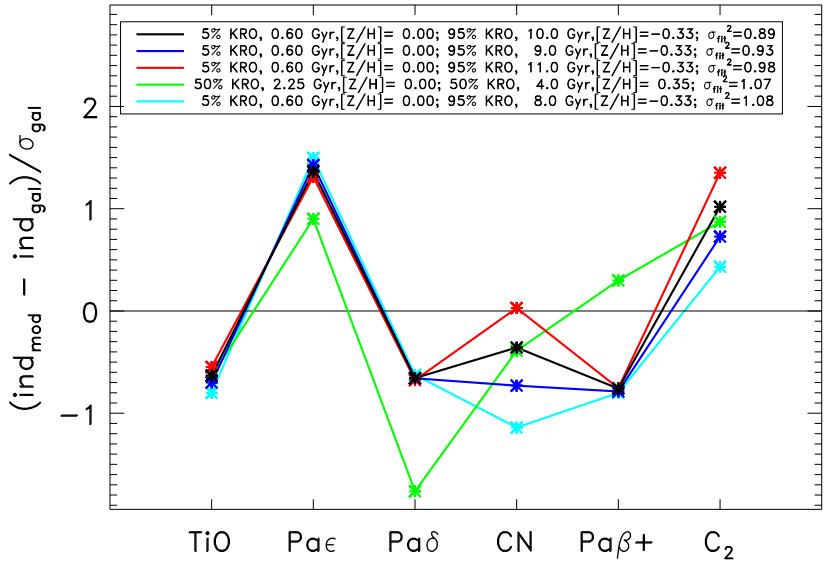

(a) Kroupa IMF.

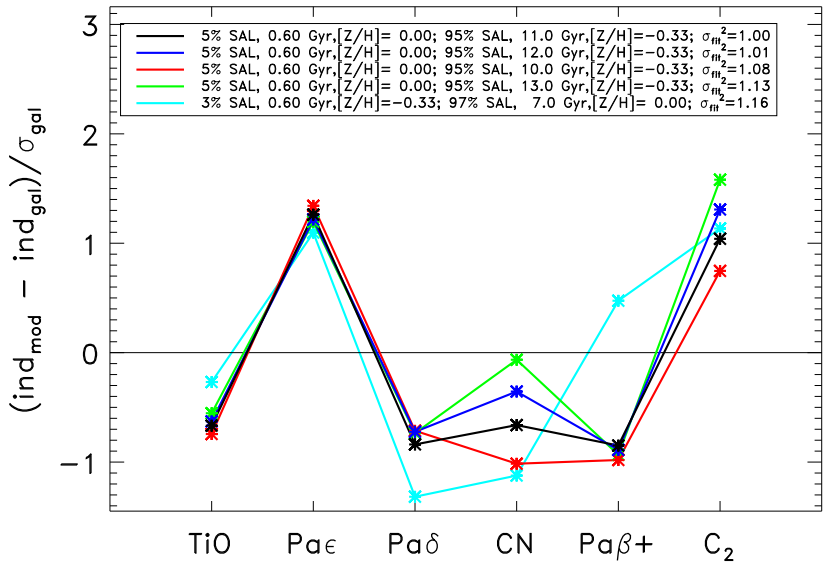

(b) Salpeter IMF.

Figure 4.3 - Best M05 model composite two-SSP fits to M32 indices.

Chapter 5

Discussion

Galaxies in the local universe show a staggering variety of sizes and morphologies. Quiescent massive spheroidal galaxies, grand design spirals steadily forming stars, dwarf irregulars burning through their supply of star-forming fuel at a prodigious rate, and many intermediate objects, are observed. Moving towards higher redshifts, we still see a similar variety of morphologies, but the vigorous star formation observed locally mostly in dwarf galaxies is occurring in more massive and luminous galaxies at $z \sim 1$ (the so-called "downsizing" effect, Cowie et al. 1995). By $z \gtrsim 2$, galaxies tend to be more compact and irregular, although selection effects can lead to biases against detection of more quiescent galaxies at these redshifts. It is clear, however, that that the broad properties of galaxies show a strong dependence on redshift, and this picture points to the bulk of stars being formed before $z \sim 1$ (e.g., Madau et al. 1996). The objective of the study of galaxy evolution is to determine the physical processes responsible for this diversity and redshift dependence of galaxy properties we observe. Techniques for accurately determining physical properties of galaxies are then essential for providing a complete picture of galaxy evolution over cosmic time.

In this thesis I focus on determining the stellar content of galaxies, because our understanding of the properties and evolution of stars allows us to use stellar populations as clocks for their host galaxies. Specifically, I present spectroscopic chronometers that are particularly sensitive to young stars, and measure features from two different stel-

lar sources: hot MSTO stars that are present in integrated light up to ∼100 Myr in a population, and cool TP-AGB stars whose strong molecular absorption will be prominent up to ∼3 Gyr. In general, integrated light methods require model comparisons, because the models can predict stellar population properties for a wide range of ages and metallicities, and we consult the M05 SPS models. However, calibrating objects are needed to test the accuracy of these predictions and to gauge the effects of model uncertainties.

I have obtained IRTF/SpeX NIR spectroscopy of the young PSB galaxy NGC 5102 and the intermediate-age compact elliptical M32 to determine the accuracy of model-derived SFHs using the NIR spectroscopic indices. The following conclusions can be made from the analysis presented in the previous chapters:

1. By examining the NIR spectrum of the young PSB galaxy NGC 5102, I have defined spectroscopic indices and tracked their dependence on age and metallicity with the M05 SPS models. Because the indices probe different timescales, their relative strengths can provide important information about SFH, and differentiate between young and intermediate-age populations.
2. The derived SFH for NGC 5102 using the M05 SPS models is consistent with previous studies, when assumptions are made about the metallicity ($[Z/H] \geq -0.33$). Specifically, the best-fitting models consist of a slightly sub-solar metallicity ∼20 Myr burst and a several hundred Myr sub-solar population. The IMFs provided by the M05 models do not strongly affect these results.
3. The TP-AGB contribution to the NIR flux in stellar populations is still a source of systematic uncertainty, but the NGC 5102 results indicate that, at least within the error limits, the TP-AGB treatment in the M05 models is accurate. Because the age estimates are derived from TP-AGB features, any large errors in the TP-AGB contribution would affect the derived age. However, because we only have one calibrating object, we cannot make a strong statement about the TP-AGB contributions. More galaxies are required whose stellar populations are dominated by young stars to place robust limits on TP-AGB flux in populations.

4. I performed a similar examination of the intermediate-age M32, to determine whether the NIR indices could place limits on the presence of young stars contributing to its central light. The SSP-equivalent age derived from the NIR indices is consistent with previous studies and suggests a population slightly younger than 3 Gyr. A two-SSP fit returned a population that is not consistent with the optical spectrum, indicating that caution is necessary when increasing the fitting parameters in composite population models, which is the case for any integrated light technique. By performing fits to models with extended SF, a degeneracy between population age and SFR was evident in that old populations with extended SF have index values similar to young SSPs (or young populations with a rapid decline in SF). This is due to the fact that the index values are being driven by contributions from young stars, and young stars can be produced either in a recent burst, or due to ongoing SF in an older population.

5. The results of the M32 analysis illustrate that the utility of the NIR indices is diminished when applied to intermediate-age populations, because the index values are close to the values for old populations where the age sensitivity disappears. As seen in the application of a two-SSP model to M32, inconsistent SFHs can be derived. This suggests that for populations approaching SSP-equivalent ages of 3 Gyr, the ability to uniquely determine SFH is compromised. However, the indices can still be utilized to place meaningful limits on contributions from young populations. In the case of M32, we see that there is evidence of an appreciable contribution from stars younger than 3 Gyr.

To conclude, I have demonstrated the ability to detect signatures of young populations in integrated NIR spectra. Aside from being a general age-dating technique, it has particular significance for high redshift galaxies because such galaxies will necessarily have young stellar populations. Measuring the SFHs of high-z galaxies will provide a record of when the bulk of star formation occurred, and how it may depend on galaxy properties such as mass and environment. The work presented here is part of a larger concerted effort to develop observational techniques to measure galaxy

properties, and can aid in describing the stellar mass buildup in galaxies. Characterizing the contribution of TP-AGB stars to integrated light in young populations is key, because luminous TP-AGB stars will drive the M/L.

As described in previous chapters, NIR spectroscopic techniques suffer from two sources of systematic uncertainties: telluric absorption effects, and model uncertainties due to the poorly understood physical processes that determine the evolution of evolved stars. The results I present here are preliminary, and a larger sample of calibrating galaxies will be necessary to disentangle these systematic errors. However, I have demonstrated that the NIR indices provide useful chronometers for young populations, and that this technique will complement the scientific goals of the next generation of IR-optimized observatories.

Chapter 6

Future Work

6.1 Further calibration with PSB galaxy sample

A useful next step in the process of testing the robustness of the NIR chronometers presented here is to obtain optical and NIR spectroscopy of a sample of galaxies and perform a large-scale calibration similar to that described in §§ 3 and 4 for NGC 5102 and M32. The age range during which the TP-AGB and MSTO features are prominent in a population's spectrum is ∼100 Myr – 3 Gyr, and it would be ideal to sample galaxies whose SSP-equivalent ages are in this range. By populating the index vs. age plots with galaxies having a range of index values, and comparing the predictions of SSP-equivalent age and composition derived from the models to measurements using optical spectroscopy, calibrations can be performed. Specific questions about the NIR contribution of the TP-AGB in stellar population models, the metallicity dependence of TP-AGB features, and the intrinsic scatter in the indices can be addressed. Also, targets with recessional velocities above a few thousand km/s will avoid the critical systematic uncertainties in the Paschen lines described in § 3.3.2, and will provide more robust measurements of the Paschen indices.

The ideal targets for this work are PSB galaxies, as they will have a young population whose NIR light is dominated by the TP-AGB or MSTO. Goto (2007) has compiled a catalog of PSB galaxies from the Sloan Digital Sky Survey (SDSS) of

galaxies whose optical spectra have Hδ equivalent widths >5 Å with no detectable emission in [O II] λ3727Å or Hα, providing hundreds of possible northern hemisphere targets with redshifts $\sim 0.1 < z < 1$. On 8 or 10 m class telescopes such as Gemini and Keck, spectroscopic observations of ∼1 hour (in cross-dispersed mode) will achieve sufficient signal to noise ratio (SNR, ∼50 per pixel for typical galaxy with K mag ∼14). With such a sample, the NIR indices would be used to find the corresponding SSP-equivalent ages from the M05 models, and these predicted ages compared to results from optical spectroscopy in order to test the accuracy of the models fits.

The optical spectroscopic technique described in § 3.3.4 utilizing the spectral indices of (Rose 1985, 1994) could provide estimates of SFH for the sample of galaxies. While this technique relies also on models of stellar evolution, it has been calibrated using MC globular clusters in integrated light (Leonardi & Rose 2003). Because it is based on features in well-understood main sequence stars, it has a fundamental physical underpinning that makes it an ideal calibrator and will allow for testing of the reliability of NIR-derived ages and metallicities. The Goto (2007) sample is selected from SDSS spectroscopy, thus optical spectra will be available for the sample of PSB galaxies.

Optical calibrations of the NIR predictions are essential because there is still a great amount of uncertainty in characterizing the effect of the TP-AGB in SPS models. For example, Conroy et al. (2010) and Kriek et al. (2010) suggest that the M05 models do not accurately reproduce the NIR spectral energy distribution (SED) of some galaxies, and suggest that a 'flexible' SPS model, with adjustable temperature and luminosity of the TP-AGB, is necessary to account for uncertainties. While we have found that the M05 model fits to the NIR spectra of NGC 5102 and M32 are consistent with other studies, it is clear that the TP-AGB is difficult to characterize, and empirical calibrations are essential. The results of such a program could determine the extent to which the uncertainties in the TP-AGB contribution in SPS models affect NIR-derived estimates of SFH and composition.

6.2 Application to ULIRGS

Ultra-luminous infrared galaxies (ULIRGs) represent a fascinating stage of evolution in which galaxies in a merger stage of dissipative collapse fuel a central disky starburst region and/or active galactic nucleus (AGN) (Sanders et al. 1988a,b), create outflows that remove gas, quench star formation, and ultimately produce visible quasars and gas-poor elliptical galaxies (e.g., Davies et al. 2007). While these objects represent a fundamental phase of galaxy evolution, the extremely energetic processes involved are not well understood. Therefore, observational measurements of outflows in ULIRGs are necessary to constrain the effects of these feedback mechanisms on the stellar population properties of the galaxy (e.g., Rupke et al. 2005a). For example, Fischer et al. (2010) find evidence of massive molecular outflows powered by an advanced starburst and AGN in the local ULIRG Mrk 231, indicating the fundamental connection between gas removal and star formation. Likewise, Engel et al. (2010) find evidence of recent starbursts (20 Myr) in the merging system NGC 6240, and suggest that the nuclear stellar populations consist of merger-induced bursts on top of the progenitors' bulge remnants.

Archived NIR spectra of a sample of ULIRGs in the IRAS Revised Bright Galaxy Sample (RBGS, Sanders et al. 2003) are available from the UKIRT 1-5 μm Imager-Spectrometer (UIST), as well as the Keck NIRSPEC spectrograph. With these data, one could measure the NIR indices described above to estimate ages of the stellar populations in the merging galaxies. Much work has been done on measuring outflow velocities in RBGS ULIRGs (e.g., Rupke et al. 2005a), and thus a large sample of galaxies exists for which both NIR spectroscopy and outflow measurements are available. The results will allow for a better understanding of the interplay between the stars in merging systems and the resulting galaxy winds, and a large sample of targets in different merger states could be used to describe the progression of star formation throughout the merging process.

As described in e.g., Rupke et al. (2005b), AGN contribute energy to galaxy winds

as well, and therefore many ULIRGs will be composite starburst/AGN. Therefore, it will be necessary to differentiate the NIR contribution from each source. Davies et al. (2007) describe methods for isolating the stellar continuum. Furthermore, Landt et al. (2011) study the NIR AGN continuum, and show that it can be approximated by a simple accretion disk + hot dusty blackbody. These previous studies will provide the tools necessary for investigating the underlying stellar sources in composite SF/AGN systems.

6.3 High Resolution Stellar Population Modeling

As described in § 3, the NIR spectra were smoothed to the low resolution of the M05 models, but it is obvious from visual inspection of high resolution TP-AGB spectra, and the NIR spectra we obtained with SpeX, that many features are lost due to the smoothing. I have begun preliminary work on constructing approximate high resolution SSP models using stellar NIR spectroscopic libraries to better understand how spectral resolution affects the NIR indices and to find features not present in the low resolution models. The models are constructed semi-empirically by finding a single stellar spectrum from the Rayner et al. (2009) catalog of IRTF/SpeX stellar spectra that best matches the M05 model SED, at the resolution of the model, for each evolutionary phase up to the TP-AGB. These spectra are then combined at high resolution, weighted by the total NIR flux contributions of the phase that it represents. The TP-AGB contribution is similarly constructed using the Lançon & Mouhcine (2002) spectra, which are also used in the M05 models, albeit at lower resolution. Effectively, this method reproduces approximate M05 models at high resolution, and limited to $Z_{\odot}$ because the Rayner et al. (2009) library only include solar-neighborhood stars. While these models are not exact, they can be useful for determining how features from each phase contribute to the integrated flux, and may reveal spectroscopic indices that are lost at low resolution. Maraston (private communication) will be publishing high resolution models in the near future as well, allowing me to define indices

in resolution better matched to medium-resolution NIR spectrographs.

In Figure 6.1, I show that the higher resolution model displays detailed line structure that is lost in the lower resolution spectrum. The discrepancy in the values of the Paβ+ index indicates that consideration of spectral resolution is necessary when defining indices. While much less work has been done in the NIR than in the optical in terms of defining spectral indices such as the Lick system (e.g., Worthey 1994), recent studies have identified several more indices in high resolution NIR spectra of globular clusters and galaxies. For example, Silva et al. (2008) define several K-band indices and show that they correlate well with optical indices, such as Mgb and Ca II H and K, and depend similarly on age and metallicity. It is clear that a necessary next step is to investigate the effect of resolution on the indices we have already defined, and to search for other potential indices to improve the accuracy of the technique and to aid in breaking any age/metallicity/dust degeneracies.

6.4 The JWST connection

The *James Webb Space Telescope* (JWST) will be a space-borne infrared-optimized 6.6 m telescope that will provide unprecedented access to galaxies, conceivably up to $z \gtrsim 7$. JWST will have two infrared spectrographs, NIRSpec ($0.6 < \lambda < 5.0$ μm) and the Mid-Infrared Instrument (MIRI, $5.0 < \lambda < 29$ μm), both with medium resolutions of $\Delta\lambda/\lambda \approx 2000 - 3000$. JWST will also employ a tunable filter over the whole wavelength range. These instruments, and other medium-to-high resolution instruments on planned ground-based observatories illustrate the motivation to pursue higher resolution model SEDs to match the instrumental resolution. NIR observations from space will also avoid the telluric effects that plagues ground-based observations, and the systematic uncertainties described in § 3.3.2 will be absent.

The science goals of JWST are categorized into four themes, two of which have direct implications for galaxy evolution: the objectives of the First Light and Reionization theme are to trace the history of ionization in the early universe and to observe

the first luminous sources, while the Assembly of Galaxies theme seeks to describe the evolution of galaxy properties such as dark matter, stellar and gas mass, chemical composition, AGN, and morphology[12]. The NIR spectroscopic technique described in this thesis is well-suited to contribute to the JWST science goals in two complementary ways. First, by performing the calibrations described above for a large sample of galaxies observed with ground-based telescopes, the contributions from TP-AGB stars to the integrated light of populations can be better understood. Because deep imaging surveys of high redshift galaxies will be performed with JWST, stellar mass can be measured from NIR colors, but stellar population models with accurate TP-AGB contribution will be required because the M/L ratio is strongly affected by TP-AGB stars. Second, the NIR indices can be measured in a large sample of galaxies with JWST NIR spectroscopy, up to redshifts of $\sim$2. Observations in this cosmological epoch are particularly well suited to measuring the NIR indices because galaxy evolution models predict that by z$\sim$2 many galaxies will have had rigorous star formation episodes, and will be settling into PSB phases (e.g., Fritze-v. Alvensleben & Bicker 2006). The TP-AGB and MSTO features will be prominent in the NIR light in galaxies after star formation has ramped down, and measurements of the SFHs and metallicities will provide useful information about the timescales of their formation and evolution.

Estimates of observations that will provide adequate S/N for accurate index measurements in galaxy spectra ($\sim$30 per pixel) with JWST instrumentation indicate that NIR spectroscopy of a sample of galaxies if feasible. The continuum sensitivity for NIRSpec is $\sim$1 μJy, which corresponds to a K magnitude $\sim$20, allowing for observations of galaxies similar to nearby PSBs in the Goto (2007) sample out to a redshift of $\sim$3. However, by z$\sim$2 the 1.77μm feature is redshifted past 5μm, the limit of NIRSpec. The sensitivity of the spectrograph on MIRI is poorer, with a continuum flux limit of $\sim$50 μJy, but will still allow for 10σ exposures in 10^4s for PSBs at z$\sim$2–3. Therefore, it is clear that achieving necessary signal-to-noise ratios will be possible with exposure

[12]See (Gardner et al. 2006) for a detailed description of the JWST science goals, instrumentation, and planned implementation.

times on the order of 10^3s for a large sample of galaxies in the z$\sim$2–3 range. Also, the tunable filter could be utilized by placing narrowband filters around absorption-break TP-AGB features. This would allow for shorter exposure times, although previous redshift information would be required for each object. Candidate PSB galaxies could be selected from red NIR colors, and follow-up tunable filter observations could be obtained to find galaxies with strong TP-AGB features.

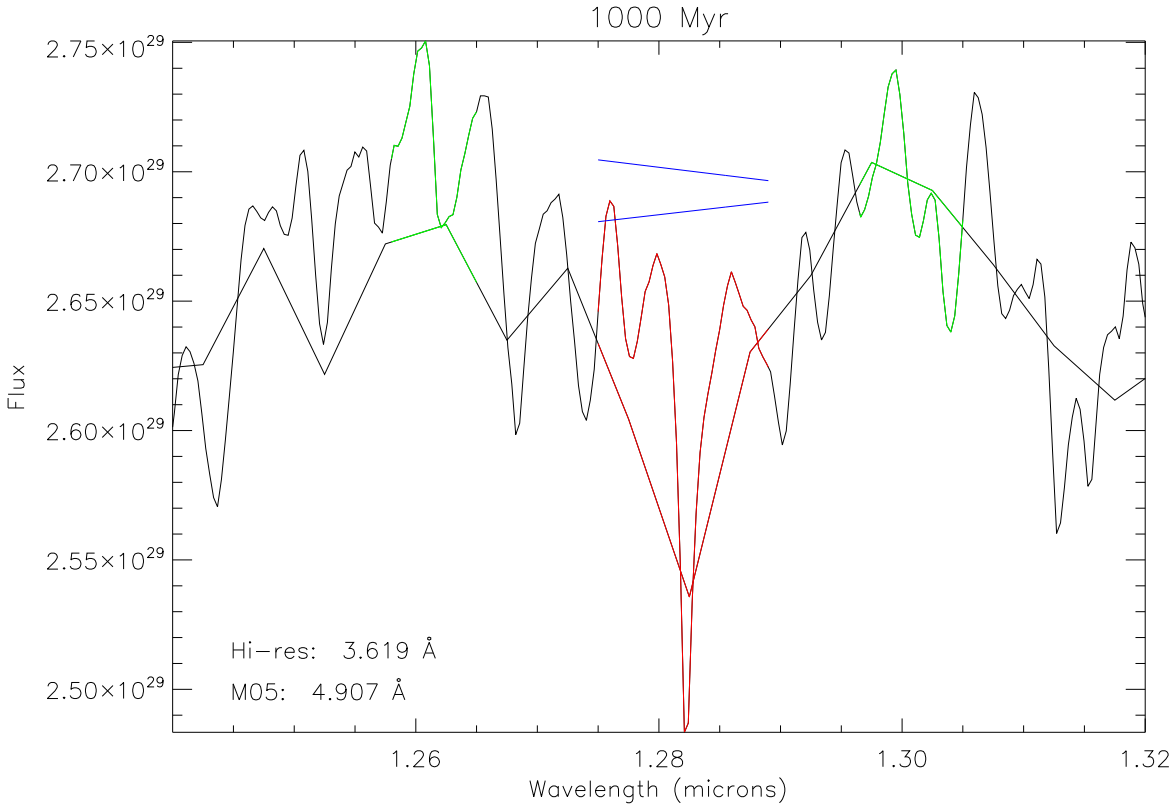

Figure 6.1 - Region around the 1.28μm Paβ+ index showing the difference between high-resolution semi-empirical model spectra for a 1 Gyr SSP. The colored lines show the pseudo-continua (green) and the line (red). The blue horizontal lines show the continuum calculated from interpolating over the pseudo-continua.

REFERENCES

Abt, H. A. & Morrell, N. I. 1995, ApJS, 99, 135

Avila-Reese, V. 2006, arXiv:astro-ph/0605212

Battinelli, P. & Demers, S. 2004, A&A, 418, 33

Baugh, C. M. 2006, Reports on Progress in Physics, 69, 3101

Beaulieu, S. F., Freeman, K. C., Hidalgo, S. L., Norman, C. A., & Quinn, P. J. 2010, AJ, 139, 984

Birnboim, Y. & Dekel, A. 2003, MNRAS, 345, 349

Bloecker, T. & Schoenberner, D. 1991, A&A, 244, L43

Bressan, A., Granato, G. L., & Silva, L. 1998, A&A, 332, 135

Bromm, V. & Yoshida, N. 2011, Annual Review of Astronomy and Astrophysics, 49

Brown, T. M., Bowers, C. W., Kimble, R. A., Sweigart, A. V., & Ferguson, H. C. 2000, ApJ, 532, 308

Bruzual, G. & Charlot, S. 1993, ApJ, 405, 538

—. 2003, MNRAS, 344, 1000

Burstein, D., Bertola, F., Buson, L. M., Faber, S. M., & Lauer, T. R. 1988, ApJ, 328, 440

Buzzoni, A. 1989, ApJS, 71, 817

Cassisi, S., Castellani, M., & Castellani, V. 1997, A&A, 317, 108

Cassisi, S., Castellani, V., Ciarcelluti, P., Piotto, G., & Zoccali, M. 2000, MNRAS, 315, 679

Chandar, R., Leitherer, C., & Tremonti, C. A. 2004, ApJ, 604, 153

Charbonnel, C., Meynet, G., Maeder, A., & Schaerer, D. 1996, A&AS, 115, 339

Clemens, J. C., Crain, J. A., & Anderson, R. 2004, in Presented at the Society of Photo-Optical Instrumentation Engineers (SPIE) Conference, Vol. 5492, Society of Photo-Optical Instrumentation Engineers (SPIE) Conference Series, ed. A. F. M. Moorwood & M. Iye, 331–340

Coelho, P., Mendes de Oliveira, C., & Cid Fernandes, R. 2009, MNRAS, 396, 624

Cohen, M., Wheaton, W. A., & Megeath, S. T. 2003, AJ, 126, 1090

Conroy, C., Gunn, J. E., & White, M. 2009, ApJ, 699, 486

Conroy, C. & Wechsler, R. H. 2009, ApJ, 696, 620

Conroy, C., White, M., & Gunn, J. E. 2010, ApJ, 708, 58

Conselice, C. J., Bundy, K., Trujillo, I., Coil, A., Eisenhardt, P., Ellis, R. S., Georgakakis, A., Huang, J., Lotz, J., Nandra, K., Newman, J., Papovich, C., Weiner, B., & Willmer, C. 2007, MNRAS, 381, 962

Cowie, L. L., Hu, E. M., & Songaila, A. 1995, Nature, 377, 603

Cushing, M. C., Vacca, W. D., & Rayner, J. T. 2004, PASP, 116, 362

Davidge, T. J. 1990, AJ, 99, 561

—. 2008, AJ, 135, 1636

Davidge, T. J. & Jensen, J. B. 2007, AJ, 133, 576

Davies, R. I. 2007, MNRAS, 375, 1099

Davies, R. I., Muller Sanchez, F., Genzel, R., Tacconi, L. J., Hicks, E. K. S., Friedrich, S., & Sternberg, A. 2007, ApJ, 671, 1388

Davis, M., Efstathiou, G., Frenk, C. S., & White, S. D. M. 1985, ApJ, 292, 371

De Propris, R. 2000, MNRAS, 316, L9

Deharveng, J., Jedrzejewski, R., Crane, P., Disney, M. J., & Rocca-Volmerange, B. 1997, A&A, 326, 528

Dekel, A., Birnboim, Y., Engel, G., Freundlich, J., Goerdt, T., Mumcuoglu, M., Neistein, E., Pichon, C., Teyssier, R., & Zinger, E. 2009, Nature, 457, 451

del Burgo, C., Peletier, R. F., Vazdekis, A., Arribas, S., & Mediavilla, E. 2001, MNRAS, 321, 227

Depoy, D. L., Atwood, B., Byard, P. L., Frogel, J., & O'Brien, T. P. 1993, in Society of Photo-Optical Instrumentation Engineers (SPIE) C onference Series, Vol. 1946, Society of Photo-Optical Instrumentation Engineers (SPIE) C onference Series, ed. A. M. Fowler, 667–672

Engel, H., Davies, R. I., Genzel, R., Tacconi, L. J., Hicks, E. K. S., Sturm, E., Naab, T., Johansson, P. H., Karl, S. J., Max, C. E., Medling, A., & van der Werf, P. P. 2010, A&A, 524, A56+

Faber, S. M., Friel, E. D., Burstein, D., & Gaskell, C. M. 1985, ApJS, 57, 711

Fagotto, F., Bressan, A., Bertelli, G., & Chiosi, C. 1994, A&AS, 105, 29

Fioc, M. & Rocca-Volmerange, B. 1997, A&A, 326, 950

Fischer, J., Sturm, E., Gonz´alez-Alfonso, E., Graci´a-Carpio, J., Hailey-Dunsheath, S., Poglitsch, A., Contursi, A., Lutz, D., Genzel, R., Sternberg, A., Verma, A., & Tacconi, L. 2010, A&A, 518, L41+

Fritze-v. Alvensleben, U. & Bicker, J. 2006, A&A, 454, 67

Frogel, J. A., Mould, J., & Blanco, V. M. 1990, ApJ, 352, 96

Gallagher, J. S., Faber, S. M., & Balick, B. 1975, ApJ, 202, 7

Gardner, J. P., Mather, J. C., Clampin, M., Doyon, R., Greenhouse, M. A., Hammel, H. B., Hutchings, J. B., Jakobsen, P., Lilly, S. J., Long, K. S., Lunine, J. I., McCaughrean, M. J., Mountain, M., Nella, J., Rieke, G. H., Rieke, M. J., Rix, H., Smith, E. P., Sonneborn, G., Stiavelli, M., Stockman, H. S., Windhorst, R. A., & Wright, G. S. 2006, Space Sci. Rev., 123, 485

Girardi, L., Bressan, A., Bertelli, G., & Chiosi, C. 2000, A&AS, 141, 371

Goto, T. 2007, MNRAS, 381, 187

Grillmair, C. J., Lauer, T. R., Worthey, G., Faber, S. M., Freedman, W. L., Madore, B. F., Ajhar, E. A., Baum, W. A., Holtzman, J. A., Lynds, C. R., O'Neil, Jr., E. J., & Stetson, P. B. 1996, AJ, 112, 1975

Habing, H. J. & Olofsson, H., eds. 2003, Asymptotic Giant Branch Stars.

Herwig, F. 2005, ARA&A, 43, 435

Iben, Jr., I. & Renzini, A. 1983, ARA&A, 21, 271

Jarrett, T. H., Chester, T., Cutri, R., Schneider, S. E., & Huchra, J. P. 2003, AJ, 125, 525

Kaufmann, T., Bullock, J. S., Maller, A. H., Fang, T., & Wadsley, J. 2009, MNRAS, 396, 191

Kormendy, J. & Richstone, D. 1995, ARA&A, 33, 581

Kraft, R. P., Nolan, L. A., Ponman, T. J., Jones, C., & Raychaudhury, S. 2005, ApJ, 625, 785

Kriek, M., Labbe, I., Conroy, C., Whitaker, K. E., van Dokkum, P. G., Brammer, G. B., Franx, M., Illingworth, G. D., Marchesini, D., Muzzin, A., Quadri, R. F., & Rudnick, G. 2010, ApJ, 722, L64

Kroupa, P. 2001, MNRAS, 322, 231

Kurucz, R. L. 1992, in IAU Symposium, Vol. 149, The Stellar Populations of Galaxies, ed. B. Barbuy & A. Renzini, 225

Lacey, C. & Cole, S. 1994, MNRAS, 271, 676

Lançon, A. & Mouhcine, M. 2000, in Astronomical Society of the Pacific Conference Series, Vol. 211, Massive Stellar Clusters, ed. A. Lançon & C. M. Boily, 34–+

Lançon, A. & Mouhcine, M. 2002, A&A, 393, 167

Lançon, A., Mouhcine, M., Fioc, M., & Silva, D. 1999, A&A, 344, L21

Lançon, A. & Wood, P. R. 2000, A&AS, 146, 217

Landt, H., Elvis, M., Ward, M. J., Bentz, M. C., Korista, K. T., & Karovska, M. 2011, ArXiv e-prints

Le Borgne, J., Bruzual, G., Pell´o, R., Lan¸con, A., Rocca-Volmerange, B., Sanahuja, B., Schaerer, D., Soubiran, C., & V´ılchez-G´omez, R. 2003, A&A, 402, 433

Lejeune, T., Cuisinier, F., & Buser, R. 1997, A&AS, 125, 229

Leonardi, A. J. & Rose, J. A. 2003, AJ, 126, 1811

Lilly, S. J., Le Fevre, O., Hammer, F., & Crampton, D. 1996, ApJ, 460, L1+

Lyubenova, M., Kuntschner, H., Rejkuba, M., Silva, D. R., Kissler-Patig, M., Tacconi-Garman, L. E., & Larsen, S. S. 2010, A&A, 510, A19+

Madau, P., Ferguson, H. C., Dickinson, M. E., Giavalisco, M., Steidel, C. C., & Fruchter, A. 1996, MNRAS, 283, 1388

Maiolino, R., Rieke, G. H., & Rieke, M. J. 1996, AJ, 111, 537

Maraston, C. 1998, MNRAS, 300, 872

—. 2005, MNRAS, 362, 799

Maraston, C., Daddi, E., Renzini, A., Cimatti, A., Dickinson, M., Papovich, C.,

Pasquali, A., & Pirzkal, N. 2006, ApJ, 652, 85

Maraston, C., Kissler-Patig, M., Brodie, J. P., Barmby, P., & Huchra, J. P. 2001, A&A, 370, 176

Maraston, C. & Thomas, D. 2000, ApJ, 541, 126

McMillan, R., Ciardullo, R., & Jacoby, G. H. 1994, AJ, 108, 1610

Messias, H., Afonso, J., Hopkins, A., Mobasher, B., Dominici, T., & Alexander, D. M. 2010, ApJ, 719, 790

Miner, J., Rose, J. A., & Cecil, G. 2011, ApJ, 727, L15

Mo, H., van den Bosch, F. C., & White, S. 2010, Galaxy Formation and Evolution, ed. Mo, H., van den Bosch, F. C., & White, S.

Mouhcine, M. & Lançon, A. 2002, A&A, 393, 149

—. 2003, MNRAS, 338, 572

Mouhcine, M., Lançon, A., Leitherer, C., Silva, D., & Groenewegen, M. A. T. 2002, A&A, 393, 101

O'Connell, R. W. 1976, ApJ, 206, 370

—. 1980, ApJ, 236, 430

O'Connell, R. W. 1986, in Stellar Populations, ed. C. A. Norman, A. Renzini, & M. Tosi, 167–189

Persson, S. E., Aaronson, M., Cohen, J. G., Frogel, J. A., & Matthews, K. 1983, ApJ, 266, 105

Pritchet, C. 1979, ApJ, 231, 354

Rayner, J. T., Cushing, M. C., & Vacca, W. D. 2009, ApJS, 185, 289

Rayner, J. T., Onaka, P. M., Cushing, M. C., & Vacca, W. D. 2004, in Society of Photo-Optical Instrumentation Engineers (SPIE) Conference Series, Vol. 5492, Society of Photo-Optical Instrumentation Engineers (SPIE) Conference Series, ed. A. F. M. Moorwood & M. Iye, 1498–1509

Rayner, J. T., Toomey, D. W., Onaka, P. M., Denault, A. J., Stahlberger, W. E., Vacca, W. D., Cushing, M. C., & Wang, S. 2003, PASP, 115, 362

Renzini, A. & Buzzoni, A. 1986, in Astrophysics and Space Science Library, Vol. 122, Spectral Evolution of Galaxies, ed. C. Chiosi & A. Renzini, 195–231

Renzini, A. & Voli, M. 1981, A&A, 94, 175

Riffel, R., Ruschel-Dutra, D., Pastoriza, M. G., Rodriguez-Ardila, A., Santos, Jr., J. F. C., Bonatto, C. J., & Ducati, J. R. 2011, MNRAS, 410, 2714

Rocca-Volmerange, B. & Guiderdoni, B. 1987, A&A, 175, 15

Rose, J. A. 1985, AJ, 90, 1927

—. 1994, AJ, 107, 206

Rose, J. A., Arimoto, N., Caldwell, N., Schiavon, R. P., Vazdekis, A., & Yamada, Y. 2005, AJ, 129, 712

Rupke, D. S., Veilleux, S., & Sanders, D. B. 2005a, ApJS, 160, 87

—. 2005b, ApJS, 160, 115

Salaris, M. & Cassisi, S. 2005, Evolution of Stars and Stellar Populations, ed. Salaris, M. & Cassisi, S.

Salasnich, B., Girardi, L., Weiss, A., & Chiosi, C. 2000, A&A, 361, 1023

Sanders, D. B., Mazzarella, J. M., Kim, D., Surace, J. A., & Soifer, B. T. 2003, AJ, 126, 1607

Sanders, D. B., Soifer, B. T., Elias, J. H., Madore, B. F., Matthews, K., Neugebauer, G., & Scoville, N. Z. 1988a, ApJ, 325, 74

Sanders, D. B., Soifer, B. T., Elias, J. H., Neugebauer, G., & Matthews, K. 1988b, ApJ, 328, L35

Santos, Jr., J. F. C. & Frogel, J. A. 1997, ApJ, 479, 764

Schaller, G., Schaerer, D., Meynet, G., & Maeder, A. 1992, A&AS, 96, 269

Schiavon, R. P., Caldwell, N., & Rose, J. A. 2004, AJ, 127, 1513

Serra, P. & Trager, S. C. 2007, MNRAS, 374, 769

Silva, D. R., Kuntschner, H., & Lyubenova, M. 2008, ApJ, 674, 194

Spinrad, H. & Taylor, B. J. 1971, ApJS, 22, 445

Steidel, C. C., Adelberger, K. L., Giavalisco, M., Dickinson, M., & Pettini, M. 1999, ApJ, 519, 1

Tinsley, B. M. & Gunn, J. E. 1976, ApJ, 203, 52

Tonini, C., Maraston, C., Thomas, D., Devriendt, J., & Silk, J. 2010, MNRAS, 403, 1749

Tremonti, C. A., Heckman, T. M., Kauffmann, G., Brinchmann, J., Charlot, S.,White, S. D. M., Seibert, M., Peng, E. W., Schlegel, D. J., Uomoto, A., Fukugita, M., & Brinkmann, J. 2004, ApJ, 613, 898

Vacca, W. D., Cushing, M. C., & Rayner, J. T. 2003, PASP, 115, 389

van den Bergh, S. 1976, AJ, 81, 795

van Woerden, H., van Driel, W., Braun, R., & Rots, A. H. 1993, A&A, 269, 15

Vassiliadis, E. & Wood, P. R. 1993, ApJ, 413, 641

Vazdekis, A. 1999, ApJ, 513, 224

Westera, P., Lejeune, T., Buser, R., Cuisinier, F., & Bruzual, G. 2002, A&A, 381, 524

White, S. D. M. & Frenk, C. S. 1991, ApJ, 379, 52

White, S. D. M. & Rees, M. J. 1978, MNRAS, 183, 341

Worthey, G. 1992, PhD thesis, California Univ., Santa Cruz.

—. 1994, ApJS, 95, 107

—. 2004, AJ, 128, 2826

Yan, H., Dickinson, M., Eisenhardt, P. R. M., Ferguson, H. C., Grogin, N. A., Paolillo, M., Chary, R., Casertano, S., Stern, D., Reach, W. T., Moustakas, L. A., & Fall, S. M. 2004, ApJ, 616, 63